Phosphorescence spectroscopy and its application to the study of colloidal dynamics

Fosforescentie-spectroscopie en haar toepassing op de studie van colloïdale dynamica

(MET EEN SAMENVATTING IN HET NEDERLANDS)

PROEFSCHRIFT

TER VERKRIJGING VAN DE GRAAD VAN DOCTOR AAN DE UNIVERSITEIT UTRECHT OP GEZAG VAN DE RECTOR MAGNIFICUS PROF. DR. H.O. VOORMA, INGEVOLGE HET BESLUIT VAN HET COLLEGE VOOR PROMOTIES IN HET OPENBAAR TE VERDEDIGEN OP MAANDAG 6 SEPTEMBER 1999 DES MIDDAGS TE 14.30 UUR.

DOOR

Minne Paul Lettinga

GEBOREN OP 15 JUNI 1970 TE DELFT

Promotores: Prof. dr. Y.K. Levine
Faculteit der Natuur- en Sterrenkunde
Universiteit Utrecht
Prof. dr. A.P. Philipse
Faculteit Scheikunde
Universiteit Utrecht
Co-promotor: Dr. M.A.M.J. van Zandvoort
Faculteit der Geneeskunde
Universiteit Maastricht

ISBN: 90-393-2189-2

Contents

Chapter 1

General Introduction

1.1 Translation and Rotation

Consider a particle taking a bath in a vessel filled with solvent. If the particle has colloidal dimensions, it will move freely throughout the vessel. Observe the particle one would see that the particle describes a random trajectory as it tumbles and zigzags across the bath. In other words: the particle undergoes random translations and rotations. The particle is taken out of the bath and put in a very long but also very thin tube filled with the same solvent. The displacements of the particle are now restricted to almost one dimension, while the tumbling of the particle is not markedly reduced. Or, to put it differently, translations are reduced to one dimension while the rotations of the particle are relatively unaffected.

If the particle is incorporated in a system that forms effectively a labyrinth, then the translational diffusion will be confined to displacements over very small distances. On the other hand, the particle will keep turning over and over in its confined space, unless it sticks to the wall of the labyrinth by some sort of interaction (hydrogen bonding, hydrophobic interactions, etc.). This example illustrates a fundamental difference between rotational and translational diffusion. It shows that in complex media the translational diffusion over a large range can be completely quenched, while the rotational diffusion is unaffected. If the resolution of the microscope, or the visualization technique, is less than the range of the displacements, one would even tend to think that the particles are immobilized. It thus appears that rotational diffusion measurements are very suitable for monitoring local interactions between particles and their surrounding. Translational diffusion measurements, on the other hand, give information on the overall structure of the complex.

Another important difference between rotational and translational diffusion is an experimental one. Suppose one is looking through a microscope at perfectly

spherical particles. Again particles will be observed that move across in a zigzag fashion through the vessel, but no tumbling of the particles can be observed because of their spherical symmetry. The only way to make the rotation of the spherical particles visible is to mark the particle with a dot or a line. In other words, one has to make a mechanically isotropic sphere anisotropic for the detection technique used.

1.2 Studying rotational diffusion

Most techniques for determining rotational diffusion make use of probe molecules that exhibit some sort of anisotropy. Nuclear Magnetic Resonance (NMR) and Electron Spin Resonance[1] (ESR) can be used to monitor the reorientational motions of ^{13}C or spin-labeled probes. Luminescent probe molecules are also often used because of their superior sensitivity.[2] When excited with a polarized light pulse, these dyes will absorb a photon. The efficiency of the absorption depends on the orientation of the dye molecule relative to the polarization direction of the excitation light. The emitted polarized light is detected and the degree by which the polarization changes between absorption and emission is a measure of rotational motion.[3] This technique relies on the delay between the absorption and emission processes. The time-scale on which the photon is emitted determines the rate of rotation the technique can access.

Measurements of the rotational diffusion of unbound dye molecules have been used to determine the local viscosity in a variety of polymer solutions and gels.[4,5,6] The dye molecules can also be used as tags for large particles like proteins that do not have an intrinsic response. In this way the interactions between proteins and their environment can be studied. Examples are interactions in muscle fibers,[7] membrane proteins,[8,9] and in matrices as erythrocytes[10,11] and the cytoplasm.[12]

The main difficulty in interpreting the observed signals from rotational dynamics experiments is the theoretical description of the physical processes involved. For instance, studies of proteins and their environment are hampered, even for model systems,[13] by factors such as the mobility of the probe relative to the protein and the flexibility of the protein molecule itself. Moreover, it is not a simple matter to describe the complex interactions between the proteins and their environment. Many of these drawbacks can, however, be overcome in studies of synthesized spherical model colloids. Monodisperse silica spheres are examples of widely studied colloids. Their surface modification with compounds such as long-chain alcohols[14] and silane coupling agents[15,16] allow dispersibility of spheres in a wide variety of solvents.

As mentioned above, in order to monitor the rotational diffusion of spherical particles the particles have to exhibit an anisotropic response. Depolarized Dynamic Light-Scattering and Forward Depolarized Light-Scattering experiments have been performed on fluorinated, spherical, polymer colloids with partially crystalline internal structure.[17,18] Forced Rayleigh Scattering[19] is another light scattering method, where internal anisotropy is created by the bleaching of photosensitive dyes attached to the polystyrene sphere. Similarly, NMR experiments have exploited the ^{13}C chemical shift anisotropy.[20]

Another approach for studying rotational dynamics in colloidal systems is to make use of luminescent molecules incorporated in the silica spheres. Such particles have already been exploited for monitoring translational diffusion with Fluorescence Recovery After Photobleaching (FRAP).[21] The rotational dynamics of the dye molecules in the spheres may then be followed with depolarization experiments. The advantages of the luminescence depolarization technique over conventional light scattering methods are its selectivity and its application to slightly scattering samples. Consequently, it can be applied to a large variety of confining media. Light scattering techniques are restricted to optically transparent samples, such as dispersions of colloids,[17,18,20] polymer gels,[22] and solutions of macromolecules.[23] With depolarization experiments, however, the rotational dynamics of specifically tagged spherical particles in matrices such as porous glasses and packings of host spheres can now be followed. For the same reasons, the translational diffusion of fluorescent dye-labeled spheres have been studied with the FRAP technique.[24,25]

In this thesis we present, among other things, studies of the rotational diffusion of silica spheres tagged with phosphorescence dyes in colloidal sphere packings. We were able to obtain information about the system, which cannot be monitored with translational diffusion techniques as FRAP. A prerequisite for phosphorescence depolarization studies is, however, the characterization of the spectral properties of suitable dyes.

1.3 Time-resolved Phosphorescence Anisotropy

Luminescence depolarization

In a generalized luminescence depolarization experiment an instantaneous pulse of polarized light illuminates a sample containing luminescent dye molecules. A transition from the electronic ground state to the excited state and vice versa will take place if the energy of the photons corresponds to the energy gap between the two states of the dye molecule. Furthermore, a fixed direction in the frame of the molecule relative to the polarization direction (denoted by $\vec{e}_i$ for excitation and $\vec{e}_f$ for detection) of the light is associated with the transitions between the ground and excited state. This fixed direction is called the transition dipole moment, denoted by $\vec{m}$ and $\vec{n}$ for the absorption and emission dipole moment, respectively. Following Fermi's Golden Rule, the excitation and emission probabilities of a given molecule are proportional to $(\vec{e}_i \cdot \vec{m})^2$ and $(\vec{e}_f \cdot \vec{n})^2$ respectively.

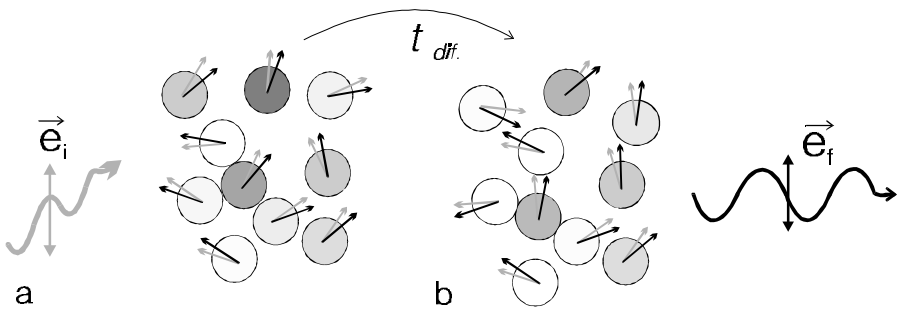

Figure 1.1 *The luminescence anisotropy experiment in two steps. The gray-scale of the spheres indicates the excitation (a) and detection (b) probability. The particles are excited with a polarized light beam. The excitation probability is proportional to the angle between the gray arrows depicting the absorption process and the polarization vector* $\vec{e}_i$. *The particles will diffuse during* $t_{dif.}$ *before emitting a photon. The probability of emitting a photon of polarization* $\vec{e}_f$ *depends on the angle between the black arrows depicting the emission dipole moments and* $\vec{e}_f$.

When a population of dye molecules, $f(\Omega_p)$, where Ω_p denotes the orientation of the molecules in space, is excited with a polarized light pulse, a sub-population of dyes in the excited state, $f(\Omega_p)\cdot(\vec{e}_i\cdot\vec{\mu})^2$, is created. This sub-population is not in orientational equilibrium and will therefore relax to its equilibrium distribution $f(\Omega_p)$. As the excited dye decays to the ground state after a time t, the polarization of the emitted light reflects the rotational motion of the dye. The probability that molecules excited at $t = 0$ emit a photon at time t, is given by $F(t)$, whose time course is characterized by the lifetime of the excited state. The lifetime depends on the photophysical processes, which in turn are determined by the electronic structure of the dye. If the photon is emitted directly from the excited singlet state, the time-window within which the rotational dynamics can be followed, lies in the order of nanoseconds. If the photon is emitted from the triplet state, the time-window is typically micro- to milliseconds. In general, the lifetime does not depend on the orientation of the dye molecules. Now, the general expression for the luminescence intensity is

$$I_{if}(t) \propto \int \frac{d\Omega_p}{8\pi^2} (\vec{e}_f\cdot\vec{n})^2\Big|_t (\vec{e}_i\cdot\vec{\mu})^2\Big|_0 F(t)\,, \tag{1.1}$$

where the integration is performed over the orientation of the molecules, Ω_p.

Equation (1.1) is the central equation of the luminescent depolarization experiment. However, in order to extract information about the orientation of the tagged particles equation (1.1) has to be expressed explicitly as a product of factors describing the properties of the sample and factors describing the geometry of the experiment.[26] This is done most conveniently on using the Wigner functions, D^L_{mn}, which represent the rotational transformation between two coordinate systems.[27] To this end, the inner products in equation (1.1) are expressed in terms of the Legendre polynomial P_2, which is equal to the Wigner function D^2_{oo}. On using the closure relation,[26] we obtain:

$$P_2(\vec{e}_i\cdot\vec{\mu}) = \tfrac{1}{2}(3(\cos(\vec{e}_i\cdot\vec{\mu})^2 - 1) = \sum_{i=-2}^{2} D^{2*}_{i0}(\Omega_{eL}) D^2_{i0}(\Omega_{Lm}) \tag{1.2}$$

and

$$P_2(\vec{e}_i\cdot\vec{n}) = \tfrac{1}{2}(3(\cos(\vec{e}_f\cdot\vec{n})^2 - 1) = \sum_{i=-2}^{2} D^{2*}_{i0}(\Omega_{fL}) D^2_{i0}(\Omega_{Ln})\,. \tag{1.3}$$

The angles Ω_{eL} and Ω_{fL} represent the orientations of the polarization factors of the excitation and emission relative to the laboratory frame. Ω_{Lm} and Ω_{Ln} represent the

orientation of the laboratory frame relative to the absorption and emission dipole moments $\vec{m}$ and $\vec{n}$, respectively. After some laborious but straightforward algebra, (1.1) can be expressed as

$$I_{if}(t) \propto \left(1 + 2D_{00}^{2*}(\Omega_{eL})S_{\mathrm{m}} + 2D_{00}^{2}(\Omega_{fL})S_{\mathrm{n}} + 4\sum_{k=-2}^{2} D_{k0}^{2*}(\Omega_{eL})D_{k0}^{2}(\Omega_{fL})G_k\right)F(t), \quad (1.4)$$

where the order parameters S_μ and S_ν for the absorption and emission dipole moment and the correlation functions G_k are defined by

$$S_{\mathrm{m}} = \left\langle D_{00}^{2}(\Omega_{L\mathrm{m}})\right\rangle \quad (1.5a)$$

$$S_{\mathrm{n}} = \left\langle D_{00}^{2*}(\Omega_{L\mathrm{n}})\right\rangle \quad (1.5b)$$

$$G_k = \left\langle D_{k0}^{2*}(\Omega_{L\mathrm{n}}^{t})D_{k0}^{2}(\Omega_{L\mathrm{m}}^{0})\right\rangle \qquad k=0,1,2. \quad (1.5c)$$

Here the brackets $\langle\ldots\rangle$ denote integration over Ω_{p}, the orientation of the molecules in space.

In a time-resolved anisotropy experiment the sample is illuminated with a short vertically (*V*) polarized light pulse. The horizontal (*H*) or vertical (*V*) component of the emitted light is detected in a standard 90° geometry (see Figure 1.1). The anisotropy $r(t)$ is then defined by

$$r(t) = \frac{I_{VV}(t) - I_{VH}(t)}{I_{VV}(t) + 2I_{VH}(t)} \quad (1.6)$$

For isotropic samples $S_\mu=S_\nu=0$ and $G_0=G_1=G_2$. With (1.4) we find that the anisotropy then can be expressed as a single correlation function:[28]

$$r(t) = 2\left\langle D_{00}^{2*}(\Omega_{L\mathrm{n}}^{t})D_{00}^{2}(\Omega_{L\mathrm{m}}^{0})\right\rangle \quad (1.7)$$

The closure relation can again be used to separate $\Omega_{L\mathrm{mn}}$ in the angle of interest, i.e. the orientation of the long axis of the dye *l* relative to the laboratory frame L,

Ω_{Ll}, and the angles between l and the absorption and emission dipole moment Ω_{lm} and Ω_{ln}, respectively.

$$r(t) = \tfrac{2}{5} \sum_{m,n=-2}^{2} \left\langle D_{0m}^{2*}(\Omega_{Ll}) D_{0n}^{2}(\Omega_{Ll}) \right\rangle D_{m0}^{2}(\Omega_{lm}) D_{n0}^{2}(\Omega_{ln}) \tag{1.8}$$

The zero-time anisotropy $r(0)$ depends solely on the difference angle between the absorption and emission dipole moment $\Omega_{\mu\nu}$, which is an intrinsic property of the dye molecule. Its value has to be determined prior to the actual experiment, in order to avoid ambiguities in the interpretation of the measurements.

$$r(0) = D_{00}^{2}(\Omega_{mn}) \tag{1.9}$$

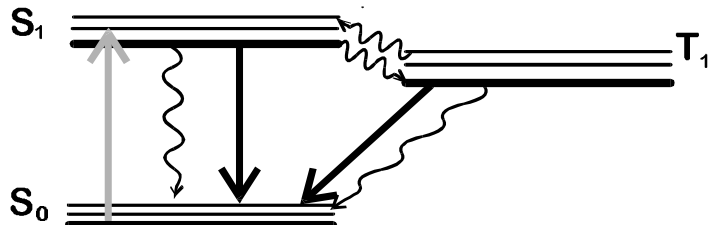

Figure 1.2 *The Jablonski diagram, which gives a schematic overview of the photo-excitation and emission processes.*

Phosphorescence lifetime and quantum yield

The time-window in which a photon is emitted depends on the processes taking place in the excited state. All molecules studied in this thesis return to the ground state through two pathways. The most probable pathway is the direct return from the first excited singlet state S_1 either by the emission of a photon (fluorescence) or by a radiationless decay. The effective fluorescence lifetime is defined as the average residence time in the first excited singlet state and is typically of the order of nanoseconds.

The second route is followed when the molecules can undergo intersystem crossing to the triplet state T_1. In this scenario the spin of the excited electron flips during the transition due to the presence of spin-orbital coupling. Again the molecule will return from the triplet state to the ground state with the emission of a photon or via a radiationless decay. The photon emitting process is called

phosphorescence. In marked contrast with fluorescence, the probability of phosphorescent emission is small, so that the effective phosphorescence lifetime is typically of the order of micro- to milliseconds. This means that the same dye molecules can be used to study rotational dynamics in the nanosecond time-window as well as in the micro- to millisecond time-window.

Another important difference between the two luminescent processes is the quantum yield. The quantum yield of the excited state S_1 or T_1 is defined as the fraction of molecules relaxing to the ground state with the emission of a photon. Competing processes such as collisional quenching play a far more important role for phosphorescence than for fluorescence, since the residence time in the triplet state is substantially longer. Therefore the quantum yield is orders of magnitude higher for fluorescence than for phosphorescence. The phosphorescence quantum yield is increased when the coupling between the triplet state and the ground state is enhanced. This depends solely on the efficiency of spin-orbit interaction, which increases with the number of conjugated heavy atoms and their Z number.

The low quantum yield of phosphorescence raises a challenging technical problem. The detection channel must be sensitive and at the same time be protected from an overload during the excitation light pulse and the following instant strong fluorescence emission. In practice this means that the detection unit has to be gated. This, however, introduces an experimental dead-time of at least a few hundred nanoseconds into the time-resolved phosphorescence measurements.

1.4 Thesis outline

The scope of this thesis is twofold. In the first place, dye molecules are scanned for their suitability as probe in Time-resolved Phosphorescence Anisotropy (TPA) experiments. The applicability of the dye depends on its phosphorescence quantum yield, lifetime, and zero-time anisotropy, $r_p(0)$. The number and type of substituted heavy atom in a dye molecule mainly influence these three factors. For this reason, we study the spectral properties of the commonly used probes erythrosine (4-iodo-fluorescein), eosin (4-bromo-fluorescein) as well as the 2-iodo- and 2-bromo-fluorescein derivatives. The results are presented in chapter 2.

The interpretation of depolarization experiments on orientationally anisotropic systems such as membranes[29] and muscle fibers[30] not only requires knowledge of $r_p(0)$, but also of the absolute orientation of the transition dipole moments in the frame of the dye. In chapter 3 we determine the orientation of the absorption and fluorescence dipole moments for eosin and erythrosine. To this end we exploit

angle-resolved fluorescence depolarization (AFD) measurements on dye molecules macroscopically aligned in stretched polymer films.

The results of chapter 3 are used in chapter 4, where we determine the orientations of the phosphorescence dipole moment of the four fluorescein derivatives. This information is obtained on combining phosphorescence anisotropy measurements at two excitation wavelengths with the results of AFD experiments.

The second goal of this thesis was the synthesis and characterization of colloidal silica spheres tagged with phosphorescent dye molecules, and their use in TPA experiments. In chapter 5 we show how the incorporation of the dye molecule in the silica sphere influences the spectral properties of the dye. We monitor the internal restricted orientational motions of the dyes within the silica particles on exploiting the fact that this motion takes place on the time-scale of fluorescence. Importantly, we demonstrate that the rotational diffusion rate of tagged colloidal spheres can be determined quantitatively.

In chapter 6 we present a study of the rotational diffusion rates of the phosphorescent tracer spheres in packings and dispersions of host spheres. The results are compared with measurements of translational diffusion on the same systems. In this way we show that our experiments provide more detailed information about the local structure and environment in complex media.

References

[1] J. Buitink, M. A. Hemminga, and F. A. Hoekstra (1999), *Biophys. J.* **76**, 3315-3322

[2] G.L. Hoatson and Y.K. Levine (1994) in *The Molecular Dynamics of Liquid Crystals*, G.R. Luckhurst and C.A. Veracini (Ed.). Kluwer Academic Publishers, 1-9.

[3] C.R. Cantor and P.R. Schimmel (1980), *Biophysical Chemistry, part II*¸W. H. Freeman and Company, New York

[4] M. Hermansson (1999), *Colloids and Surfaces A* **154**, 303-309

[5] W. Mikosch, Th. Dorfmüller, and W. Eimer, (1994), *J. Phys. Chem.* **101** 11044-11051 and 11052-11059

[6] M.T. Cicerone, F.R. Blackburn, and M.D. Ediger (1995), *J. Chem. Phys.* **102**, 471-479

[7] C.L. Berger and D.D. Thomas (1994), *Biophys. J* .**67**, 250-261; D.D. Thomas, S. Ramachandran, O. Roopnarine, D.W. Hayden, and E. M. Ostap (1995), *Biophys. J.* **68**, 135s-141s and other work by D.D. Thomas and his group.

[8] D.A. Roess, M. A. Jewell, C.J. Philpott, and B.G. Barisas (1997), BBA **1375**, 98-106

[9] R. Zidovetski, M.Bartholdi, D. Arndt-Jovin, and T. M. Jovin (1986), *Biochemistry* **25**, 4397-4401

[10] A. M. Genaro, A. Luquita, and M. Rasia (1996), *Biophys. J.* **71**, 389-393

[11] D. Wang, U. Kreatzer, Y. Chung, and T. Jue (1997), *Biophys. J.* **73**, 2764-2770

[12] R. Swaminathan, C.P. Hoang, and A.S. Verkman (1997), *Biophys. J.* **72**, 1900-1907
[13] D. Lavalette, C. Tétreau, M. Tourbez, and Y. Blouquit (1999), *Biophys. J.* ,**76** 2744-2751
[14] A.K. van Helden, J.W. Jansen, and A. Vrij (1981), *J. of Coll. and Interf. Sci.* **81**, 354-358
[15] A.P. Philipse and A. Vrij (1989), *J. of Coll. and Interf. Sci.* **128**, 121-136
[16] A.P. Philipse and A. Vrij (1988), *J. Chem. Phys.* **88**, 6459-6470
[17] V. Degiorgio, R. Piazza, and R.B. Jones (1995), *Phys. Rev. E* **52**, 2707-2712
[18] V. Degiorgio, R. Piazza (1996), *J. Phys.Chem.* **52**, 9497-9502
[19] J. Kanetakis and H. Sillescu (1996), *Chem. Phys. Let.* **252**, 127-134
[20] J. Kanetakis, A. Tölle, and H. Sillescu (1997),) *Phys. Rev. E* **55**, 3006-3013
[21] A. van Blaaderen, I. Peetermans, G. Maret, and J.K.G. Dhont (1992), *J. Chem. Phys.* **96**, 4591-4603
[22] B. Camins and P.S. Russo (1994), *Langmuir* **10**, 4035-4059
[23] T. Jamil and P.S. Russo (1998), *Langmuir* **14**, 264-270
[24] S.G.J.M. Kluijtmans, E.H.A. de Hoog , and A.P. Philipse (1998), *J. Chem. Phys.* **108**, 7469-7477
[25] S.G.J.M. Kluijtmans and A.P. Philipse (1999), *Langmuir* **15,** 1896-1898
[26] C. Zannoni (1979) in *The molecular physics of liquid crystals,* G.R. Luckhurst and C. A. Veracini (Ed.). Academic Pres, New York
[27] M.E. Rose (1957), *Elementary theory of angular momentum*. Wiley, New York.
[28] C. Zannoni (1979), Distribution functions and order parameters. *The molecular Physics of Liquids, eds.* G. R. Luckurst and G. W. Gray, Acedemic Press, London
[29] M. van Gurp, H. van Langen, G. van Ginkel, and Y.K. Levine (1988), in *Polarized spectroscopy of ordered systems*, B. Samori, and E.W. Thulstrup (Ed). Kluwer Academic Publishers, 455-489
[30] U.A. van der Heide, B. Orbons, H.C. Gerritsen, and Y.K. Levine (1994), *Eur. Biophys. J.* **21**, 263-272

Chapter 2

Luminescent characterization of fluorescein derivatives in various immobilizing matrices

Abstract

The phosphorescence quantum yield, zero-time anisotropy, and lifetime are the three factors determining the suitability of a phosphorescent dye for rotational diffusion experiments. These factors have been characterized here for four dye molecules, consisting of a fluorescein core with two or four substituted heavy-atoms (iodine and bromine). The characterization has been performed by a combination of spectral and time-resolved luminescence measurements on dye molecules embedded in various immobilizing matrices. We found that the Z number of the substituted heavy atoms primarily influences the luminescent properties of the dyes. The number of substituted heavy atoms appears to play a subsidiary role. More importantly, we have formulated a quantitative measure for selecting a dye molecule for a particular phosphorescence experiment. In addition, we have delineated the optimal concentration range of dye molecules for phosphorescence depolarization experiments.

2.1 Introduction

Luminescence depolarization is a widely used technique for studying order and reorientational motions in biological systems.[1] It makes use of luminescent dyes incorporated in the system of interest. The order and dynamics of the dyes are conveniently monitored when the orientation of the absorption dipole moment relative to that of the emission dipole moment of the dye is followed in time. This orientation is defined by the fluorescence or phosphorescence anisotropy (depending on the emission process). The effectiveness of the depolarization technique depends on both the spectral properties of the dye and the time-window of the reorientational dynamics.

The luminescence properties of the dye ideally satisfies three requirements. First, the initial anisotropy of the dye should be as close as possible to the

theoretical maximum of 0.4, in order to reach the highest dynamic range. Second, the lifetime of the emission process should be in the same range as the reorientational motion in order to monitor the full reorientational decay. Third, the quantum yield of the emitting process should be sufficiently high. Since luminescence quantum yield, lifetime, and initial anisotropy are intrinsic properties of the dye molecule, it is expedient to have prior knowledge of these properties for the quantitative analysis of the experimental data. In addition the analysis is facilitated by knowledge of the orientations of the absorption and emission dipole moments (i.e. the transition dipole moments) within the frame of the dye molecule.

Phosphorescence depolarization studies often utilize dye molecules such as eosin and erythrosine.[2,3] These consist of a fluorescein core with four substituted heavy-atoms: iodine for erythrosine and bromine for eosin. The number of substituted heavy atoms and their Z number are known to influence the phosphorescence properties significantly.[4] However, it is not known which of the two latter factors is of greater importance. Furthermore, little is known of how these factors influence the orientations of the transition dipole moments in the molecular frame. To this end it is interesting to compare the spectral properties of erythrosine and eosin with the spectral properties of fluorescein with two substituted bromine or iodine atoms. With the knowledge of the spectral properties of the four dyes one is able to select the most suitable probe for a particular experiment.

The spectral properties of the four fluorescein derivatives are the focus of this chapter. They can be determined using a model system in which the dyes are immobilized within the phosphorescence time-scale (micro- to milliseconds). In such a system the phosphorescence anisotropy is independent of time and equal to the zero-time anisotropy. The model system is chosen judiciously, so that it is reasonable to assume that the spectral properties are transferable to the dye in the system of interest, e.g. a protein or colloidal particle. One of the considerations which had been overlooked in the past,[3,5,6] is the accessibility of the UV region of the spectrum where the $S_0 \rightarrow S_2$ absorption band is found. It will be argued in chapters 3 and 4, that this knowledge is necessary for determining the orientation of the phosphorescence dipole moment within the molecular frame.

We have shown in previous studies[7,8] that systems like nitrocellulose (NC) and polyvinylalcohol (PVA) films are suitable for fluorescence anisotropy studies in both the visible and the UV regions. Dye molecules embedded in these matrices were found to be immobilized on the nanosecond fluorescence time-scale. Here we report time-resolved phosphorescence anisotropy measurements showing that the dynamics of the molecules are also quenched on the

phosphorescence time-scale (μs to ms) in these polymer matrices. In addition, the optimal dye concentration was investigated to find a trade off between signal intensity depolarization effects arising from energy transfer in the excited state (ET).[7] For this reason also a framework for describing the influence of ET on the phosphorescence anisotropy is presented. In order to gain insight into the influence of the heavy atom substituents on the luminescent properties of the dye, we determined the fluorescence and phosphorescence quantum yields from the spectral information and measurements of fluorescence and phosphorescence lifetimes. It is found that the luminescent properties of the dyes are primarily influenced by the Z number of the substituted heavy atoms. The number of substituted heavy atoms appears to play a subsidiary role. This information is useful in considerations of the choice of a dye molecule for time-resolved phosphorescence studies.

2.2 Theory

Phosphorescence mechanism for fluorescein derivatives

Phosphorescence is a process whereby a molecule relaxes from the triplet excited state T_1 to the singlet ground state S_0 by the emission of a photon. Since this is a spin-forbidden transition, phosphorescence lifetimes are in general much longer than fluorescence lifetimes, i.e. microseconds rather than nanoseconds.

For organic dyes like eosin and erythrosine, the main route for populating the triplet state is intersystem crossing from the first excited singlet state S_1. The depopulation of the first excited singlet state depends on the fluorescence rate k_f, the rate of intra- and intermolecular quenching (e.g. radiationless transitions) rate k_{qf}, and the intersystem crossing rate k_{isc}. The depopulation of the triplet state depends on the phosphorescence rate k_p, the quenching rate k_{pq}, and the back transfer process $f \cdot k_{isc}$. Delayed fluorescence occurs when the molecule returns from the T_1 to the S_1 with a subsequent emission of a photon. When this process is thermally activated it is called *E-type* (eosin-type) *delayed fluorescence*.[9] The *E-type* process thus depends on the S_1-T_1 energy band gap and the temperature. The processes considered here are summarized schematically in the Jablonski diagram shown in Figure 2.1.

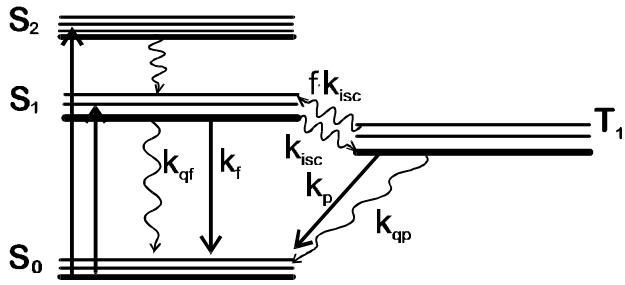

Figure 2.1 *Generalized Jablonski diagram for E-type luminescent molecules.*

Several mechanisms are known to promote intersystem crossing. The most important are internal rotations, the external heavy atom effect, and the internal heavy atom effect. Internal rotations in the excited state of a molecule cause a difference in parity between the excited state and the ground state. This results in a partially forbidden transition from the first excited singlet state to the ground state.[10] In the external heavy atom effect, heavy atoms of nearby molecules can perturb the electronic state of the dye molecule, resulting in a mixing of the triplet and singlet state.[4,11] A similar process takes place when heavy atoms are substituted in the molecule itself, as a result of the perturbation of the π-electronic system. The spin-orbit coupling is strongly enhanced[4,10,12] and intersystem crossing to the triplet state is promoted. This type of spin-orbit coupling is called the internal heavy-atom effect. The strength of the coupling is governed by the atomic spin-orbit coupling factor ζ_K. This factor depends on the position of the substituted K^{th} heavy atom in the molecule and increases with the Z number of the atom.[11] We shall now focus on the internal heavy atom effect, since we here study the properties of four molecules with identical aromatic ring structure, but differing in the number and type of the substituted heavy atoms.

The relation between the coupling factor ζ_K and the natural phosphorescence lifetime ($\tau_P^0 = 1/k_p$) is given by[12]

$$\frac{1}{\tau_P^0} = B\sum_K c_K^2 \zeta_K^2 , \qquad (2.1)$$

where the c_K's denote the Hückel Atomic Orbital coefficients of the parent carbocyclic system at center K of the atom and B is a constant. The summation is taken over all the atoms of the molecule. Thus, if ζ_K is independent of the position of the substituted atom in the molecular structure, then the natural

lifetime is linearly dependent on the number of substituted atoms with a given atomic number Z. As an example, the natural phosphorescence lifetime of a xanthene ring system with two substituted iodine atoms is in this case twice as long as that of a xanthene ring system with four substituted iodine atoms. The radiationless transition rate from the triplet state to the ground state, k_{qp}, often exhibits the ideal behavior where it has the same dependence on the coupling factor z_K as the natural phosphorescence lifetime. In these cases, the measured phosphorescence lifetime, τ_p, is also found to be linearly dependent on the number of substituted atoms with a specific Z number.

The population dynamics shown in the Jablonski diagram, Figure 2.1, can be expressed in terms of a set of rate equations, (2.2), relating the rate constants to the following experimental observables: 1) the fluorescence and phosphorescence lifetimes, τ_f and τ_p; 2) the natural fluorescence lifetime $\tau_f^0 = 1/k_f$ calculated from the excitation and fluorescence spectra (see below); 3) the relative quantum yields Φ_f/Φ_p and Φ_{df}/Φ_p obtained from the integrated spectra. This is an extension of the set of rate equations used by Lam and Lo,[5] who did not use the spectral determination of τ_f^0 and therefore had to omit the quenching rate k_{qf}.

$$\begin{aligned}
\frac{\Phi_f}{\Phi_p} &= \frac{k_f}{k_{isc}} \frac{1}{k_p \tau_p} \\
\frac{\Phi_{df}}{\Phi_p} &= \frac{f \cdot k_{isc}}{k_p} \frac{k_f}{k_f + k_{isc} + k_{qf}} \\
\tau_p &= \frac{1}{k_p + f \cdot k_{isc} + k_{qp}} \\
\tau_f &= \frac{1}{k_f + k_{isc} + k_{qf}}
\end{aligned} \tag{2.2}$$

In setting up the set of equations we assumed that the delayed fluorescence is caused by thermal activation. Now the probability f that the molecule will overcome the energy barrier between the triplet state and the first excited singlet state is governed by the Boltzmann distribution factor, $f = e^{-\Delta E/kT}$. Here ΔE is the energy difference between the T_1 and S_1 states. This energy difference can be determined from the distance between the maxima of the phosphorescence and fluorescence emission peaks. Note that the intersystem crossing rate from T_1 to S_1 is given by $f \times k_{isc}$.[13]

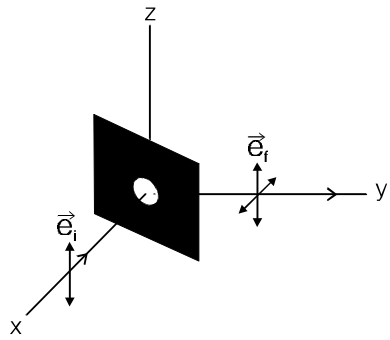

Figure 2.2 *Geometry for anisotropy measurements on a polymer film sealed between two glass plates. A diaphragm in the excitation beam ensures a well defined measuring volume.* $\vec{e}_i$ *and* $\vec{e}_f$ *are polarization vectors of the excitation beam and analyzer, respectively.*

Luminescence anisotropy of molecules in immobilized solutions

The geometry for luminescence anisotropy measurements is shown in Figure 2.2. The sample is illuminated with vertically (*V*) polarized light while the emitted light is detected with horizontal (*H*) or vertical (*V*) polarization in a direction perpendicular to the excitation beam. The anisotropy $r(t)$ is then defined by

$$r(t) = \frac{I_{VV}(t) - I_{VH}(t)}{I_{VV}(t) + 2I_{VH}(t)} \quad , \tag{2.3}$$

where the subscripts denote the polarization directions of the exciting and emitted light, respectively, in the laboratory frame. If the molecules are embedded homogeneously in the polymer matrix with a random orientation of their molecular frames, the anisotropy and its decay after a short light pulse are determined simply by the difference angle Δ between the absorption and emission dipole moments, as well as by the rotational dynamics of the dye molecules.[14] In its most general form the anisotropy can be written as a sum of exponentials:[15,16]

$$r(t) = r(0)\sum_i a_i \cdot e^{-t/\rho_i} \quad , \tag{2.4}$$

where $r(0)$ is the anisotropy at t=0

$$r(0) = \frac{1}{5}\left\{3(\cos\Delta)^2 - 1\right\} \tag{2.5}$$

and j $_i$ are decay times whose explicit forms depend on the symmetry and rotational modes of the dye molecules. Thus, the presence of rotational motions can be inferred from the decay of the anisotropy. If the dye molecules are immobilized on the time-scale of the luminescing process, j $_i$ fi ¥, and thus the anisotropy is time-independent and equals *r(0).* In the latter case the steady-state experiment suffices to determine the difference angle Δ, since r_{SS}=*r*(0).

$$r_{SS} = \frac{\bar{I}_{VV} - \bar{I}_{VH}}{\bar{I}_{VV} + 2\bar{I}_{VH}} \tag{2.6}$$

Thus, steady-state anisotropy experiments on a homogenous, random, motionless system yield the difference angle between the absorption and emission dipole moments in the molecular frame. We now note that this holds for both fluorescence and phosphorescence, as the absorption process is independent of the emission process.EMBED

Förster Radiation Energy Transfer for donor-donor systems and its influence on phosphorescence anisotropy

At high dye concentrations, the energy of a molecule in an excited singlet state can migrate to a nearby dye molecule via a resonant, radiationless energy transfer. This process is called Förster Radiation Energy Transfer.[17] A prerequisite for Energy Transfer (ET) to take place is a spectral overlap between the extinction spectrum (e(l)) of the acceptor molecule and the fluorescence emission spectrum (*F*(l)) of the donor molecule. The migration of the excitation energy from one dye molecule to another with a different orientation causes the partial loss of the polarization of the excited state. The polarization loss arises from the fact that the ET process tends to randomize the distribution of orientations of the absorption dipole moments of the molecules in the S_1 state. If the intersystem crossing rate is larger than the ET rate, the excited molecules will populate the triplet state without participating in the ET process. We note that not only is the overlap between absorption and phosphorescence spectra very small, but the ET process is also spin-forbidden. Consequently, the polarization of the excited state is trapped until the phosphorescence photon is emitted.

However, in the opposite limit of an ET rate larger than the intersystem crossing rate, the polarization will be lost prior to the population of the triplet state. Thus, no phosphorescence depolarization will be observed. In order to gain insight into the conditions under which ET processes compromise the observed phosphorescence depolarization, we shall now consider the singlet-singlet ET process in some detail.

The efficiency of the ET process is commonly described in terms of the Förster radius R_0, defined by

$$R_0^6 = 8.79\times10^{-25}\frac{\langle \kappa^2 \rangle}{n^2}\frac{\int F(\lambda)\varepsilon(\lambda)\lambda^2 d\lambda}{\int F(\lambda)\lambda^{-2} d\lambda}[cm^6], \tag{2.7}$$

where n is the refractive index of the medium and $\langle\kappa^2\rangle$ is a factor determined by the mutual orientation of two interacting molecules which is conventionally taken to be equal to 2/3, the value for a random orientational distribution. R_0 is the distance between two molecules when the probability of ET equals 0.5.

A simple model describing the depolarization effect of ET in the singlet state has been formulated by Galanin.[18] This approach assumes that the polarization is completely lost when the excitation migrates from one dye molecule to the other, so that polarized fluorescence emission is only observed from those dye molecules excited at $t=0$. The probability that a molecule excited at time t=0 is still excited at time t is given by $N_0(t)$. It has been shown[19,20] that under these conditions the time-dependent fluorescence anisotropy $r_f(t)$ is related to N_0 by

$$r_f(t) = r_f(0)\frac{N_0(t)}{N(t)}. \tag{2.8}$$

$N(t)$ is simply the total fluorescence decay e^{-t/τ_f}, where τ_f is the lifetime of the excited state, i.e. the fluorescence lifetime.

$N_0(t)$ is given accurately by the heuristic approach of the Huber, Hamilton, and Barnett (HBB) model.[19,20,21] In the limit of a three-dimensional system of immobilized and isotropically distributed dyes this latter model yields:

$$\log N_0(t) = -\frac{t}{\tau} - \sqrt{\frac{\pi}{2}}\gamma_{stat}\sqrt{\left(\tfrac{4}{3}\pi R_0^3\rho\right)^2\frac{t}{\tau_0^f}}. \tag{2.9}$$

Here, γ_{stat} is a factor arising from the orientational averaging of κ^2 over the dye ensemble. γ_{stat} is equal to 0.8452 for immobilized, isotropically distributed dyes.

ρ is the average dye concentration and τ_f^0 is the natural fluorescence lifetime in absence of competing processes like intersystem crossing and quenching. The natural lifetime is obtained directly from the absorption spectrum ($\varepsilon(\lambda)$ in $M^{-1}cm^{-1}$) and the emission spectrum ($F(\lambda)$):

$$\frac{1}{\tau_f^0} = 2.88\times10^{-9} n^2 \frac{\int F(\lambda)\lambda^{-2}d\lambda}{\int F(\lambda)\lambda\, d\lambda}\int \varepsilon(\lambda)\lambda^{-1}d\lambda \ [s^{-1}]. \tag{2.10}$$

As discussed above the loss of polarization by ET processes amongst molecules in the first excited state will leak into the triplet state when the ET rate is of the same order or larger than the intersystem crossing rate. Thus, depolarization of the phosphorescence is governed by $N_0(t)/N(t)$ (see (2.8)) and its time dependence is given by

$$r_P(t) = r_P(0)\frac{\int_0^t \exp\left[-g_{stat}(\tfrac{4}{3}\pi R_0^3\rho)\sqrt{\frac{\pi}{2}\frac{t'}{\tau_f^o}} - t'\cdot k_{isc}\right]dt'}{\int_0^t \exp(-t'\cdot k_{isc})dt'}. \tag{2.11}$$

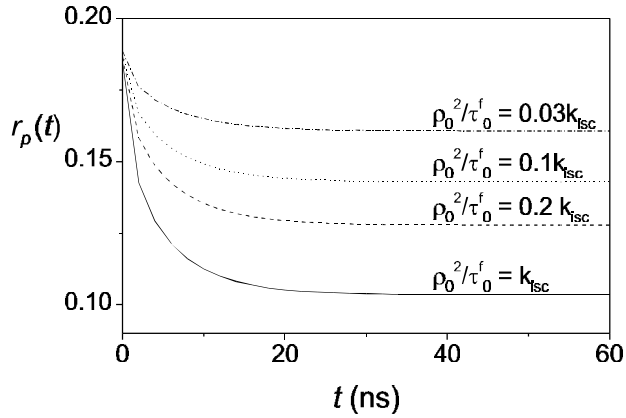

Figure 2.3 *Influence of ET on phosphorescence anisotropy for different values of the relative density* ρ_0*, taking* $1/k_{isc} = 5.4$ *ns.*

The value $r_p(t)$ decays to a plateau on the time-scale of $1/k_{isc}$. This is demonstrated in Figure 2.3, where the phosphorescence anisotropy has been calculated for different values of the relative density $\rho_0 = \frac{4}{3}\pi R_0^3\rho$.

Experimentally the phosphorescence anisotropy signal can only be captured a few hundred nanoseconds after the excitation pulse (see below). This experimental dead-time is in general much longer than $1/k_{isc}$, so $r_p(t)$ is effectively time-independent on the phosphorescence time-scale. Nevertheless, its value will be lower than the intrinsic value of $r_p(0)$. This consideration of the effect of ET on the observed phosphorescence anisotropy indicates that the experiment affords a route for determining the intersystem crossing rate. This however requires the independent determination of R_0, τ_f^0, and r.

2.3 Experimental

Sample preparation

Erythrosine B (EryB), 4'-5'dibromofluorescein (2Br) and 4'-5'diiodofluorescein (2I) were obtained from Aldrich Chemical c. inc. Eosin Y was obtained from J.T. Baker Chemicals B.V. All dyes (see Figure 2.4) were used without further purification.

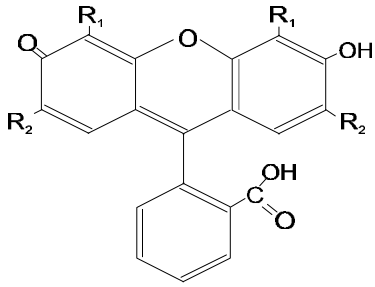

Figure 2.4 *Schematic molecular structure of EryB (R_1=I, R_2=I), 2I (R_1=I, R_2=H), Eosin (R_1=Br, R_2=Br), and 2Br (R_1=Br, R_2=H).*

dimethylsulfoxide (DMSO), *N*,*N*'-dimethylformamide (DMF), and ethanol of analytical grade purity were obtained from J.T. Baker Chemicals B.V. and used without further purification. Spectrophotometric grade glycerol was obtained from Aldrich Chemical co. inc. Completely hydrolyzed polyvinylalcohol (PVA) with an average weight of about 100 kD was obtained from Aldrich Chemical co. inc. and cleaned from side-products (acidic traces and residual acetyl groups) by the modified ethanol extraction method described by van Zandvoort *et al.*[7] Nitrocellulose (NC) powder was obtained from Wolff Walsroder A.G. and purified before use as described by van Zandvoort *et al.*[22]

Polymethylmethacrylate (PMMA) blocks were prepared as follows: Methylmethacrylate (MMA, Aldrich Chemical co. inc.) was washed free of stabilizer by pouring it over a column of neutral alumina. A concentrated stock

solution of dye molecules in DMF (10 mM) was added to 9.99 ml of MMA, followed by the addition of 0.5 mg 2,2'-azobis-(2-methyl-propanenitrile). This solution was deoxygenated for 10' with N_2 and sealed with parafilm. Next, the solution was incubated at 60 °C and then cooled at room temperature until totally polymerized. The polymerized solid was machined into a 0.9 cm x 0.9 cm x 2 cm block, polished and inserted in an optical cuvette, using glycerol for the optical contact.

A PVA solution in DMSO was prepared under nitrogen atmosphere by adding 0.5 g cleaned PVA powder to 6 ml DMSO and heating this mixture to 60 °C under continuous magnetic stirring until an optically clear solution was obtained. The PVA-DMSO solution was cooled down and then mixed with a small amount of an EryB stock solution in DMSO. A film was prepared by pouring the polymer solution onto a quartz plate. It was then dried in the dark for 24 hours at room temperature under a continuous nitrogen stream. The temperature was then increased to 60 °C for 3 days of further drying. In this way the DMSO was completely removed from the polymer film. This thorough drying procedure is crucial in order to immobilize the embedded dye molecules on the phosphorescence time-scale. The dried film was covered with a droplet of glycerol for optical contact and another quartz plate. Finally, the samples were sealed at the edges with glue and taped, leaving a small hole free for illumination.

The density of the PVA films was measured prior to experiments. The dimensions of a rectangular piece of film were measured with a micrometer and the weight was determined with an analytical balance. The thickness of the film was chosen so that its optical density was kept below 0.1 so as to avoid re-absorption effects. These parameters were then used to calculate the extinction coefficient.

Spectral measurements

The steady-state fluorescence excitation and emission anisotropy spectra were measured with a SLM-Aminco SPF 500 spectrofluorimeter equipped with an anisotropy module, using a 90° geometry. The detection wavelength for the excitation spectra was 565 ± 2.5 nm and the excitation wavelength for the emission spectra was 515 ± 2.5 nm. The correction factor (I_{HH}/I_{HV}), accounting for the difference in response of the detector to horizontally and vertically polarized light, was determined with a dilute EryB/glycerol solution.

Time-integrated fluorescence and phosphorescence spectra were measured on a Perkin Elmer LS 50 B luminescence spectrometer following the application of

an excitation light pulse. The spectra were corrected for the wavelength dependence of the response of the Hamamatzu R928 PMT. The delayed luminescence spectra ($I_{df} + I_p$) were collected using a delay time of 50 μs to screen off the fluorescence signals. A gate width of 20 ms was used to integrate over the full decay of the phosphorescence and delayed fluorescence. The time-integrated delayed luminescence spectra were corrected for the intensity decay during the experimental dead-time using the delayed luminescence lifetimes determined independently, see below.

Fluorescence spectra and phosphorescence spectra were recorded under identical conditions for direct comparison, although occasionally the fluorescence intensity was attenuated 100x times. The excitation and detection wavelengths were chosen so as to enable measurements of the entire emission or excitation spectrum. This was subsequently used for the calculation of the natural fluorescence lifetime and the Förster radius.

Time-resolved phosphorescence set-up

A Nd:YAG-laser (Continuum) running at 10 Hz was used as the excitation light source. The laser pulse was 6 ns long and may be considered a delta pulse on the microsecond time-scale used for signal capture. The second (532 nm) and third (355 nm) harmonics of the laser were used to excite the molecules in their visible and UV excitation bands. The power on the sample was kept as low as possible, in order to avoid saturation of the population of excited molecules.[23,24] The laser intensity was controlled using a liquid filter of a potassium bichromate solution and the setting of the laser Q-switch so as to keep it within the limits indicated by Peng and Barisas.[23]

The experiments were performed with a standard 90° set-up (see Figure 2.2). A vertically polarized laser beam was used for excitation. A Glen-Tayler prism was used to ensure that vertically polarized excitation light was incident on the sample. The sensitivity of the detection line for the polarization of the emission light was measured using a Soleil-Blodget adjustable quarter-wave plate. The slab-shaped film was placed with the normal to its plane at 45° to the incident beam. A sheet polarizer was used to select the polarization direction of emission light. An Omega interference filter (680 ± 10 nm) or an Omega edge filter (cut off frequency at 640 nm) was used for the spectral filtering of the phosphorescence light, depending on the intensity. An interference filter (542 ± 15 nm) was used to detect the delayed fluorescence.

Time-resolved phosphorescence experiments are often compromised by the instant scattering of the excitation light and fluorescence light, which is orders of

magnitude more intense than the phosphorescence. This initial light burst saturates the PMT. The saturation may be partially avoided by spectral filtering, on exploiting the red-shift of the phosphorescence spectrum relative to the fluorescence spectrum. Unfortunately this is often insufficient for avoiding the saturation of the PMT.[25,26] In order to overcome this problem, a home build gating device was incorporated in the bleeder circuit of the PMT, following the scheme of Ballard.[27] The device produces a 200 ns pulse of about 200 V over the first few dynodes of the PMT. Switching noise was reduced by a careful linking of the grounding. In this way the dead-time of the PMT was reduced to 300 ns. The output of the PMT was sampled with a Lecroy 9370 digitising oscilloscope capable of a maximal sampling rate of 500 Msamples/second. Consequently, every photon captured by the PMT following the gating pulse was detected. Sweeps containing up to $25 \cdot 10^3$ samples were summed, averaged, and stored on an internal memory card. Each experiment consisted on average of 2048 sweeps. The memory card was read by a PC every 256 sweeps. Low intensity signals were amplified with a Melles Griot (13 AMP 003). The captured signals were corrected for the response of the amplifier on the gating pulse.

2.4 Results

Spectral characteristics of eosin and erythrosine

Excitation spectra of eosin in glycerol (10 μM), PVA ($2 \cdot 10^{-7}$ moles/g), and PMMA (10 μM) are shown in Figure 2.5. The UV parts of the spectra are enlarged to emphasize the changes in the shape of the UV band. Going from PVA or glycerol to PMMA the two peaks of the UV band merge. The fluorescence anisotropy excitation spectrum is similarly affected, Figure 2.6. The anisotropy spectra of eosin in glycerol and PVA are virtually identical and strongly indicate that the UV band arises from a mixed transition. In marked contrast, the spectrum in PMMA is featureless. Interestingly, the visible band in PMMA is significantly lower than that in glycerol and PVA (0.33 vs. 0.36). The corresponding spectra of eosin in NC (not shown) follow those in glycerol and PVA. The spectra of EryB are found to be affected in the same way by the four matrices used. In view of these results we shall henceforth concentrate on the spectral properties of all four fluorescein derivatives in PVA and NC.

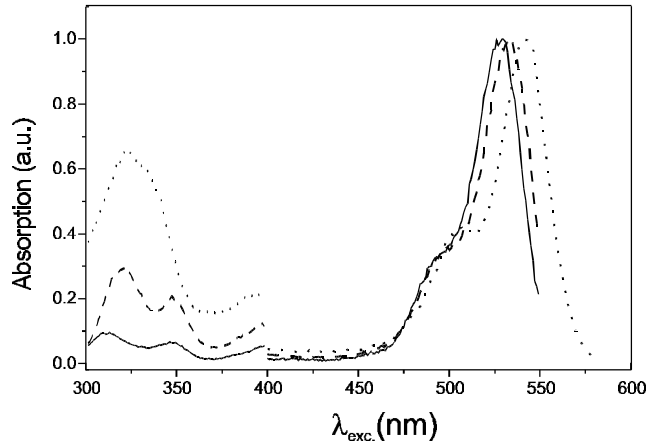

Figure 2.5 *Excitation spectrum for Eosin in PMMA (dotted), PVA (dashed), and glycerol (solid). The UV part of the spectrum is enlarged by a factor 3.*

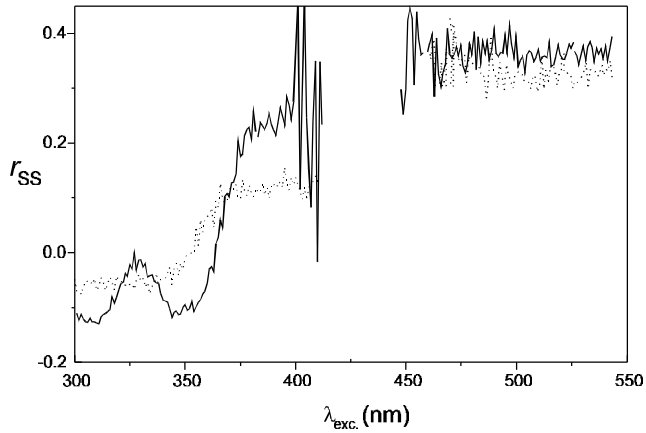

Figure 2.6 *Excitation anisotropy spectrum for Eosin in PMMA (dotted) and in glycerol cq. PVA (solid).*

Time-resolved Phosphorescence Anisotropy in polymer systems

A typical time dependence of the phosphorescence anisotropy is shown in Figure 2.7 for EryB embedded in 'wet' and 'dry' PVA films. Similar results were found for all the four fluorescein derivatives studied here. The ‘wet’ sample was dried at room temperature under a nitrogen atmosphere for two days. The dry sample was dried at 60 °C under a nitrogen atmosphere for three days. The experiments show beyond doubt that the drying procedure is crucial for the immobilization of the molecules on the phosphorescence time-scale. As can be seen from Figure 2.7, it is not straightforward to obtain the zero-time anisotropy in the case of the wet sample. The anisotropies of the delayed fluorescence were also determined on dried samples and found to coincide with the fluorescence anisotropies.

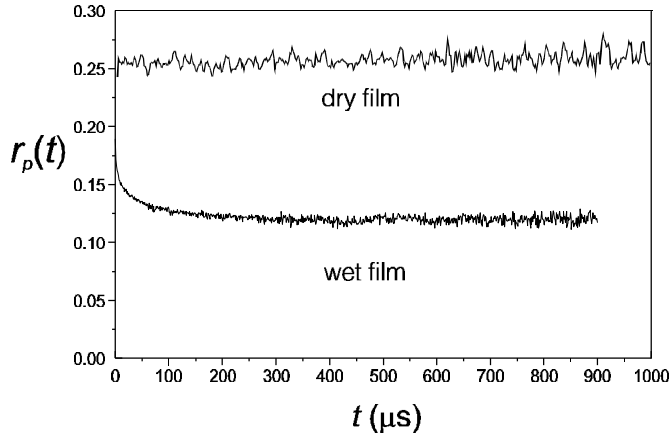

Figure 2.7 *Phosphorescence anisotropy decay of EryB in a wet PVA film (solid) and in a dry PVA film (dotted).*

[dye]·10^{-7} moles/g	1	2	5	10
r_p (EryB)	0.25	0.25	0.22	0.205
r_p (Eosin)	0.19 ± 0.01	0.19 ± 0.01	0.14 ± 0.01	0.13 ± 0.005

Table 2.1 *Influence of ET on the phosphorescence anisotropy (*$\lambda_{exc.}$*=532 nm).*

Optimal concentration and the influence of Energy Transfer on phosphorescence anisotropy

The optimal dye concentration was investigated in order to find a trade off between signal intensity and depolarization effects arising from energy transfer in the excited state (ET).[7,21] This was done by varying the concentration of eosin and erythrosine in the concentration range of $5 \cdot 10^{-8}$ to 10^{-6} moles/g and monitoring the phosphorescence anisotropy for excitation at 532 nm and emission at 680 nm. The phosphorescence anisotropy was found to be constant within the phosphorescence time-scale, though the value of the plateau decreased with concentration (see Table 2.1). Moreover, the phosphorescence lifetimes did not alter with increasing concentration. Since the spectral difference between the four fluorescein derivatives are marginal, we expect ET to affect their phosphorescence anisotropy in the same way.

The experiments indicate that dye concentrations of around $1 \cdot 10^{-7}$ moles/g are optimal for all four fluorescein derivatives.

Influence of heavy atom substitution on spectral properties

The excitation, delayed fluorescence, and phosphorescence spectra of the four fluorescein derivatives in PVA films are shown in Figure 2.8. The corresponding spectral parameters are given in Table 2.2. The differences found between the different molecules can directly be attributed to the influence of the heavy-atom substituents. As the fluorescence spectra and delayed luminescence spectra were obtained under identical conditions, the fluorescence, delayed fluorescence and phosphorescence quantum yields can be directly compared (Φ_f, Φ_{df}, and $\Phi_{p,}$ respectively). All spectra were taken at room temperature. The error margins in t_f^0 and R_0 are mainly determined by the relatively large error in the determination of the density of the films.

The measured fluorescence and phosphorescence lifetime and relative quantum yields are summarized in Table 2.3. The time-course of the fluorescence intensity of EryB and 2I was found to be better described by a double exponential decay than a single one. Therefore, the values given in Table 2.3 are the mean fluorescence lifetimes. We are now in a position to calculate the rates appearing in (2.2). The results are summarized in Table 2.4.

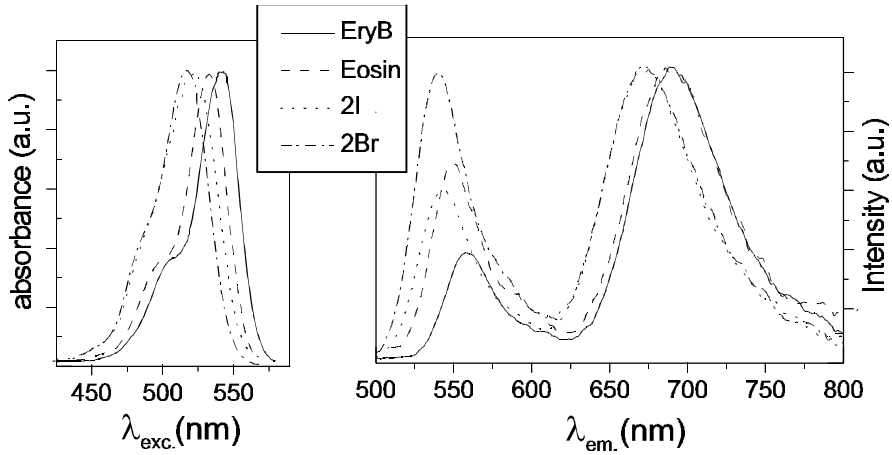

Figure 2.8 *Influence of heavy atom substitution on the absorption (left) and delayed emission (right) spectra of the four fluorescein derivatives.*

	$\lambda_{exc,max}$(nm)	$\lambda_{df,max}$(nm)	$\lambda_{p,max}$(nm)	f (10^{-8} s^{-1})	t^0_f (ns)	R_0(Å)
EryB	546 ± 1	558 ± 0.5	691 ± 2	4.6 ± 0.7	3.6 ± 0.2	57 ± 1
Eosin	534 ± 1	551 ± 2	686 ± 3	2.5 ± 0.7	3.7 ± 0.2	55 ± 3
2I	521 ± 2	544 ± 1	673 ± 1	3.2 ± 0.5	3.1 ± 0.2	53 ± 1
2I	517 ± 1	542 ± 2	670 ± 2	3.2 ± 0.7	3.6 ± 0.4	55 ± 3

Table 2.2 *Spectral properties of all four derivatives. The films were dried for 3 days at 60 °C and the dye concentration was 10^{-7} moles/g.*

dye	t_f (ns)	t_{df} (ms)	t_p (ms)	Φ_f/Φ_p	Φ_{df}/Φ_p
EryB	0.65 ± 0.10	0.67 ± 0.04	0.65 ± 0.04	9.4 ± 0.7	0.23 ± 0.002
Eosin	2.1 ± 0.08	4.0 ± 0.5	4.1 ± 0.4	165 ± 32	0.46 ± 0.005
2I	0.98 ± 0.04	0.98 ± 0.06	1.1 ± 0.2	18 ± 3	0.32 ± 0.03
2I	2.7 ± 0.05	7.4 ± 0.4	7.7± 0.5	304 ± 53	0.62 ± 0.01

Table 2.3 *Results from fluorescence and phosphorescence time-resolved measurements.*

	k_{qf} ($\cdot 10^8$ s^{-1})	k_{isc} ($\cdot 10^8$ s^{-1})	k_p (s^{-1})	k_{pq} ($\cdot 10^3$ s^{-1})	Φ_f	Φ_p ($\cdot 10^{-3}$)
EryB	1.6±1.5	11±1	41±3	1.46±0.12	0.18±0.03	19±3
Eosin	0.9±0.2	1.15±0.15	3.5±0.6	0.25±0.03	0.57±0.02	3.5±0.6
2I	0.8±0.8	6.3±0.8	19±2	0.63±0.09	0.31±0.03	17±3
2I	0.3±0.3	0.56±0.06	2.2±0.3	0.126±0.008	0.75±0.09	2.4±0.4

Table 2.4 *Determination of all relevant rates using (2.2).*

2.5 Discussion

Choice of Matrix

The ideal matrix for a spectroscopic study of dye molecules should not affect the properties of the embedded dye so that it is reasonable to assume that they are transferable to the dye in the system of interest, e.g. a protein or colloidal particle.[28] Moreover, the dye should be immobilized on the phosphorescence time-scale (micro- to milliseconds). In the past boric and sucrose glasses and PMMA matrices were used for this purpose.[3,5,6] However, these studies neglected the UV region of the spectrum where $S_0 \rightarrow S_2$ absorption band is found. We have shown above that PVA and NC systems are suitable for this purpose as they not only closely approximate the ideal requirements, but also allow measurements to be performed in the UV region of the spectrum.[29,8] This in contrast to PMMA. We note further that the PVA matrix was used earlier for phosphorescence studies.[30] The suitability of PVA and NC is not a general feature for all embedded probes and should always be checked prior to the experiment.[28]

The sample preparation method was found to be crucial for ensuring the quenching of the reorientational motions of the dye molecules on the phosphorescence time-scale. The time-resolved phosphorescence anisotropy experiments showed that complete immobilization is only reached after drying the films for three days at 60 °C under a nitrogen atmosphere.

Influence of Energy Transfer on phosphorescence anisotropy

The influence of radiationless singlet-singlet energy transfer on the phosphorescence anisotropy has in the past not been considered explicitly. We have shown in Table 2.1 that the phosphorescence anisotropy decreases when the dye concentration increases above $2 \cdot 10^{-7}$ moles/g, equivalent to 0.22 mM. It is thus necessary to include effects of energy transfer when analyzing phosphorescence depolarization experiments on samples exceeding this dye concentration.

We now note that values for the intersystem crossing rate k_{isc} can be extracted from both the rate equation (2.2) and the effects of ET on the phosphorescence anisotropy. The agreement between the values obtained in these two independent ways indicates the correctness of the approach used here.

	$k_{isc}(\cdot 10^8\ s^{-1})$ from (2.2)	$k_{isc}(\cdot 10^8\ s^{-1})$ from ET at $5 \cdot 10^{-7}$ moles/g	$k_{isc}(\cdot 10^8\ s^{-1})$ from ET at $1 \cdot 10^{-6}$ moles/g
Eosin	1.15 ± 0.15	1.2 ± 0.4	3.2 ± 0.8
EryB	11 ± 1	8 ± 4	16 ± 4

Table 2.5 *Comparison of intersystem crossing rate k_{isc} found by solving the rate equations or from the Energy Transfer treatment.*

The decrease of the phosphorescence anisotropy is related to the ratio of the intersystem crossing rate k_{isc} to the energy transfer probability (see (2.10)). Table 2.5 shows the intersystem crossing rates obtained by solving the rate equation (2.2) and from the phosphorescence anisotropy measurements at high concentrations (Table 2.1). The errors for the latter values were derived from the statistical uncertainties in the phosphorescence anisotropy experiments. The large error margins in the latter values of k_{isc} arise from their sensitivity to the exact value of the phosphorescence anisotropy. In both cases we found a good agreement between the values of k_{isc} extracted from the rate equation and from the ET measurements at $5 \cdot 10^{-7}$ moles/g. The values for k_{isc} obtained at 10^{-6} moles/g were too high. We may conclude that the phosphorescence anisotropy is not as low as expected from the ET treatment. This deviation can be attributed to the formation of so-called statistical pairs.[7] Statistical pairs are formed at high concentrations, where the intermolecular distance is sufficiently small to act as an excitation trap.

Influence of heavy-atom substitution on shape and position of the spectra

We have shown above that while the excitation energy is strongly influenced by the number of substituted heavy atoms, the Z number of the heavy atom is of less relevance. The Stokes-shift between the excitation and the fluorescence spectra is larger for 2I and 2Br than for eosin and EryB. We thus infer that the number and Z number of the substituted heavy atoms had no influence on the energy difference between the first excited singlet and the triplet state (ΔE_{S1-T1} = $22 \cdot 10^3$ cm^{-1}) in accord with theoretical predictions.[4,12] Heavy-atom substitution did not significantly change the spectral overlap between the excitation and fluorescence spectra and the extinction coefficients. Consequently, the same values of the Förster radius R_0 and τ_0 were found for all four molecules.

Interestingly, the delayed fluorescence peaks are red-shifted relative to the fluorescence peaks: 3 nm for EryB and 6 nm for the other derivatives. As this shift indicates an energy drop, it may well arise from losses during the prolonged residence in the excited state. This explanation is consistent with the observation of a smaller shift for EryB, which has the shortest delayed fluorescence lifetime.

Influence of heavy-atom substitution phosphorescence lifetime

It can be seen from equation (2.1) that the natural phosphorescence lifetime is expected to decrease linearly with the number of substituted heavy atoms. Experimentally we found that the phosphorescence lifetime decreases by a factor 2.2 ± 0.3 on the substitution of additional iodine atoms and by a factor 1.6 ± 0.3 on substituting two additional bromine atoms. The observed deviation from a factor 2 may well be caused by the difference in the strength of the interaction, which itself depends on the substitution site (see Figure 2.4REFMERGEFORMAT).

The dependence of the natural phosphorescence lifetime on the Z number of the substituted heavy atom is not immediately transparent. The observed natural phosphorescence lifetime was found to differ by a factor 12 ± 2 between derivatives containing 4 bromine and 4 iodine, and a factor 9 ± 1 between molecules with 2 bromine and 2 iodine atoms. This finding implies that the coupling factor ζ for iodine is a factor 3.0 to 3.4 bigger than for bromine. In contrast, a factor 2 was reported for naphthalene derivatives by McGlynn *et al.*[31] The coupling in fluorescein derivatives is thus demonstrably higher than in the naphthalenes and accounts for their relatively high phosphorescence quantum yield. The intersystem crossing rate and phosphorescence quenching rate follow

the same trend as the natural phosphorescence lifetime, as predicted earlier.[4]

Comparison with earlier studies

Previous spectroscopic studies of EryB and eosin were reported by Lam and Lo in gelatine and sol-gel matrices[5] and by Garland and Moore,[6] who used dye-protein complexes in deoxygenated buffers. The ratios of the fluorescence, phosphorescence, and delayed fluorescence quantum yield of EryB in a PVA matrix presented above are relatively lower than those found by Lam and Lo. The differences, however, are primarily due to the omission of k_{qf} in the analysis of the latter authors as well as the large spectral shift between the fluorescence maximum and phosphorescence maximum in the matrices they used. Importantly, our values for the phosphorescence quantum yields for eosin and EryB are in excellent agreement with those of Garland and Moore.

In addition, the advanced instrumentation used here, enabled the measurement of delayed fluorescence for weakly phosphorescent molecules such as eosin and 2Br. Experimentally, this meant that the instrumental response was determined and used in the data analysis. It is also important to stress that unlike Lam and Lo, we do not need to invoke bimolecular processes, such as triplet-triplet annihilation,[32] in the interpretation of the experiments. This is because we have taken care to avoid a too high dye concentration, the dyes were immobilized on the time-scale of the phosphorescence lifetime and we observed no decrease in phosphorescence lifetime with concentration.

Selection of dye molecule

The values of the zero-time phosphorescence anisotropies and lifetimes, enable us to choose a suitable dye molecule for time-resolved phosphorescence studies. In making this choice we need to consider factors such as the dynamic range of the phosphorescence anisotropy (r_P), its quantum yield (Φ_P), and its lifetime (t_P). This may be defined quantitatively in terms of the sensitivity of a dye molecule on time *t* after excitation, *S(t)*,

$$S(t) = r_P \cdot \Phi_P \cdot e^{-t/\mathrm{t}_P} . \qquad (2.12)$$

This quantity is plotted for the four fluorescein derivatives. Figure 2.9 can be used as a guide for the selection of the most suitable dye for an experiment sensitive to rotational dynamics on a given time-scale. Clearly, EryB is the most suitable dye for fast rotation on a time-scale of a few μs to 1.3 ms, while the

range of 2I is limited to between 1.3 and 1.9 ms. eosin is the most suitable dye for monitoring slow dynamics in the range of 1.9 to 8.8 ms and 2Br is effective for even slower motions. We note that for time-scales longer than 9 ms, the sensitivity is very small, so that high dye concentrations must be used. However, we have shown above that high dye concentrations may lead to loss of sensitivity due to the lowering of the zero-time phosphorescence anisotropy. One can also conclude that the commercially available dyes with a reactive group, eosin and EryB, in practice cover the whole regime of slow rotational motions.

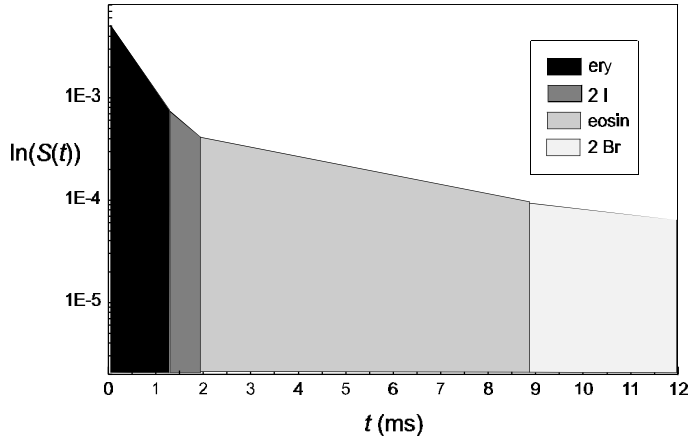

Figure 2.9 *The sensitivity ($r_P \cdot \Phi_P \cdot e^{-t/t_P}$) for the four fluorescein derivatives. EryB is the most sensitive in the first time-window, followed by 2I, eosine, and 2Br.*

2.6 Conclusions

We have here characterized the spectral properties of four phosphorescent dyes in a model system. The values of the zero-time phosphorescence anisotropies and lifetimes enabled us to formulate a quantitative measure for selecting a dye molecule for phosphorescence. Moreover, we have delineated the optimal concentration range of dye molecules for phosphorescence depolarization experiments.

The model systems of PVA-dye and NC-dye characterized above will be used in the following chapters for the determination of the directions of the transition dipole moments in the molecular frame.

Acknowledgements

We thank T.J. Cleij, department of Physical- Organical Chemistry University Utrecht, for the preparation of the PMMA blocks. Dr. E.L. de Beer, Department of Medical Physiology and Sports Medicine, University Utrecht, is thanked for the use of the Nd:YAG laser system.

References

[1] J.R. Lakowicz (1983), *Principles of Fluorescence Spectroscopy*, Plenum Press, New York
[2] R.A. Stein, R.D. Ludescher, S. Dahlberg, P.G. Fajer, L.H. Bennet, and D.D. Thomas (1990), *Biochemistry* **29**, 10023-10031
[3] R.D. Ludescher and Z. Liu (1993), *Photochem. and and Photobiol.* **58**, 858-886
[4] S.P. McGlynn, T. Azumi, and M. Kinoshita (1969), *Molecular spectroscopy of the Triplet state* Prentice-Hall, Inc.
[5] S.K. Lam and D. Lo (1997), *Chem. Phys. Let.* **281**, 35-43
[6] P.B. Garland and C.H. Moore (1979), *Biochem. J.* **183**, 561-572
[7] M.A.M.J. van Zandvoort, D. Wróbel, P. Lettinga, G. van Ginkel, and Y.K. Levine (1995), *Photochem. and Photobiol.* **62**, 279-289
[8] U.A. van der Heide, B. Orbons, H.C. Gerritsen, and Y.K. Levine (1994), *Eur. Biophys. J.* **21**, 263-272
[9] C.A. Parker in *Advances in Photochemistry* (1964), V.2 Interscience
[10] C. Orlandi and W. Siebrand (1981), *Chem. Phys. Let.* **80**, 399-403
[11] G.G. Giachino and D.R. Kearns (1970), *J. Chem. Phys.* **53**, 3886-3892
[12] M. Zander and G. Kirsch (1989), *Z. Naturforschung*, **44a**, 205-209
[13] C.A. Parker and C.G. Hatchard (1962), *J. Phys. Chem.* **66**, 2506-2520
[14] M. van Gurp, Y.K. Levine, and G. van Ginkel (1988), *J. Polym. Sci. B.* **26**, 1613-1625
[15] C. Zannoni , A. Arcioni, and P. Cavartorta (1983), *Chem. Phys. Lipids* **32**, 179-250
[16] Ph. Wahl (1983) in *Time-Resolved Fluorescence Spectroscopy in Biochemistry and Biology*, R. B. Cundall and R. E. Dale (Ed.) Plenum Press, New York, 483-522
[17] Th. Förster (1948**)**, *Ann. Phys.* **2**, 55-73
[18] M.D. Galanin (1955), *Sov. Physics-JETP.* **1**, 317-325.
[19] J. Knoester and J. E. van Himbergen (1984), *J. Chem. Phys.* **80**, 4200-4203
[20] J. Knoester and J. E. van Himbergen (1986), *J. Chem. Phys.* **84**, 2990-2997
[21] J. Baumann. and M.D. Fayer (1986), *J. Chem. Phys.* **85,** 4087-4107
[22] M.A.M.J. van Zandvoort, D. Wróbel, A.J. Scholten, D. de Jager, G. van Ginkel, and Y.K. Levine (1993), *Photochem. and Photobiol.* **58**, 600-606
[23] H. Peng and B.G. Barisas (1997), *J. of Fluorescence* **7**, 139-145
[24] J.R. Lakowicz, I. Gryczynski, V. Bogdanov, and J. Kusba (1994), *J. Phys. Chem.* **98**, 334-342
[25] J.R. Herman, T.R. Londo, N.A. Rahman, and B.G. Barisas (1992), *Rev. Sci. Instrum.* **63**, 5454-5458
[26] L. Yang, D. McStay, A.J. Rogers, and P.J. Quinn (1993), *Optical Engineering* **32**, 354-360

[27] S.G. Ballard (1983), *Rev. Sci. Instrum.* **54**, 1473-1475
[28] M.A.M.J. van Zandvoort, D.L.J. Vossen, G. van Ginkel, R. Torre, P. Bartolini, M. Ricci, J. Thomas-Oates, and H. Zuilhof *to be published*
[29] M.A.M.J. van Zandvoort, D. Wróbel, P. Lettinga, G. van Ginkel, and Y. K. Levine (1995), *Photochem. and Photobiol.* **62**, 299-308
[30] F. Dörr, J. Kern, and V. Zanker (1962), *Z. Naturforsch.* **17**, 93-111
[31] S.P. McGlynn, R. Sansuri, and N. Chroistodouleas (1962), *J. Chem. Phys.* **37**, 1818-1829
[32] B.P. Singh, G. Raindra Kumar, and K.K. Sharma (1995), *Chem. Phys. Let.*, **237**, 485-492

Chapter 3

The orientation of the fluorescence and absorption dipole moments of erythrosine B and eosin-5-maleimide within their molecular frame

Abstract

The absolute orientations of the absorption and fluorescence dipole moments in the frame of the molecule have been determined for erythrosine and eosin. This information is needed for an unequivocal interpretation of depolarization experiments on anisotropic systems. The orientations were recovered from angle-resolved fluorescence depolarization measurements on dye molecules macroscopically aligned in stretched polymer films. We found that the fluorescence dipole moment lies between the visible and UV absorption dipole moments for both molecules, eosin and erythrosine.

3.1 Introduction

Optical techniques have conveniently been used to study the orientational order and reorientational dynamics of dyes incorporated in biological systems.[1] Fluorescence depolarization experiments have been performed in the studies of dynamic processes in lipid membranes[2,3] and muscle fibers[4] on the nanosecond time scale. Phosphorescence depolarization studies were used to monitor the rotational dynamics of large membrane proteins on the micro- to millisecond time scale. As the systems are often not luminescent, they need to be tagged with an appropriate dye molecule. Thus, depolarization experiments on dye molecules only monitor the behavior of the system indirectly.

The depolarization effects arise from the change in the angle between the absorption dipole moment at the time of excitation and the emission dipole moment of the dye at the time of luminescence. This change is determined by three independent factors: 1) the overall orientation and reorientational dynamics

of the system; 2) the orientation and reorientational dynamics of the dye molecule relative to the system and 3) the orientation of the absorption and emission dipole moments in the molecular frame of the dye molecule. All the parameters describing these factors enter the analysis of the experimental data, but only those pertaining to factor 3 depend on the intrinsic properties of the dye. Knowledge of these latter parameters is a prerequisite for an unambiguous interpretation of the experimental data, especially for orientationally anisotropic systems.

The resolution of the different factors contributing to anisotropy has been addressed in studies on oriented systems as crossbridges in a muscle fiber[5] and in time-resolved anisotropy measurements on membrane systems.[6,7] It was shown that the difficulties in the analysis of depolarization experiments could be overcome if the orientation of the transition dipole moments in the frame of the dye was determined in a separate experiment. This is preferably done in an environment resembling the biological system under study as much as possible.

The orientation of the absorption and fluorescence dipole moments can be determined from the angle-resolved fluorescence depolarization (AFD) measurements. Here the steady-state fluorescence depolarization of dyes aligned macroscopically in stretched polymers[8,9,10,11] is measured under various angles. The orientations of the transition dipole moments of several molecules, including the two fluorescein derivatives eosin-5-maleimide[9] and 5-iodoacetamidotetramethylrhodamine,[10] have been determined in this way. Here we report an extension of the work to the determination of the orientations of the fluorescence transition dipole moments of erythrosine. This knowledge is necessary for the extraction of the phosphorescence dipole moment direction. The latter determination is the subject of the next chapter.

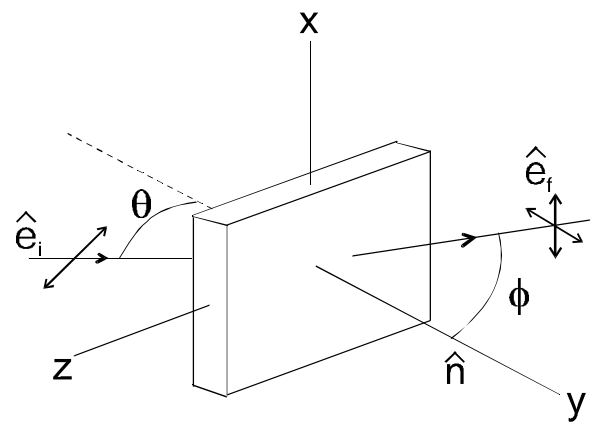

Figure 0.1 *Schematic view of the set-up used in AFD experiments on flat samples. The incoming light is horizontally polarized ($\hat{e}_i$), while the emitted light is detected, either in horizontal or vertical polarization direction ($\hat{e}_f$). The stretching direction of the film is positioned along the y-axis.*

3.2 Theory

The orientation of the transition dipole moments in the molecular frame can be determined applying the AFD method,[8,9] whose geometry is shown in Figure 3.1. In this experiment, the dyes are macroscopically aligned and immobilized in a stretched polymer film and illuminated with horizontally polarized light (*H*) under different angles of incidence, θ. The intensity of horizontally (*H*) and vertically (*V*) polarized fluorescence light is detected again on varying the detection angle, ϕ. Under these experimental conditions the fluorescence intensities I_{HH} and I_{HV} and their ratio $R_e(=I_{HV}/I_{HH})$ are given by the following expressions:[6,12]

$$\begin{aligned} I_{HV} &= (k/9)\cdot(1+2S_m - S_n - 2G_0 - 3(S_n - G_0 + G_2)\sin^2\theta) \\ I_{HH} &= (k/9)\cdot(1+2S_m + 2S_n + 4G_0 - 3(S_m + 2G_0)\sin^2\theta - (S_n + 2G_0)\sin^2\phi \\ &\quad 3(3G_0 + G_2)\sin^2\theta\sin^2\phi - 3G_1\sin 2\theta\sin 2\phi) \end{aligned} \qquad (3.1)$$

The terms in this expression have the following meaning:

I_{IF} the intensity of the fluorescence light with polarization direction F, on exciting the sample with a light beam with polarization direction I (see also Figure 0.1).

k a constant determined by the excitation light intensity and the probe concentration and illuminated volume.

$$S_m = \sum_{i=-2}^{2} \left\langle D_{0i}^{2}(\Omega_{sm}) \right\rangle D_{i0}^{2}(\Omega_m) \tag{3.2}$$

$$S_n = \sum_{j=-2}^{2} \left\langle D_{0j}^{2*}(\Omega_{sm}) \right\rangle D_{jo}^{2*}(\Omega_n) \tag{3.3}$$

$$G_k = \sum_{i,j=-2}^{2} \left\langle D_{kj}^{2*}(\Omega_{sm})\, D_{ki}^{2}(\Omega_{sm}) \right\rangle D_{j0}^{2*}(\Omega_n)\, D_{i0}^{2}(\Omega_m) \tag{0.4}$$

$D_{mn}^{L}(\Omega)$ Wigner rotation matrix elements.[13]

Ω_μ $(\alpha_\mu,\beta_\mu,\gamma_\mu)$ The set of Euler angles of the absorption dipole moment in the molecular frame shown in Figure 3.2.

Ω_ν $(\alpha_\nu,\beta_\nu,\gamma_\nu)$ The set of Euler angles of the emission dipole moment in the molecular frame shown in Figure 3.2.

$\langle X_{sm} \rangle$ The ensemble average $\int d\Omega_{sm} f(\Omega_{sm}) X(\Omega_{sm})$ of $X(\Omega_{sm})$ over the orientational distribution function $f(\Omega_{sm})$.

$f(\Omega_{sm})$ The orientational distribution function of the dye molecules relative to the stretch direction.

Equation (3.1) expresses the separation of the geometrical factors q and f, dictated by the experimental set-up, in the molecular properties, the order parameters S_m and S_n, and the correlation functions G_k. The correlation functions are related to the anisotropy by

$$r = 0.4 \sum_{k=-2}^{2} G_k \tag{3.5}$$

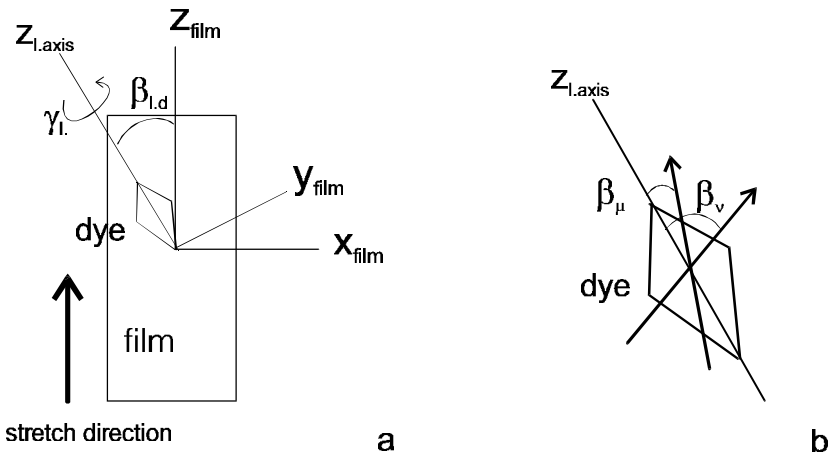

Figure 3.2 *Two independent orientations determine the polarization for a probe embedded in a polymer film: a) the orientation of the dye molecule relative to the director of the film.* $z_{l.\,axis}$ *is the inertial axis of the dye.* γ *gives the internal rotation of the molecule around this long axis and* $\beta_{l.\,d}$ *gives the angle between the inertial axis of the dye and the director of the film. b) the orientation of the transition dipole moments relative to the inertial axis of the dye, where the index of the angles represents the transition dipole moment.*

In the following we will limit ourselves to the case of quenched reorientational motions, since in polymer films the probes are immobilized on the fluorescence time-scale. We shall also assume the orientational distribution of the pigments in the polymer matrix to be either isotropic (unstretched film) or uniaxially symmetric around the stretch direction (stretched film).[8,12] Note that for these two cases $G_k = G_{-k}$. Equation (3.1) indicates that the AFD experiment yields a maximum of 5 independent parameters, S_m, S_n, G_0, G_1, and G_2. These experimental parameters contain all the accessible molecular information. The question arising now is how to extract the orientational distribution function and directions of the transition dipole moments from the 5 experimental parameters.

EryB and E5M consist of a planar chromophoric xanthene system, to which a phenyl ring is attached. The ring is twisted by 90 degrees relative to the plane of the xanthene rings.[14] The absorption and fluorescence dipole moments are thus expected to lie in the xanthene plane. Thus the absorption and fluorescence dipole moments are fully defined by the Euler angles β_μ and β_ν with the long axis of the chromophoric plane. For films stretched uniaxially along the Z-axis, the distribution of the planar pigments is invariant under rotations around this axis. Therefore the orientational distribution possesses mirror-symmetries in the

XY- and the XZ-plane of the film and, moreover, is invariant to reflections in the xz- and the yz-planes of the molecular frame. The orientational information in the experimental parameters (S_m, S_n, G_0, G_1 and G_2) can now be expressed in terms of only 5 order parameters: [8,13] $\langle P_2 \rangle = \langle D^2_{00} \rangle$, $\langle P_4 \rangle = \langle D^4_{00} \rangle$, $\langle D^2_{02} \rangle$, $\langle D^4_{02} \rangle$, and $\langle D^4_{04} \rangle$.

As we need two angles to describe the orientation of the transition moments, there are in total seven parameters to be extract from the five experimentally available parameters S_m, S_n, G_0, G_1, and G_2. We shall now assume that the order parameters $\langle P_2 \rangle$, $\langle P_4 \rangle$ and $\langle D^2_{02} \rangle$ are the most significant. The smoothest possible orientational distribution function $f(\Omega_{sm})$ consistent with them may now be reconstructed with the maximum entropy formalism (Levine and Bernstein[15]) given by van Gurp *et al*:.[6]

$$f(\Omega_{sm}) = A \cdot e^{\lambda_2 P_2(\Omega_{sm}) + \lambda_4 P_4(\Omega_{sm}) + \varepsilon [D^2_{02}(\Omega_{sm}) + D^2_{0-2}(\Omega_{sm})]} \tag{3.6}$$

In this equation A is a normalization constant. λ_2, λ_4 and ε are variables whose values are uniquely related to the three order parameters. Any order parameter $\langle X \rangle$ can be calculated from this equation with the above expression, since $\langle X \rangle = \int d\Omega_{sm} f(\Omega_{sm}) X(\Omega_{sm})$. This approach now expresses the five experimental parameters S_m, S_n, G_0, G_1, and G_2 in terms of the three variables (λ_2, λ_4, and ε) and the two angles β_μ and β_ν, defining the orientation of the transition dipole moments relative to an in-plane axis of the molecular ring, (3.2) to (3.4).

3.3 Experimental

Sample preparation

EryB was obtained from Sigma Chemical Co. and used without further purification. *N,N'*-dimethylformamide (DMF) and ethanol of analytical grade purity were obtained from J.T. Baker chemicals B.V. and used without further purification. Spectrophotometric grade glycerol was obtained from Aldrich Chemical c. inc. Nitrocellulose (NC) powder was obtained from Wolff Walsroder A.G. and purified before use as described by van Zandvoort *et al*.[16]

A NC solution in DMF was prepared under nitrogen atmosphere by adding 0.8 g NC to 6 ml DMF and stirring this mixture at room temperature until an optically clear solution was obtained. The desired amount of an EryB stock solution in DMF was added and the resulting solution homogenized. The

concentration of dye in the polymer film was $2 \cdot 10^{-7}$ moles/g. This concentration was chosen in order to minimize energy transfer processes.[10]

Films for the AFD measurements were prepared by pouring out a NC solution on a glass plate and drying it in the dark for 40 hours under a continuous nitrogen stream. A rectangular piece of film was cut and put in a homemade stretching bank and placed in a desiccator under saturated DMF vapor for about 30 minutes. The film was then stretched to at least twice its original length. A piece was cut from the center, dried, and placed between quartz plates using glycerol to improve optical contact. Finally, the sample was sealed at the edges with glue and taped, leaving a small hole free for illumination. The refractive index of stretched NC films was measured with an Abbe-refractometer and found to be 1.52 ± 0.02 with a birefringence within the experimental error.

The uniaxiality of the stretched NC films was checked previously by us,[17] using the methods described in.[12,18] The spectral properties and zero-time anisotropy of the dye were tested prior to the AFD experiment. It appeared that the spectral properties were the same for PVA and NC as host matrix, implying that measurements performed on NC films can be correlated with measurements performed on PVA films (see chapter 2).

Steady-state angle resolved fluorescence depolarization

Steady-state AFD experiments were carried out on the set-up as described by van Gurp *et al.*[12] The excitation light was selected to be either 338 nm or 528 nm. The 338 nm wavelength was selected with an 338 ± 10 nm interference filter and two broadband filters. The 528 nm wavelength was selected with a 528 ± 5 nm interference filter and a 540 low-pass filter. The excitation light was polarized with a horizontally aligned Glan-Taylor prism. The emission light was detected through a 573 ± 5 nm interference filter and a GG560 cut-off filter. The horizontally and vertically polarized emission light was detected using a sheet polarizer. Polarization ratios were determined for 63 different angles of excitation and emission. The correction factor (I_{HH}/I_{HV}) reflecting the difference in response of the emission line to horizontally and vertically polarized light, was determined on the same set-up in a 90° set-up using a dilute solution of EryB in ethanol.

Data analysis

The 126 polarization ratios obtained for both wavelengths were analyzed simultaneously with a Global target approach using a non-linear least squares Marquard (ZXSSQ) procedure from the IMSL library. The values for λ_2, λ_4 and ε were allowed to vary, while the value for β_v was kept fixed.[9] The difference angles, β_v-β_μ, between absorption dipole moments and the emission dipole moment were kept fixed at the values determined by the anisotropy measurement at the two wavelengths of excitation. The sign of the difference angle was left as a variable since the anisotropy is determined by cos (β_v-β_μ). In this way the χ^2 minima were found for a sequence of fixed values of β_v.

Calculation of molecular structure

The molecular structures where drawn in ChemOffice (CambridgeSof Corporation, Cambridge, MA 02139, USA; ChemDraw version 4.0/Chem3D version 4.5, 1997) and pre-optimized with MM2 force field implemented in this program. Subsequently, the geometry was fully optimized via PM3 computations.[19] The resulting geometry was verified to correspond to real minima on the potential energy surface via computation of the vibrational frequencies. These computations were performed on a Silicon Graphics R10000 O2 computer using MOPAC 93 [20] and MOPAC 97 programs within ChemOffice. The species were placed in a dielectric continuum with epsilon=1, mimicking the polymer, using the COSMO method.[21]

The results of the molecular structure calculations were used to calculate the positions and eigenvalues of the inertial axes in the molecular frame.

3.4 Results

Molecular structure calculations

The principal moments of inertia of E5M and EryB were calculated from the positions of the atoms obtained from the structure calculations, Figure 3.3. The eigenvalues of the moment of inertia matrices (shown in brackets) and the corresponding eigenvectors were found to be

EryB:

$$I_1(12.4) = \begin{pmatrix} 0.998 \\ 0.03 \\ -0.049 \end{pmatrix}, I_2(6.958) = \begin{pmatrix} -0.046 \\ 0.93 \\ -0.364 \end{pmatrix}, I_3(0.517) = \begin{pmatrix} 0.034 \\ 0.366 \\ 0.93 \end{pmatrix}.$$

E5M:

$$I_1(6.27) = \begin{pmatrix} -0.989 \\ 0.151 \\ -0.004 \end{pmatrix}, I_2(9.149) = \begin{pmatrix} 0.056 \\ 0.997 \\ 0.058 \end{pmatrix}, I_3(1.624) = \begin{pmatrix} -0.016 \\ -0.057 \\ 0.998 \end{pmatrix}$$

It can be seen from Figure 3.3 that the xanthene ring structure of both molecules is planar. The molecules effectively possess two equivalent principal moments of inertia, I_1 and I_2, consistent with the assumption of a D_{2h} used in the theoretical section. The main difference between E5M and erythrosine is the interchange of the principal axis due to the presence of the maleimide group in E5M.

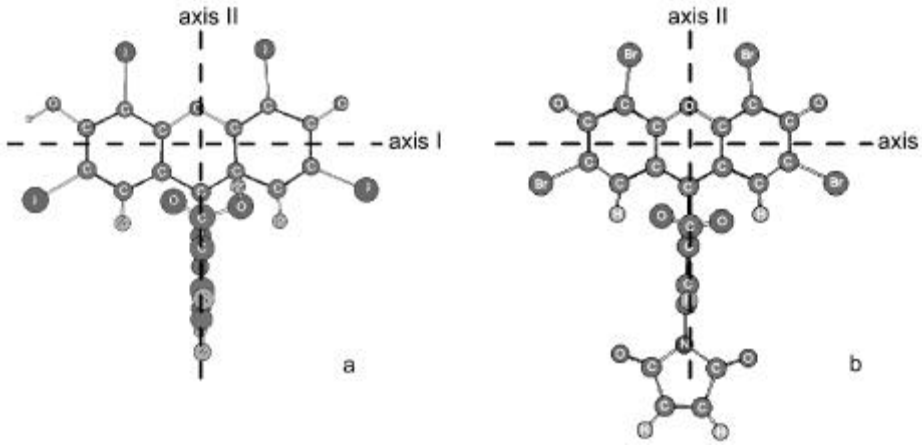

Figure 3.3 *The computed structures of EryB (a) and E5M (b).*

AFD results for Erythrosine B

AFD measurements were performed on EryB in NC film (concentration $2 \cdot 10^{-7}$ moles/g), stretched to three times its original length. The polarization ratios were measured at 63 different angle combinations. Each film was excited in two absorption bands, while the fluorescence was detected at one emission wavelength. Thus, for each film two data sets of 63 points were acquired. The two data sets were fitted simultaneously to the same orientational distribution function. The number of adjustable parameters was reduced by systematically varying the angle characterizing the emission dipole moment, β_ν , and constraining the two difference angles $\Delta\mu = \beta_\nu - \beta_\mu$ to the region indicated by the anisotropy experiments, chapter 2. The analysis was carried out for both positive and negative values of $\Delta\mu$.

Figure 3.4 shows two profiles of χ^2 vs. β_ν, one for $\beta_{\mu,528} < \beta_\nu < \beta_{\mu,338}$ and the other for $\beta_\nu < \beta_{\mu,528} < \beta_{\mu,338}$. Solutions were found from the minima in the χ^2 surface. It can be clearly seen that the χ^2 surface in the latter case was consistently higher than for the former and consequently this solution region was not considered further. The solutions for $\beta_{\mu,528} < \beta_\nu < \beta_{\mu,338}$ are given in Table 3.1, and the corresponding orientational distribution functions are shown in Figure 3.5. The error margins in the values of the adjustable variables were estimated from the width of the minimum of the χ^2 profile. The main features of the orientational distribution functions were unaffected within these error margins.

	1	2	3	4
χ^2	2.10	2.24	2.21	2.40
λ_2	-1.7 ± 0.5	0.6 ± 0.03	3 ± 1	-3 ± 1
λ_4	2.0 ± 0.5	-1.0 ± 0.04	1.0 ± 0.5	-3 ± 1
ε	0.0 ± 0.05	-0.6 ± 0.03	-4 ± 2	-0.1 ± 0.05
β_ν	117 ± 3	163 ± 3	213 ± 3	258 ± 3

Table 3.1 *Results of the AFD experiments on EryB in a stretched NC film (3x its original length, $2 \cdot 10^{-7}$ moles/g). $\beta_{\mu,528} = \beta_n - 13°$ and $\beta_{\mu,338} = \beta_n + 54°$. The error margins are estimated from the width of the χ^2 minimum.*

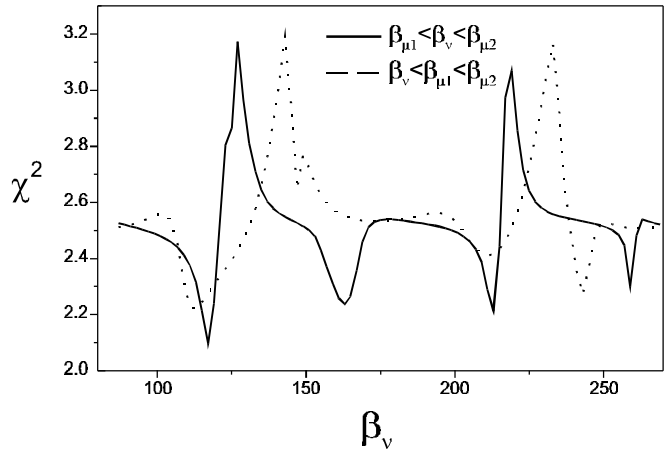

Figure 3.4 *The* c^2 *profiles of the AFD-fit for EryB in stretched NC film for four relative orientations of the absorption and fluorescence dipole moments.*

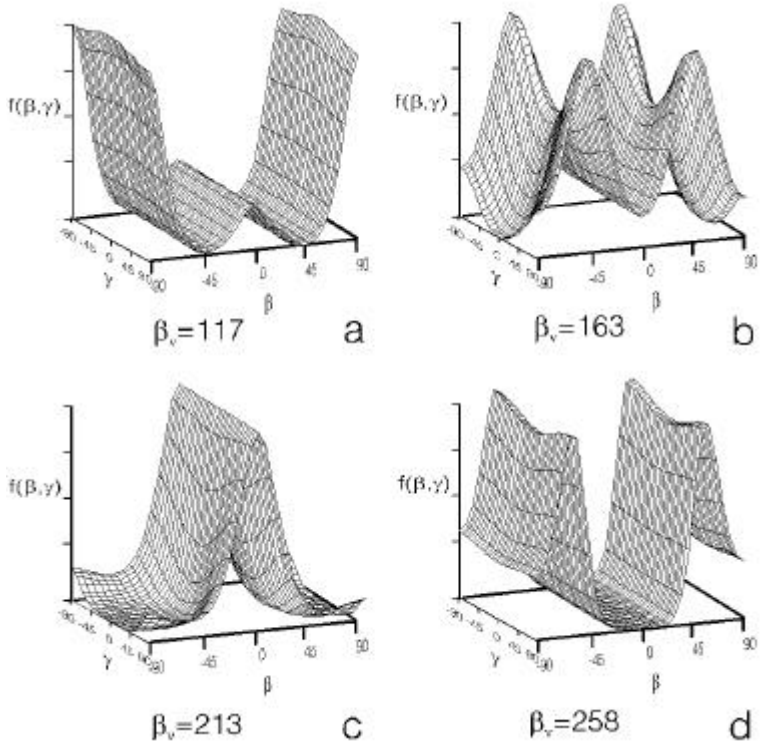

Figure 3.5 *Orientational distribution functions describing the orientation of EryB in a stretched NC film. The functions a) to d) belong to the solutions 1 to 4 as given in Table 3.1.*

AFD results for E5M

In view of the results presented above for EryB, where the solution region $\beta_{\mu,528}<\beta_{v}<\beta_{\mu,338}$ yielded a lower χ^2 surface than the $\beta_{v}<\beta_{\mu,528}<\beta_{\mu,338}$ region, we have re-examined the AFD experiments on E5M in PVA films reported earlier by van der Heide *et al.*[11] The analysis of the results was carried out in an analogous way to that described above for EryB. In doing this we selected three data sets using excitations at 330 nm, 345 nm and 518 nm, as these correspond to three distinctly different values for the anisotropy, Figure 2.6. Now the solution region $\beta_{\mu,345}<\beta_{\mu,330}<\beta_{v}<\beta_{\mu532}$ was found to exhibit the lowest χ^2 surface (Figure 3.6). Nevertheless, we note that the results are relatively insensitive to the relative values of $\beta_{\mu,330}$ and β_{v} as $\beta_{\mu,330}$ lies near 54.7°. The solutions are shown in Table 3.2 and the corresponding orientational distribution functions are given in Figure 3.7. We note that van der Heide *et al.* only considered solutions whereby $\beta_{v}<\beta_{\mu,x}$.

	1	2	3	4
χ^2	1.95	0.95	3.54	0.95
λ_2	0.34 ± 0.02	1.5 ± 0.5	-0.3 ± 0.2	6 ± 2
λ_4	-1.7 ± 0.3	0.32 ± 0.05	-0.6 ± 0.3	0.26 ± 0.04
ε	0.04 ± 0.03	3 ± 2	0.14 ± 0.03	7 ± 2
β_v	106	165	214	255

Table 3.2 *Results of the AFD experiments on E5M in a stretched PVA film (3x its original length, concentration $2\cdot10^{-7}$ moles/g).* $b_{m518} = b_n - 22°$, $b_{m330} = b_n + 60°$ *and* $b_{m345} = b_n + 64°$. *The error in the angles is 3°. The error margins are estimated from the width of the* c^2 *minimum.*

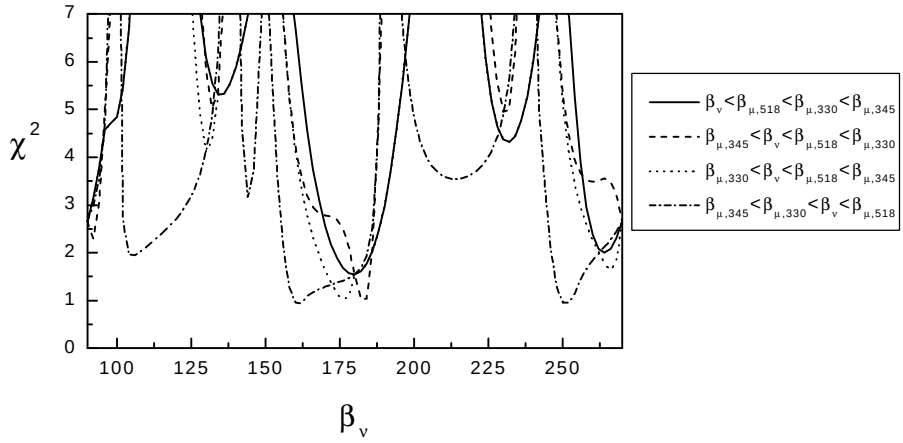

Figure 3.6 *The c^2-profiles of the AFD-fit for E5M in stretched PVA film for four relative orientations of the absorption and fluorescence dipole moments.*

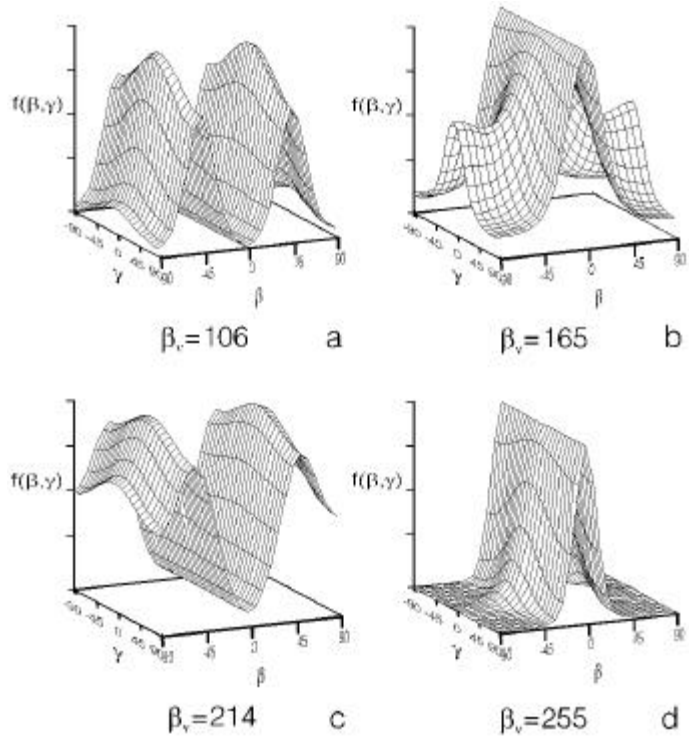

Figure 3.7 *Orientational distribution functions describing the orientation of E5M in a stretched PVA film. The functions a) to d) belong to the solutions 1 to 4 as given in Table 3.2.*

3.5 Discussion

The numerical analysis of the AFD experiment searches for the best fit of the observed depolarization ratios by looking at combinations of molecular orientational distribution functions $f(\beta,\gamma)$ of the molecular frame and orientations of the absorption and emission dipole moments relative to the long axis of that frame. The search procedure is only constrained by the imposed symmetry of the molecular structure. Thus, the analysis can yield different forms for $f(\beta,\gamma)$ all conforming to the imposed symmetry, but not all describing physical situations. Each orientational distribution function yields a similar set of angles describing the direction of the dipole moments relative to the presumed long molecular axis. This is because effectively the different solutions simply describe a mathematical choice for the alignment of the long molecular axis in the sample. Knowledge of the principal moments of inertia of the molecule enables now the selection of physically acceptable orientational distribution functions in the film. Given this choice, the directions of the moments relative to the principal inertial axis of the molecule can be assigned.

It was shown above that both EryB and E5M behave to a good approximation as elongated planar molecules with D_{2h} symmetry. For this reason we expect the molecules to align with their long axis along the stretch direction of the film and/or perpendicular to it. Thus the functions $f(\beta,\gamma)$ should only exhibit local and/or global maxima for β = 0 and 90°. Functions exhibiting maxima at intermediate angles, which correspond to a collective molecular tilt, can be excluded a priori.

There remains, however, degeneracy in the solutions regarding the relative orientations of the three dipole moments. Does the emission dipole moment lie between the two absorption moments, $\beta_{\mu,528}<\beta_{\nu}<\beta_{\mu,338}$, or does it lie to one side, $\beta_{\nu}<\beta_{\mu,528}<\beta_{\mu,338}$? In the following discussion we shall address this problems.

Selection of physical orientational distributions for the inertial axis of EryB

The calculations of the molecular structure of EryB show that the molecule possesses a principal inertial axis (axis I in Figure 3.8), which is oriented within 3° of the long axis of the xanthene ring structure, and a second principal axis perpendicular to axis I. The eigenvalue belonging to axis I is a factor two higher than the eigenvalue belonging to axis II. Thus, upon stretching the polymer film, we expect the embedded dye to align either with axis I or axis II along the polymer chains. This situation corresponds to an orientational distribution

function exhibiting maxima at $\beta = 0$ and 90°. This expectation is borne out in two of the orientational distribution functions depicted in Figure 3.5. The distribution function belonging to solution c has a clear maximum around $\beta = 0°$, while small wings at $\beta = \pm 90°$, $\gamma = \pm 90°$. This implies that in this case the molecular z-axis is chosen so as to preferentially align parallel to the stretching axis, while a small probability remains for the orientation of this axis perpendicular to the stretching direction. It is thus reasonable to identify it with the inertial axis with the highest eigenvalue, axis I. The angles of the transition dipole moments belonging to solution c thus refer to axis I. The solution indicated in Figure 3.5 a, corresponds to the choice of axis II as the molecular z-axis. The orientational distribution function of the z-axis belonging to solution a can indeed be related to the orientational distribution function of the z-axis belonging to solution c by a rotation of the axis by 90 degrees. The two solutions b and d, whose orientational distribution functions peak around 45 degrees, reflect a collective tilt of the molecules and can thus be discarded as non-physical.

Relative orientation of fluorescence and absorption dipole moments of EryB

As indicated in the section Results, solutions were found for $\beta_{\mu,528}<\beta_{\nu}<\beta_{\mu,338}$ as well as for $\beta_{\nu}<\beta_{\mu,528}<\beta_{\mu,338}$. However, some features of both types of solutions were clearly different. These differences will enable us to make a choice between them. The most important difference is that the χ^2 of the $\beta_{\mu,528}<\beta_{\nu}<\beta_{\mu,338}$ solutions is lower than the χ^2 of the $\beta_{\nu}<\beta_{\mu,528}<\beta_{\mu,338}$ solutions. Given the absence of conspicuous outliners and the fact that every experimental point contributes fairly equally to the value of χ^2, we believe that the solution region $\beta_{\mu,528}<\beta_{\nu}<\beta_{\mu,338}$ should be preferred. This choice will be further justified below when we consider the absolute directions of the moments in the molecular frame.

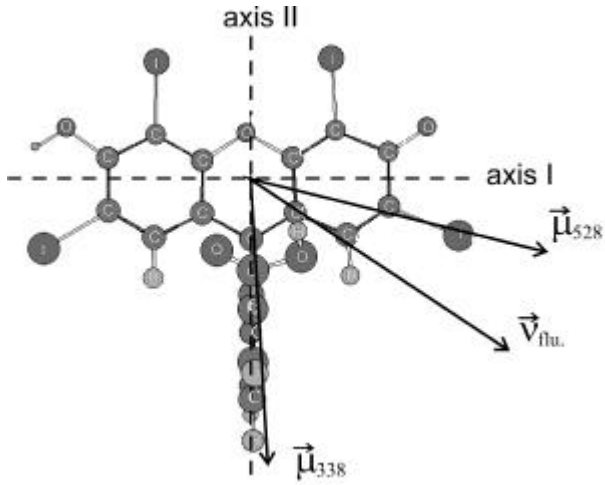

Figure 3.8 *Calculated structure of EryB, with inertial axes indicated. The orientations of the transition dipole moments within the molecular frame, as deduced from AFD and TPA experiments, are given by the arrows.*

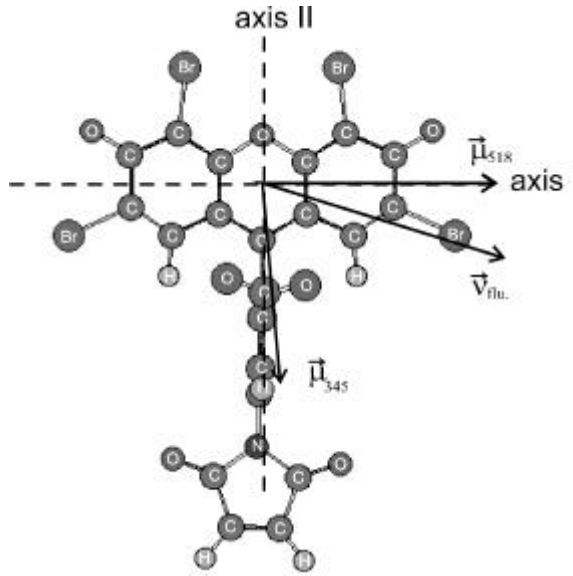

Figure 3.9 *Calculated structure of E5M, with inertial axes indicated. The orientations of the transition dipole moments within the molecular frame, as deduced from AFD and TPA experiments, are given by the arrows.*

Absolute orientation of the transition dipole moments within the molecular frame of EryB

Given the orientational distribution functions of solutions a and c above and the structural calculations, the transition dipole moments can be placed within the plane of the xanthene ring system. In doing this we shall neglect the small effect of the pendant phenyl ring on the electronic properties of the xanthene chromophore. Taking now our preferred solution $\beta_{\mu,528}<\beta_{v}<\beta_{\mu,338}$, we find that the S_0-S_1 dipole moment $\vec{m}_{532}$ is tilted 20 ± 5° away from the axis I of the xanthene ring structure. The fluorescence dipole moment $\vec{n}_{flu}$ is tilted 33 ± 5° from this axis. The errors in the angles are estimates based on differences in measurements on different samples. The finding that $\vec{m}_{532}$ and $\vec{n}_{flu.}$ are not parallel is not surprising and similar observations have been reported for other molecules.[9,22,23] A quantum mechanical discussion of this can be found in reference 2. The orientation of the effective 338 nm absorption dipole moment $\vec{m}_{338}$ is -3 ± 5° from the short axis of the xanthene part (axis II). The angle between the two absorption dipole moments, $\Delta\mu$ (= $\beta_{\mu,532}$ - $\beta_{\mu,338}$), is 68°. The fact that the two absorption dipole moments lie so close to the principal inertial axis supports our choice for the solution with $\beta_{\mu,338}<\beta_{v}<\beta_{\mu,528}$. Since the anisotropy at 338 nm is about the same as the anisotropy at 355 nm, we believe that the effective dipole moment at 355 nm has essentially the same orientation as the 338 nm dipole moment. The results are summarized in Figure 3.8.

Absolute orientation of the transition dipole moments within the molecular frame of E5M

The determination of the directions of the dipole moments in E5M follows the procedure described above for EryB. Here we have an extra degeneracy to consider, because we use three instead of two excitation wavelengths. Figure 3.6 shows that the solution $\beta_{\mu,345}<\beta_{\mu,330}<\beta_{v}<\beta_{\mu532}$ has the lowest overall χ^2 profile, i.e. better than the solutions where $\vec{m}_{330}$ or $\vec{m}_{345}$ are positioned on the same side of $\vec{n}_{flu.}$ as $\vec{m}_{528}$.

The main difference between EryB and E5M is the maleimide group, which is attached to the phenyl group of eosin. In contrast to EryB, the eigenvalue belonging to axis I is now a factor 1.5 smaller than the eigenvalue belonging to axis II. Using a similar reasoning as used for EryB, we relate the z-axis belonging to solution d (see Figure 3.7) to axis II, because for this solution a population is found around 0 degrees. This implies that axis II, which is oriented

at 90 degrees from axis I, is the main orientational axis. With this choice of axis we find that the S_0-S_1 dipole moment $\vec{m}_{518}$ is oriented parallel (0 ± 5°) to axis I of the xanthene ring structure and that the fluorescence dipole moment $\vec{n}_{flu}$ is directed 22 ± 5° from this axis. The two UV absorption dipole moments make angles of 77° ($\vec{m}_{330}$) and 81° ($\vec{m}_{345}$) with this axis. The results are depicted in Figure 3.9.

A consequence of our choice of the relative directions of the dipole moments is that $\vec{m}_{518}$ lies close to the long axis of the xanthene ring. This contrasts with the choice of van der Heide *et al.*[9] which assigns $\vec{n}_{flu}$ to this direction. The main reason for this difference is that the latter authors took the emission dipole moment to lie to one side of the absorption dipole moments.

3.6 Conclusions

We have here shown how the directions of the absorption and fluorescence dipole moments of EryB and E5M can be obtained from AFD experiments on molecules embedded in polymer matrices in a reliable way. In particular, we have demonstrated that the relative orientation of the dipole moments is $\beta_{\mu,528}<\beta_{\nu}<\beta_{\mu,338}$ for EryB and $\beta_{\mu,345}<\beta_{\mu,330}<\beta_{\nu}<\beta_{\mu,518}$ for E5M. This information is a prerequisite for the determination of the direction of the phosphorescence emission dipole moment described in the following chapter.

Acknowledgements

Han Zuilhof, Department of Biomolecular Science, Wageningen Agricultural University, is thanked for the calculations of the molecular structures.

References

[1] J.R. Lakowicz (1983) *Principles of Fluorescence Spectroscopy*, Plenum Press, New York.

[2] Y.K. Levine and G. van Ginkel (1994) in *The Molecular Dynamics of Liquid Crystals*, G.R. Luckhurst and C.A. Veracini (Ed.). Kluwer Academic Publishers, 537-571

[3] E. Grell (1981) *Membrane Spectroscopy*, Springer Verlag, Berlin.

[4] S.C. Hopkins, C. Sabido-David, J.E.T. Corrie, M. Irving, and Y.E. Goldman (1998), *Biophys. J.* **74**, 3093-3110

[5] U.A. van der Heide, O.E. Rem, H.C. Gerritsen, E.L. de Beer, P. Schiereck, I.P. Trayer, and Y.K. Levine (1994), *Eur. Biophys. J.* **23**, 369-378

[6] M. van Gurp, H. van Langen, G. van Ginkel, and Y.K. Levine (1988) in *Polarized spectroscopy of ordered systems*, B. Samori and E. W. Thulstrup (Ed). Kluwer Academic Publishers, 455-489

[7] M.A.M.J. van Zandvoort, H.C. Gerritsen, G. van Ginkel, Y.K. Levine, R. Tarroni, and C. Zannoni (1997), *J. Phys. Chem. B* **101**, 4149-4154

[8] M.A.M.J. van Zandvoort, D. Wróbel, P. Lettinga, G. van Ginkel and Y.K. Levine (1995), *Photochem. and Photobiol.* **62**, 299-308

[9] J.C.D. Verhagen, M.A.M.J. van Zandvoort, J.M. Vroom, B-Å. Johansson, and G. van Ginkel (1997), *J. Phys. Chem. B* **101**, 10568-10575

[10] M.A.M.J. van Zandvoort, D.L.J. Vossen, G. van Ginkel, R.Torre, P. Bartolini, M. Ricci, J. Thomas-Oates, H. Zuilhof, *To be published.*

[11] U.A. van der Heide, B. Orbons, H.C. Gerritsen, and Y.K. Levine (1994), *Eur. Biophys. J.* **21**, 263-272

[12] M. van Gurp, Y.K. Levine, and G. van Ginkel (1988), *J. Polym. Sci. B.* **26**, 1613-1625

[13] M.E. Rose (1957), *Elementary theory of angular momentum*, Wiley, New York

[14] J. Arden, G. Deltau, V. Huth, U. Kringel, D. Peros, and K.H. Drexhage (1991), *J. of Luminescence* 48&49, 352-358

[15] R.D. Levine and R.B. Bernstein (1975), in *Modern theoretical Chemistry, Volume III, Dynamics of molecular collisions*, W. H. Miller (Ed.), Plenum, New York.

[16] M.A.M.J. van Zandvoort, D. Wróbel, A.J. Scholten, D. de Jager, G. van Ginkel, and Y.K. Levine (1993), *Photochem. and Photobiol.* **58**, 600-606

[17] D. Wróbel, M.A.M.J. van Zandvoort, P. Lettinga, G. van Ginkel, and Y.K. Levine (1995), *Photochem. and Photobiol.* **62**, 290-298

[18] Y. Nashijima, Y. Onogi, R. Yamazaki, and K. Kawakami (1968), *Rep. Prog. Polym. Phys. Jpn.* **11**, 407-410

[19] J. J. P. Stewart (1989) *J. Comp. Chem.* 10, 209-220,(b) J. J. P. Stewart (1989) *J. Comp. Chem.* 10, 221

[20] J. J. P. Stewart (1993) *MOPAC93* Fujitsu Ltd, Tokyo

[21] Klamt and G. Schuurman (1993), *J. Chem. Sco., Perkin Trans. II* **5**, 799-806

[22] F.W. Langkild, E. Thulstrup, and J. Michl (1982), *J. Chem. Phys.* **78**, 3372-3381

[23] L.B-Å. Johansson (1990), *S. Chem. Soc. Faraday Trans.* **86**, 2103-2107

Chapter 4

The orientation of the phosphorescence dipole moments of fluorescein derivatives within their molecular frame

Abstract

The absolute orientation of the phosphorescence dipole moment in the molecular frame is a prerequisite for a quantitative analysis of TPA measurements in orientationally anisotropic systems. We demonstrated that the orientation of phosphorescence dipole moment could be found by the combination of the fluorescence AFD experiments, discussed in the previous chapter, with measurements of the fluorescence and phosphorescence anisotropies at two excitation wavelengths. The tilt of the phosphorescence dipole moment relative to the S_0-S_1 absorption dipole moment is primarily sideways towards the fluorescence dipole moment and not so much out of the molecular plane. Studies of four fluorescein derivatives indicate that the effect of the spin-orbital coupling is to pull the phosphorescence dipole moment towards the fluorescence dipole moment, causing an increase of the phosphorescence quantum yield (see chapter 2).

4.1 Introduction

Optical techniques have been conveniently used to study the orientational order and reorientational dynamics of dyes incorporated in biological systems.[1] In particular, the technique of time-resolved phosphorescence anisotropy (TPA) is frequently used to study reorientational dynamics of membrane proteins,[2,3,4,5] of muscle proteins during contraction,[6,7,8] and in protein gel systems.[9] These motions typically take place on the micro- to millisecond time-window of phosphorescence. However, one has to bear in mind that time-resolved phosphorescence anisotropy monitors the reorientation of the transition dipole moments of the attached dye and is thus an indirect technique for studying the rotational dynamics of the protein molecules themselves.

The interpretation of phosphorescence anisotropy experiments relies on knowledge of the difference angle between the absorption and emission dipole moments. This angle is characterized by the anisotropy at zero time. This quantity is not accessible experimentally in view of the dead-time of the detection channel, ≈ 300 ns. While it can be deduced by back extrapolation in quasi-static systems, for most biological systems it needs to be determined in a separate experiment.[3,9,10,11] As the rotational motion of dyes embedded in polymer matrices can be quenched on the phosphorescence time-scale, the observed anisotropy is constant in time and equals its initial value.

While knowledge of the anisotropy at t=0 affords the analysis of anisotropy experiments on macroscopically isotropic systems, it needs to be augmented by additional information when addressing motions in orientationally anisotropic ones such as membranes,[12] muscle fibres,[17] and stretched polymer films. The required information is the absolute orientation of the transition dipole moments in the frame of the dye. This can only be obtained from separate experiments. In view of the low quantum yield of the phosphorescence process, we have here chosen to obtain the necessary information in two steps. The first, described in the previous chapter 3, involves the determination of the orientations of the absorption and fluorescence dipole moments in the molecular frame using angle-resolved techniques and stretched polymer films. Subsequently, the orientation of the phosphorescence emission dipole moment relative to the latter ones is obtained from time-resolved anisotropy measurements on unstretched films. In addition, we exploit the presence of two non-collinear absorption dipole moments to determine the component of the phosphorescence dipole moment in the plane defined by the absorption and fluorescence moments, but also its component out of that plane. The analysis of previous studies, which utilized only a single excitation wavelength, rested on the assumption that the in-plane component of the phosphorescence dipole moment was parallel to the absorption dipole moment. Thus the difference angle was assigned to the tilt out of the plane.

Studies of the excitation phosphorescence spectra of simple organic molecules[11,13] indicated that the phosphorescence dipole moment is tilted out of the molecular plane, in contrast to the absorption and fluorescence dipole moments. Interestingly, the addition of heavy atoms appeared to have a strong influence on both the phosphorescence quantum yield and the tilt of the phosphorescence dipole moment. This effect was attributed to the influence of the spin-orbit coupling[11] on their spectroscopic properties. We will address the question of the tilt of the phosphorescence dipole moment out of the plane of the xanthene ring structure in Erythrosine B (EryB), 4'-5' dibromofluorescein (2Br), 4'-

5'diiodofluorescein (2I), and Eosin Y (eosin) which differ in the number and nature of the substituted heavy atoms, chapter 2.

4.2 Theory

Luminescence anisotropy of molecules in immobilized solutions

In a steady state anisotropy experiment the sample is continuously illuminated with vertically (*V*) polarized light, while the emitted light is detected with horizontal (*H*) or vertical (*V*) polarization in a direction perpendicular to the excitation beam. The steady state anisotropy r_{ss} is then defined by

$$r_{SS} = \frac{\bar{I}_{VV} - \bar{I}_{VH}}{\bar{I}_{VV} + 2\bar{I}_{VH}}. \tag{4.1}$$

In this equation the subscripts denote the polarization directions of the exciting and emitted light, respectively, in the laboratory frame. If the dye molecules are randomly distributed in the sample and immobilized on the time-scale of the luminescing process, then the anisotropy will be determined by the difference angle Δ between the absorption and emission dipole moment.[14]

$$r_{SS} = \frac{1}{5}\left\{3(\cos\Delta)^2 - 1\right\}. \tag{4.2}$$

Because the absorption process is independent of the emission process, (4.2) holds for both fluorescence and phosphorescence.

Combining phosphorescence and fluorescence anisotropies

As explained in the previous section, the angle between an absorption and an emission dipole moment can be determined in an anisotropy experiment on randomly oriented and immobilized dye molecules. Thus, four independent difference angles can be obtained on using two excitation wavelengths (in two absorption bands) and two emission wavelengths (fluorescence and phosphorescence). The angles between the two absorption dipole moments and the fluorescence dipole moment will be denoted ε_{355} and ε_{532}, where the index indicates the excitation wavelength. The angles between the two absorption dipole moments and phosphorescence dipole moment will be denoted δ_{355} and δ_{532}. In the following

it is tacitly assumed that all difference angles between absorption and emission dipole moments are smaller than 90°.

The anisotropy experiment does not yield any information about the difference angle between the two absorption dipole moments ($\Delta\mu$). However, assuming that both the absorption dipole moments and the fluorescence dipole moment are located in the plane of the molecule,[15,16] there are only two possible ways of positioning the two absorption dipole moments with respect to the fluorescence dipole moment: 1) the absorption dipole moments $\vec{m}_{355}$ and $\vec{m}_{532}$ are positioned at the same side of the fluorescence dipole moment $\vec{n}_{flu.}$. Now $\Delta\mu$- is given by e_{355}-e_{532}. 2) $\vec{n}_{flu.}$ is positioned between $\vec{m}_{355}$ and $\vec{m}_{532}$. In this case $\Delta\mu_{+}$ is given by e_{355}+e_{532}.

It is now important to note that for these two cases knowledge of the difference angles between the two absorption dipole moments yields a distinct orientation of the phosphorescence dipole moment with respect to the absorption and fluorescence dipole moments (see Figure 4.1). If e_{355}+e_{532}≠ d_{355}+d_{355} (case 1, or e_{355}-e_{532}≠d_{355}-d_{355} in case 2), the only possible way to produce a consistent picture of the relative positions of all the transition dipole moments is to tilt the phosphorescence dipole moment out of the plane of the molecule. We will show below that the tilt extracted from the measurements strongly depends on the choice between case 1 and 2.

In the following we position the xz-plane in the plane of the molecule, and align the z-axis along the fluorescence dipole moment. This latter step is taken for the sake of simplifying the geometrical construction and will be removed at a later stage using the results of chapter 3. We introduce $d_{xz,355}$ and $d_{xz,532}$ as the angles between the respective absorption dipole moments and the component of the phosphorescence dipole moment in the xz-plane. j_{yz} is defined as the angle between the component of $\vec{n}_{phos}$ in the yz-plane and the z-axis, and therefore gives the tilt between the phosphorescence dipole moment and the plane of the molecule. Note that j_{yz} does not depend on the excitation wavelength. Consequently, d_{355} can be expressed in terms of j_{yz} and $d_{xz,355}$, while d_{532} is expressed in terms of j_{yz} and $d_{xz,532}$ (see Figure 4.1). j_{yz} can be written as

$$\cos j_{yz} = \frac{\cos d_{532}}{\cos d_{xz532}} = \frac{\cos d_{355}}{\cos d_{xz355}}. \qquad (4.3)$$

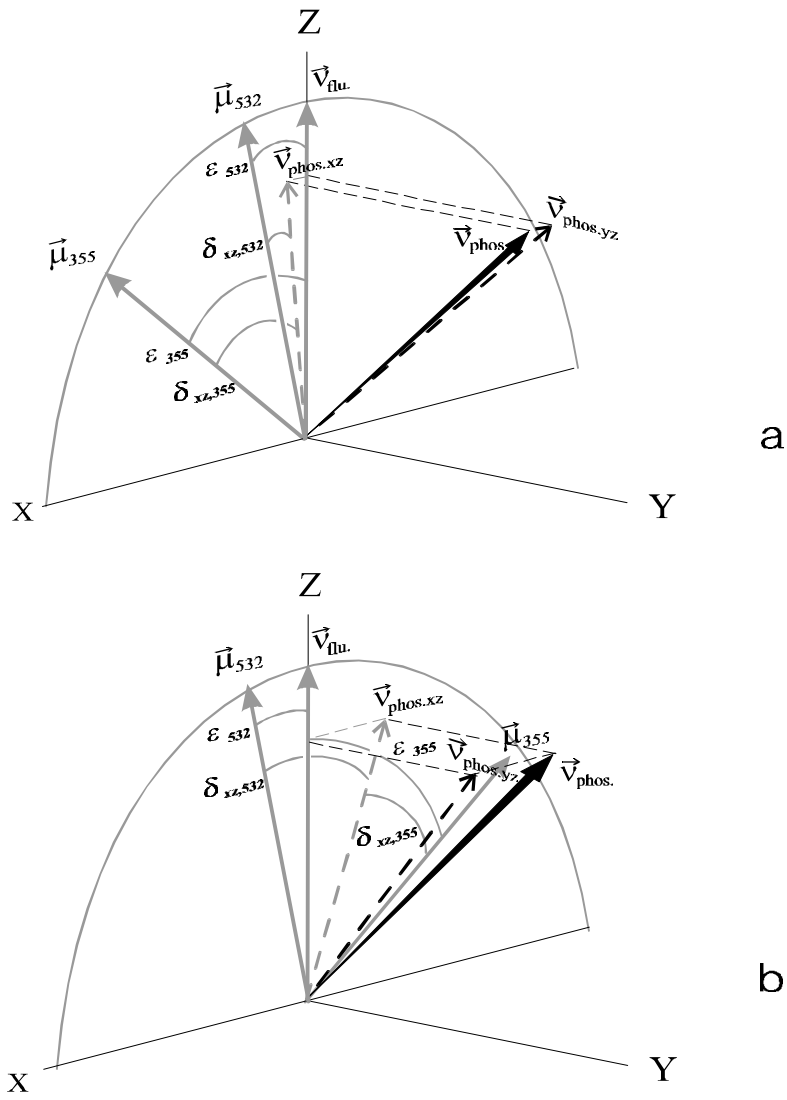

Figure 4.1 *Determination of orientation of the phosphorescence dipole moment, using fluorescence and phosphorescence anisotropies. The dotted arrows are the components of the phosphorescence dipole moment in the xz- and yx-plane. The difference angle between the two absorption dipole moments (* Δm*) is given by a)* $e_{355} - e_{532}$ *and by b)* $e_{355} + e_{532}$.

On making use of the fact that the absorption and emission processes are independent, we find for **case 1** that the difference angle between the two absorption dipole moments is given by

$$\Delta\mu_{-} = \varepsilon_{355} - \varepsilon_{532} = \delta_{xz355} - \delta_{xz532} \tag{4.4}$$

On eliminating φ_{yz} and $\delta_{xz,355}$, we obtain for $\delta_{xz,532}$

$$\delta_{xz,532} = \tan^{-1}\left\{\left(\cos\Delta\mu_{-} - \frac{\cos\delta_{355}}{\cos\delta_{532}}\right)\Big/\sin\Delta\mu_{-}\right\}. \tag{4.5}$$

As all the quantities on the right side of (4.5) are known, $\delta_{xz,532}$ can be calculated and therefore also the tilt angle φ_{yz} from (4.3).
Following a similar argument we find for **case 2** that $\Delta\mu_{+}$ is given by

$$\Delta\mu_{+} = \varepsilon_{355} + \varepsilon_{532} = \delta_{xz355} + \delta_{xz532}\ , \tag{4.6}$$

so that

$$\delta_{xz,532} = \tan^{-1}\left\{\left(\frac{\cos\delta_{355}}{\cos\delta_{532}} - \cos\Delta\mu_{+}\right)\Big/\sin\Delta\mu_{+}\right\}. \tag{4.7}$$

It is now important to realize that cases 1 and 2 represent the same physical situation only if the two absorption dipole moments are mutually orthogonal. This situation is not often encountered in practice and it has been shown that even for highly symmetric molecules the absorption and fluorescence dipole moments are not necessarily mutually orthogonal.[17,18,19]

The combination of phosphorescence and fluorescence anisotropies yields two distinct orientations of the phosphorescence dipole moment relative to the absorption and fluorescence dipole moments, depending on the position of the fluorescence dipole moment relative to the two absorption dipole moments (case 1 and 2, respectively). We have shown in chapter 3 how the orientations of the absorption and fluorescence dipole moments can be related to the inertial axis of the molecule, using angle-resolved fluorescence depolarization (AFD) measurements. This knowledge enables us to make a physical distinction between cases 1 and 2.

4.3 Results

The sample preparation procedure, the time-resolved phosphorescence depolarization set-up, and fluorescence anisotropy methodology used here were discussed extensively in chapter 2. The reader is invited to look there for details.

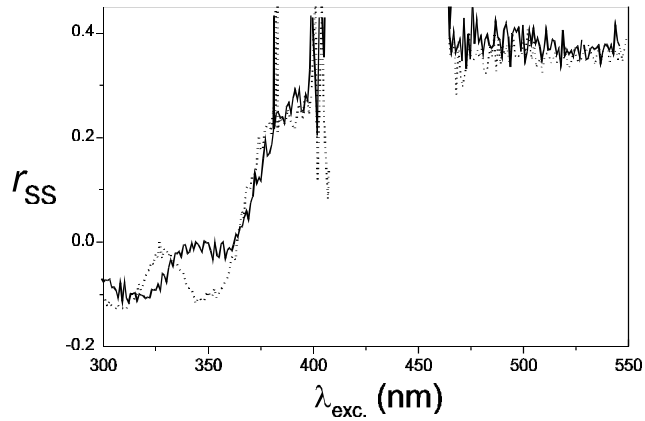

Figure 4.2 *Steady-state excitation spectrum of eosin (dotted line) and EryB (solid line) in a PVA film. The detection wavelength of the fluorescence light was 565 nm.*

Fluorescence Anisotropy

The steady-state fluorescence anisotropy spectra for EryB and eosin in polyvinylalcohol (PVA) are given in Figure 4.2. It can be seen that for EryB the anisotropy is the same for excitation at both 355 nm and 338 nm, being –0.01 ± 0.03. This indicates that the same dipole moment is excited in the AFD experiment ($\lambda_{exc.}$ = 338 nm) as in the TPA experiment ($\lambda_{exc.}$ = 355 nm). The same holds for eosin (r_{ss} at $\lambda_{exc.}$=355 nm and r_{ss} at $\lambda_{exc.}$=338 nm, being –0.11 ± 0·05 and –0.10 ± 0·05, respectively). The values of the fluorescence anisotropy at 355 nm and 532 nm are given in Table 4.1 for all four fluorescein derivatives. The difference angles between the absorption fluorescence dipole moments are given between brackets.

For EryB the steady-state fluorescence anisotropy was also measured in an nitrocellulose (NC) film. The values coincided with those in glycerol and in PVA. Therefore the results discussed in chapter 3 for angle-resolved depolarization on

EryB in a stretched NC film can be used to determine the orientation of the phosphorescence dipole moment.

	$r_{f,355}$ (ε_{355})	$r_{f,532}$ (ε_{532})	$r_{p,355}$ (δ_{355})	$r_{p,532}$ (δ_{532})
EryB	-0.01 (55º)	0.38 (13º)	0.00 (54º)	0.25 (29º)
eosin	-0.10 (66º)	0.36 (16º)	-0.01(55º)	0.19 (36º)
2I	0.12 (43º)	0.37 (14º)	0.02 (53º)	0.14 (41º)
2Br	0.03 (52º)	0.36 (16º)	0.00 (54º)	0.14 (41º)

Table 4.1 *Zero-time anisotropy for fluorescence and phosphorescence. The difference angles are given between the brackets. The errors in the anisotropies are 0.01, except for the errors of $r_{p,355}$ which are 0.02.*

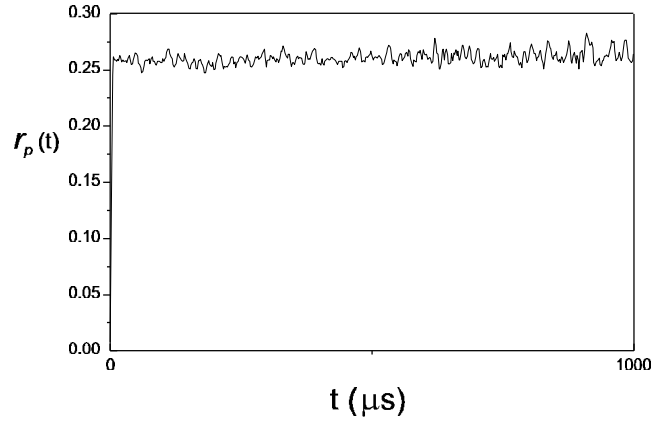

Figure 4.3 *Typical time-resolved phosphorescence anisotropy measurement on EryB in a dry for $\lambda_{exc.}$= 532 nm and $\lambda_{em.}$= 680 – 15. The concentration of dye in the polymer film was $2 \cdot 10^{-7}$ moles/g.*

Time-resolved Phosphorescence Anisotropy on polymer films

A typical TPA measurement, in this case of EryB in a PVA film, is depicted in Figure 4.3. Clearly the dyes are sufficiently immobilized so that the zero-time anisotropy can be extracted with confidence. The phosphorescence anisotropy for the four derivatives are given in Table 4.1, with the corresponding difference angles between the brackets. For the TPA experiment we used the same samples

as for the fluorescence anisotropy measurements.
The anisotropies of the delayed fluorescence were also determined (data not shown). They were found to coincide with the anisotropies of the prompt fluorescence emission.

Again, as for the fluorescence measurements, no differences are found between the phosphorescence anisotropies measured of EryB in PVA and in NC films, implying that we can combine AFD measurements on NC films with TPA measurements on PVA films.

Orientation of the phosphorescence dipole moment

It was shown in section 4.2 that the orientations of the phosphorescence dipole moment can be extracted from a combination of the fluorescence and phosphorescence anisotropies. Two possible orientations are found, depending on the orientations of the absorption dipole moments relative to the fluorescence dipole moment. For EryB we find in case 1, where the fluorescence dipole moment lies to one side of the two absorption dipole moments ($\beta_v<\beta_{\mu1}<\beta_{\mu2}$): $\chi_{yz} = 28 \pm 1°$ and $\delta_{xz532} = 9 \pm 3°$, using Equation (4.5) and (4.3). For case 2, with the fluorescence dipole moment lying between the two absorption moments ($\beta_{\mu1}<\beta_v<\beta_{\mu2}$), we find: $\chi_{xz} = 24 \pm 4°$ and $\delta_{xz532} = 16 \pm 2°$, using Equation (4.7) and (4.3). Thus, in case 2 the in-plane component of the phosphorescence dipole moment lies further from the absorption dipole moment, and closer to the fluorescence dipole moment, than in case 1. Furthermore, the out-of-plane tilt of the phosphorescence dipole moment is 4° larger for case 1 than for case 2: 24° vs. 28°.

The ambiguity between the solutions is resolved satisfactorily, simultaneously with the positioning of the z-axis, on making use of the absolute orientations of the absorption and fluorescence dipole moment in the molecular frame reported in chapter 3. It was shown that the fluorescence dipole moment is oriented between the 355 nm absorption dipole moment and the 532 nm absorption dipole moment for both EryB and eosin. This corresponds to case 2, Figure 4.1b.

The orientation of the phosphorescence dipole moment $\vec{n}_{phos}$ can be expressed in the tilt of the out-of-plane component of the phosphorescence dipole moment, χ_{yz}, relative to the xz-plane and the angle between the in-plane component of $\vec{n}_{phos}$ and the z-axis, χ_{xz}. This latter angle χ_{xz} is given by

$$\chi_{xz} = \beta_{m,532} - \delta_{xz,532} \quad , \tag{4.8}$$

where β_{m532} is the angle between the absorption dipole moment $\vec{m}_{532}$ and the long axis of the molecule (see chapter 3) and $\delta_{xz,532}$.

If we now assume that changes in the number of substituted heavy atoms do not affect the relative positions of the fluorescence and absorption dipole moments, and position $\vec{m}_{532}$ for both 2I and 2Br along the long axes of the molecules (β_{m532} = 0), we also obtain the orientations of the phosphorescence dipole moments for 2I and 2Br.

	φ_{xz} (°)	φ_{yz} (°)	$\Delta\nu$ (°)
EryB	35 ± 2	23 ± 3	4 ± 2
eosin	30 ± 2	21 ± 5	14 ± 2
2I	17 ± 4	38 ± 3	3 ± 4
2Br	24 ± 3	35 ± 3	8 ± 3

Table 4.2 *Orientation of the phosphorescence dipole moment in the molecular frame in Cartesian co-ordinates for four fluorescein derivatives.* $\Delta\nu$ *gives the difference angle between the fluorescence dipole moment and the projection of the phosphorescence dipole moment on the xz-plane.*

The results indicate that the out-of-plane orientation of the phosphorescence dipole moment is not as much influenced by the Z-number of the substituted atom as it is by the number of substituted heavy atoms. This in marked contrast to the effect on the phosphorescence quantum yields (see chapter 2), where we found that the bromide derivatives exhibited a lower quantum yield than the iodine ones. It thus appears that there is no direct correlation between the phosphorescence quantum yield and the tilt of the phosphorescence dipole moment out of the plane of the molecule. However, one feature that does coincide with the phosphorescence quantum yield is $\Delta\nu$, the difference angle between the fluorescence dipole moment and the projection of the phosphorescence dipole moment on the xz-plane. $\Delta\nu$ is around 3 degrees for both iodine derivatives, whereas $\Delta\nu$ is significantly larger for the two bromine derivatives. The fact that the phosphorescence dipole moment is oriented above the fluorescence dipole moment in the case of the two iodine derivatives suggests that this is the determining factor for the phosphorescence quantum yield. The effect of the spin-orbital coupling is that it pulls the phosphorescence dipole moment towards the fluorescence dipole moment and not necessarily towards the plane of the molecule.[11,13]

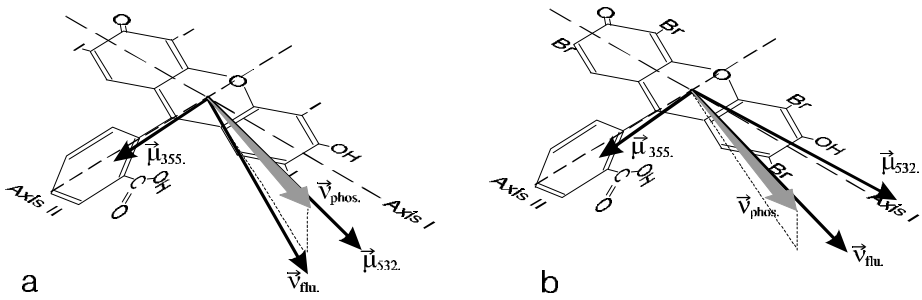

Figure 4.4 *Orientation of the transition dipole moments within the molecular frame of EryB (a) and eosin (b), as deduced from AFD and TPA experiments.* $\vec{m}_{355}$, $\vec{m}_{532}$, *and* $\vec{n}_{flu}$ *are co-planar, while* $\vec{n}_{phos}$ *is tilted out of the plane.*

4.4 Discussion

It has been long established that the phosphorescence dipole moment tilts out of the molecular frame, in marked contrast to the fluorescence dipole moment, which is co-planar with the absorption dipole moments. Previous phosphorescence studies have exclusively used a single excitation wavelength and therefore provided insufficient information to position the in-plane component of the phosphorescence dipole moment relative to the absorption one. The simplifying assumption was then made that the in-plane component of the phosphorescence dipole moment was parallel to the absorption dipole moment. One of the main objects of this investigation was to demonstrate that making use of two excitation wavelengths this problem can be circumvented, provided the associated dipole moments are not parallel. This assignment is made even more reliable on using not only the absorption dipole moments, but also the fluorescent one. The relative orientation of the absorption and fluorescence dipole moments is obtained in a fairly straightforward manner from angle-resolved measurements on dye molecules aligned in an anisotropic matrix such as a stretched polymer film (see chapter 3). Provided the spectral properties of the dye in the media used for the phosphorescence and fluorescence measurements are the same, one can safely use both sets of data in a single global analysis. We have here attempted just such an analysis using the two molecules EryB and eosin. The findings are summarized in Figure 4.4. It turns out that the phosphorescence dipole moment is not simply tilted away from the absorption dipole moment, as assumed in the past, but that its in-plane component is tilted away from the absorption dipole moments in much

the same way as the fluorescence moment is. We thus believe that the out-of-plane tilt has been overestimated in previous work by as much as 20 degrees for eosin and 5 degrees for EryB.

In principle, the orientation of the phosphorescence dipole moment could have been found from angle-resolved phosphorescence depolarization measurements. However, this experiment has two major drawbacks. The first drawback is the low quantum yield of the phosphorescence process. This aggravates a problem encountered in the fluorescence experiment, where low intensity is observed for crucial angle combinations. Thus we anticipate great experimental difficulties when measuring phosphorescence emission under these angle combinations. Second, the tilt of the phosphorescence dipole moment out of the plane introduces extra fit parameters. Since we already needed to reduce the number of fit parameters (see chapter 3, Section 3.2) this is an unsatisfactory feature. Carrying out a combined fluorescence and phosphorescence angle-resolved experiment can circumvent these problems, but this in our opinion is needlessly time consuming. The combination of AFD and TPA experiments provides an appealing and more convenient alternative.

4.5 Conclusions

We have here presented a convenient methodology for determining the absolute orientation of the phosphorescence dipole moment in the molecular frame. This method relies on the combination of the fluorescence AFD experiments discussed in the previous chapter with measurements of the fluorescence and phosphorescence anisotropies at two excitation wavelengths. In this way we have demonstrated that the tilt of the phosphorescence dipole moment relative to the S_0-S_1 absorption dipole moment is primarily sideways towards the fluorescence dipole moment and not so much out of the molecular plane.

Studies of four fluorescein derivatives indicate that the effect of the spin-orbital coupling is to pull the phosphorescence dipole moment towards the fluorescence dipole moment, causing an increase of the phosphorescence quantum yield (see chapter 2).

More importantly, the orientation of the phosphorescence dipole moment can now be used in quantitative analyses of TPA measurements in orientationally anisotropic systems.

Nomenclatura

$\vec{m}_{355}$, $\vec{m}_{532}$ absorption dipole moment for excitation at 355 nm and 532 nm, respectively.

$\vec{n}_{flu}$, $\vec{n}_{phos}$ emission dipole moment for fluorescence and phosphorescence, respectively.

e_{355}, e_{532} angle between the respective absorption dipole moment and the fluorescence dipole moment.

d_{532}, d_{532} angle between the respective absorption dipole moment and the phosphorescence dipole moment.

Δm angle between the two absorption dipole moments.

$d_{xz,355}$, $d_{xz,532}$ angle between the respective absorption dipole moments and the projection of the phosphorescence dipole moment on the xz-plane.

j_{yz} angle between the z-axis and the projection of $\vec{n}_{phos}$ on the yz-plane.

j_{xz} angle between the z-axis and the projection of $\vec{n}_{phos}$ on the xz-plane.

References

[1] J.R. Lakowicz (1983), *Principles of Fluorescence Spectroscopy*, Plenum Press, New York.

[2] R.J. Cherry and G. Schneider (1976), *Biochemistry* **15,** 3657-3661

[3] R. Zidovetski, M.Bartholdi, D. Arndt-Jovin, and T.M. Jovin (1986), *Biochemistry* **25**, 4397-4401

[4] A.M. Rubtsov, A.A. Boldyrev, L. Yang, D. McStay, and P.J. Quinn (1994), *Biochemistry* **59**, 1263-1268

[5] D.A. Roess, M.A. Jewell, C.J. Philpott, and B.G. Barisas (1997), BBA **1375**, 98-106

[6] R.D. Ludescher and D.D. Thomas (1988), *Biochemistry* **27**, 3343-3351

[7] R.A. Stein, R.D. Ludescher, S. Dahlberg, P.G. Fajer, L.H. Bennet, and D.D. Thomas (1990), *Biochemistry* **29**, 10023-10031

[8] D.D. Thomas, S. Ramachandran, O. Roopnarine, D.W. Hayden, and E.M. Ostap (1995), *Biophys. J.* **68**, 135s-141s

[9] E. Prochniewicz, Q. Zhang, E. C. Howard, and D.D. Thomas (1996), *J. Mol. Biol.* **225**, 446-457

[10] R.D. Ludescher and Z. Liu (1993), *Photochem. and Photobiol.* **58**, 858-866

[11] P.B. Garland and C.H. Moore (1979), *Biochem. J.* **183**, 561-572

[12] M. van Gurp, H. van Langen, G. van Ginkel, and Y.K. Levine (1988), in *Polarized spectroscopy of ordered systems*, B. Samori and E.W. Thulstrup (Ed). Kluwer Academic Publishers, 455-489

[13] T. Pavlopoulos and M.A. El Sayed (1964), *J. Chem. Phys.* **64**, 1082-1092

[14] M. van Gurp, Y.K. Levine, and G. van Ginkel (1988), *J. Polym. Sci. B.* **26**, 1613

[15] J. Szubiakowski, A. Balter, W. Nowak, A. Kowalczyk, K. Wisniewski, and M. Wierzbowska (1996), *Chem. Phys.* **208**, 283-296

[16] L.B-Å. Johansson and A. Niemi (1987), *J. Phys. Chem.* **91**, 3020-3023

[17] F.W. Langkild, E. Thulstrup, and J. Michl (1982), *J. Chem. Phys.* **78**, 3372-3381
[18] L.B-Å. Johansson (1990), *S. Chem. Soc. Faraday Trans.* **86**, 2103-2107
[19] U.A. van der Heide, B. Orbons, H.C. Gerritsen, and Y.K. Levine (1994), *Eur. Biophys. J.* **21**, 263-272

Chapter 5

Phosphorescent colloidal silica spheres as tracers for rotational diffusion studies

Abstract

We introduce a novel, phosphorescent, colloidal silica sphere tagged with the millisecond time-scale with time-resolved phosphorescence combination of spectral and time-resolved fluorescence and eosin is close to the value found for eosin in a dry polymer film (chapter molecules, although we report evidence that oxygen and water penetrate respectively, 4 and 10 orders slower than free diffusion in water. Energy both cause a decay of the initial phosphorescence anisotropy, but the from the TPA experiment coincides with the value found by dynamic phosphorescence lifetime and it confirms the colloidal stability of the

5.1 Introduction

Fluorescent dye-labeled silica particles are being used for many applications. Examples are their application as tracers for measuring translational diffusion in various media by fluorescence recovery after photobleaching (FRAP),[1] studies of dense colloidal materials[2] using confocal scanning light microscopy (CLSM), and various applications for photonic crystals.[3] The spectroscopical properties of the dye-labeled particles have been a major object of interest. Features like the fluorescence lifetime and the bleachability of the dye-silica complex determine the suitability of the synthesized particle for CLSM and FRAP experiments.[2,4,5]

Up till now silica spheres have been tagged with fluorescent molecules like fluorescein and tetra-methyl-rhodamine. However, tagging the spheres with *phosphorescent* molecules would significantly expand the number of applications of organic dye-labeled particles. The most important feature of phosphorescent dyes is the long lifetime of the excited state (in the order of micro- to milliseconds). The phosphorescence lifetime is of the same order as the time-window in which reorientational motions of (free) colloidal particles take place. For this reason time-resolved phosphorescence anisotropy (TPA) method may be applied to determine the rotational diffusion rates of colloidal particles tagged with phosphorescent dye. This is especially advantageous in the case of spherical particles, for which only a few techniques are available to measure the rotational diffusion. Thus, the combination of phosphorescent dye-labeled particles and TPA measurements provides us with an extra tool to study the dynamical behavior of colloids in (complex) media. In addition, the phosphorescent dye-labeled particles may be used as microsensors in biological samples, since the phosphorescence lifetime of a dye is very sensitive to the environment, such as the oxygen concentration, due to the long residence in and the triplet character of the excited state.

In this study we introduce a novel type of tracer, namely a colloidal silica sphere tagged with eosin-5-isothyocyanate. This tag is both a phosphorescent and a fluorescent dye. The primary aim of the investigations presented in this chapter is to show that the eosin-silica spheres are indeed suitable for assessing of rotational diffusion on the millisecond time-scale. Ideally, a phosphorescent silica sphere should meet the following requirements: 1) colloidal stability of the spheres in solvents of interest, i.e. the spheres should not aggregate; 2) phosphorescence lifetime comparable with the time-window of the expected dynamics; 3) a high phosphorescence quantum yield of the dye; 4) a high initial phosphorescence anisotropy.

Aggregation of the spheres would cause, amongst other things, a contribution of slow rotational diffusion components to the total decay of the TPA signal, which may seriously hamper the interpretation of the measurements. The stability of dye-labeled particles has been the object of extensive studies.[2,5] Here we will verify whether the particles indeed are colloidal stable, using visual observation as well as dynamic light scattering.

With respect to requirement 2 and 3 it should be noted that the phosphorescence lifetime and quantum yield are strongly affected by the environment of the probe. Therefore we will investigate to what extent dyes incorporated in silica spheres are shielded from the bulk environment of the tracer particles by the surrounding silica. This is done by varying the

composition of the solvent in which the particles are dispersed and by varying the oxygen concentration in the solvent.

The initial phosphorescence anisotropy is determined by the intrinsic anisotropy of the dye and by depolarizing effects that take place within the first few hundreds of nanoseconds after the excitation pulse. This is the experimental dead-time, t_d, during which the detection unit is protected for the instant light burst of fluorescence and scattered light. In the specific case of labeled dye particles two effects influence the initial phosphorescence anisotropy, namely energy transfer (ET) between dye molecules at high dye concentrations and the free volume that is available around the incorporated dye. A combination of time-resolved fluorescence and phosphorescence anisotropy measurements together with spectral measurements will be used to separate and quantify these two effects (see chapter 2).

While exploring the spectral properties of the eosin-silica spheres in various solvents and under several oxygen conditions, we observed an apparent permeability of silica matrix for oxygen and solvents. These observations are also discussed in this chapter with the purpose to gain further insight in the properties and possible applications of the phosphorescent dye-silica spheres, e.g. as microsensors.

5.2 Theory

Determination of the hydrodynamic radius of dye-labeled silica spheres

In this study, we assess the hydrodynamic radius a of a sphere by using two independent techniques. The first technique measures the translational diffusion coefficient, which depends on a^{-1}, while the second technique measures the rotational diffusion coefficient, which shows an a^{-3}-dependence.

The translational diffusion coefficient for a freely moving Brownian sphere is given by the Stokes-Einstein relation,

$$D_0^t = \frac{k_B T}{6\pi\eta_0 a}, \tag{5.1}$$

with k_B the Boltzmann constant, T the absolute temperature, and η_0 the viscosity of the solution. The D_0^t can be found from Dynamic Light Scattering (DLS) measurements, where the time-dependence of the light scattered by the particles

is monitored. In the case of free Brownian particles, D_0^t can be extracted directly from the normalized autocorrelation function

$$\hat{g}_E(t) = \exp(-D_0^t K^2 t) = \exp(-\Gamma(K)t). \tag{5.2}$$

Here the wavevector K is given by $K = 4\pi n\lambda_0 \sin(\theta/2)$, with n is the refractive index of the solvent, λ_0 the wavelength of the incident light *in vacuo* and θ the scattering angle. Thus, the translational diffusion coefficient D_0^t can be obtained from the normalized autocorrelation function measured at several scattering angles θ.

The mean rotational diffusion coefficient of a freely moving Brownian spherical particle with volume $V=(4/3)\pi a^3$ is given by the Stokes-Einstein relation for rotating spheres

$$D_0^r = \frac{k_B T}{8\pi\eta_0 a^3}. \tag{5.3}$$

The rotational diffusion coefficient for a sphere tagged with a luminescent label can be found from TPA measurements. For a rotating sphere the anisotropy is given by[6]

$$r_P(t) = r_P(t_d)\exp(-6D_0^r \cdot t), \tag{5.4}$$

where $r_P(t_d)$ is the initial phosphorescence anisotropy as discussed below.

Influence of Energy Transfer on anisotropy measurements

Energy transfer (ET) between dye molecules can seriously hamper luminescent depolarization measurements. The effect of ET can be intuitively understood considering the situation of a high concentration of immobilized dye molecules. In this case the polarization of the excited molecules can be partially lost due to migration of the excited state from one molecule to another, differently oriented, molecule. In the Galanin approximation[7] the polarization is even lost completely when such a process takes place, so that polarized emission light is observed only from those dye molecules which were initially excited at t=0. In chapter 2 the theory of ET is treated more explicitly. Here we will summarize the main features of the theory.

The fluorescence anisotropy decay caused by ET for an ensemble of randomly oriented, immobilized dyes is given by

$$r_f(t) = r_f(0) \cdot C_f^{ET}(t), \tag{5.5}$$

where $C_f^{ET}(t)$ is given by

$$C_f^{ET}(t) = \exp\left[- g_{stat} \left(\tfrac{4}{3}\pi R_0^3 \rho\right) \sqrt{\pi \frac{t}{\tau_f^0}} \right] \tag{5.6}$$

(see equations (2.8) and (2.9)). The Förster radius R_0 is a measure for the efficiency of the ET process. It describes the average distance between two interacting dye molecules for which the probability of ET equals to 0.5. The factor g_{stat} arises from the orientational averaging of the mutual orientation of two interacting molecules over the dye ensemble; g_{stat} is equal to 0.8452 for immobilized, isotropically distributed dyes. Finally, ρ is the average dye concentration and τ_f^0 is the natural fluorescence lifetime in the absence of competing processes like intersystem crossing and quenching.

The decrease of the phosphorescence anisotropy for molecules whose triplet state is populated via the first excited singlet state (with a typical rate constant k_{isc}) was derived in chapter 2. We have shown there that the phosphorescence anisotropy decreases to a constant value within tens of nanosecond, which is much shorter than the dead-time of the experiment, t_d. Consequently, the decrease of the phosphorescence anisotropy due to ET is given by $C_P^{ET}(t_d)$, with

$$C_p^{ET}(t_d) = \frac{\int_0^{t_d} \exp\left[- g_{stat}\left(\tfrac{4}{3}\pi R_0^3 \rho\right) \cdot \sqrt{\pi \frac{t'}{\tau_f^0}} - t' \cdot k_{isc} \right] dt'}{\int_0^{t_d} \exp(-t' \cdot k_{isc}) dt'} . \tag{5.7}$$

All parameters that enter (5.6) and (5.7) can be determined prior to the experiment: R_0 and τ_f^0 can be calculated from the fluorescence spectra (equations (2.7) and (2.10)); ρ is known from the sample preparation; k_{isc} can be calculated from the combination of fluorescence and phosphorescence lifetime measurements with spectral measurements (equation (2.2)).

Internal motion of the dye in the tracer particle

In the previous paragraph the influence of ET on the anisotropy was discussed for an ensemble of immobilized randomly oriented dye molecules. An additional depolarizing mechanism is the rotation of the dye molecules within an available free volume in the silica sphere. This rotation is characterized by a typical rate constant D_{dye}^{r}. The internal rotation of dye molecules in an organo-silica sphere is an important parameter to be considered when using such a particle as a tracer in studies dealing with rotational diffusion. An estimate of the free volume can be extracted from the limiting value of the fluorescence anisotropy at $D_{dye}^{r}t \to \infty$ and from the initial phosphorescence anisotropy, $r_P(t_d)$.

First we consider the fluorescence anisotropy decay. For colloidal particles the overall tumbling of the sphere takes place on a time-scale orders of magnitude longer than the fluorescence lifetime and this will therefore not influence the fluorescence anisotropy. Furthermore, the depolarization mechanisms of rotation and ET can be separated for the limit $D_{dye}^{r}t \to \infty$ EMBED although they are in principal correlated.[8,9] The limiting value of the fluorescence anisotropy in the presence of both ET and internal dye rotations can thus be written as

$$r_F(D_{dye}^{r}t \to \infty) = r_F^{rot}(D_{dye}^{r}t \to \infty) \cdot C_F^{ET}(D_{dye}^{r}t \to \infty). \tag{5.8}$$

For a particle with a local uniaxial distribution of dye molecules, like a labeled colloidal sphere, $r_F^{rot}(D_{dye}^{r}t \to \infty)$ can be written as[10]

$$r_F^{rot}(D_{dye}^{r}t \to \infty) = \frac{2}{5} \sum_{m=-2,0,2} \left\langle D_{0m}^{2} \right\rangle D_{mo}^{2}(\Omega_{\mathrm{m}}) \times \sum_{n=-2,0,2} \left\langle D_{0n}^{2} \right\rangle D_{no}^{2}(\Omega_{\mathrm{n,\,flu.}}) \tag{5.9}$$

with

$D_{mn}^{L}(\Omega)$ Wigner rotation matrix elements.

Ω_μ $(\alpha_\mu,\beta_\mu,\gamma_\mu)$ The set of Euler angles of the absorption dipole moment in the molecular frame shown in Figure 3.2.

Ω_ν $(\alpha_\nu,\beta_\nu,\gamma_\nu)$ The set of Euler angles of the emission dipole moment in the molecular frame shown in Figure 3.2.

$\langle X_{sm} \rangle$ The ensemble average $\int d\Omega_{sm} f(\Omega_{sm}) X(\Omega_{sm})$ of $X(\Omega_{sm})$ over the orientational distribution function $f(\Omega_{sm})$.

$f(\Omega_{sm})$ The orientational distribution function of the dye molecules relative to the stretch direction.

In the case of phosphorescence anisotropy measurements, the local motion of the dye will have averaged out within the dead-time of the experiment, just like $C_P^{ET}(t)$. The initial phosphorescence anisotropy $r_P(t_d)$ is therefore given by an equation similar to that for the limiting value of the fluorescence anisotropy. The important difference between $r_P(t_d)$ and $r_F(D_{dye}^r t \to \infty)$ is, however, that the fluorescence and phosphorescence emission dipole moments have a different orientation Ω_v.

$$r_P(t_d) = r_P^{rot}(t_d) \cdot C_P^{ET}(t_d) \tag{5.10}$$

$$r_P^{rot}(t_d) = \frac{2}{5} \sum_{m=-2,0,2} \left\langle D_{0m}^2 \right\rangle D_{mo}^2(\Omega_m) \times \sum_{n=-2,0,2} \left\langle D_{0n}^2 \right\rangle D_{no}^2(\Omega_{n,phos}) \tag{5.11}$$

All parameters that enter (5.9) and (5.11) can be determined in separate experiments, except for the order parameters $\left\langle D_{02}^2 \right\rangle$ and $\left\langle D_{00}^2 \right\rangle$. The orientations of the transition dipole moments of eosin have been determined in chapter 3 and 4, while $C_P^{ET}(t_d)$ and $C_F^{ET}(t)$ can be calculated using results from the spectral measurements. Therefore the two order parameters can be found using equations (5.9) and (5.11).

The orientational distribution function is fully characterized if all order parameters are known. Since we only have experimental access to two order parameters, a model orientational distribution function has to be assumed to describe the two order parameters. The simplest model is a 2-D particle-in-a-box model, in the angle space $\{\beta_0, \gamma_0\}$. Here, a dye at an orientation β_0 and γ_0 is allowed to move freely over angles $2\Delta\beta$ and $2\Delta\gamma$ within a cone of an infinitely high potential wall, while the angles β_0 and γ_0 are uncorrelated.

The orienting axis of the dye molecule is the center-line between the binding site and the center of the dye molecule. The symmetry axis of the excited state population, on the other hand, is oriented along the absorption dipole moment of the dye, $\vec{m}$, since it is induced by the polarized light pulse. β_0 is therefore given by the angle between the orienting axis and the absorption dipole moment, β_m. γ_0 equals zero, if the absorption dipole moment lies in the plane of the dye molecule, see Figure 5.1. Thus, the order parameters are calculated by integration over the following distribution function:

$$\left\langle D_{0m}^2 \right\rangle = \frac{1}{N} \int_{90-\Delta b}^{90+\Delta b} \int_{\Delta g}^{\Delta g} D_{0m}^2 d\gamma d\beta \,, \tag{5.12}$$

where N is a normalization constant.

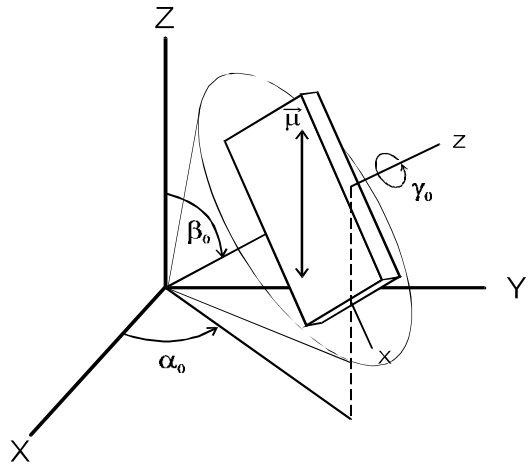

Figure 5.1 *Schematic overview for the orientational behavior of a dye molecule in a colloid.* $\vec{m}$ *gives the symmetry axis of the excited state population. The dye is allowed to move freely around the Euler angles* β_0 *and* γ_0 *, within the indicated cone.*

Influence of oxygen on phosphorescence lifetime

Both the phosphorescence quantum yield and the phosphorescence lifetime are highly sensitive to the presence of oxygen. This sensitivity is caused by the high electron affinity of oxygen, which affects the triplet excited state of the dye molecule. The quenching of phosphorescence by oxygen can be described quantitatively by the Stern-Volmer equation (5.13). This equation relates the phosphorescence lifetime τ_P to an oxygen concentration $[O_2]$ via the quenching constant k_q.[11]

$$\tau_P / \tau_P^0 = 1 + \tau_P^0 \cdot k_q [O_2] \,, \tag{5.13}$$

where τ_P^0 is the phosphorescence lifetime in the absence of oxygen.

The mobility of both the quencher and the dye plays an important role in the quenching of the excited state. In the case of quenching in a complex matrix like

a silica matrix with embedded dye molecules, the diffusion of the quencher will be very limited and k_q will decrease drastically as compared to quenching in the free solvent. Although details on the interaction between dye molecule and oxygen are revealed in the time-dependence of the quenching constant k_q, we will here use a simplified time-independent description of the quenching constant:

$$k_q = \gamma 4\pi DRN', \tag{5.14}$$

where D and R are the sum of the diffusion coefficients and molecular radii, respectively, of the quencher and the dye molecule, N` is Avogadro's number divided by 1000, and γ is the quenching efficiency.[12] k_q can be determined by measuring the phosphorescence lifetime while varying the oxygen concentration. In this way an estimate can be made of the difference between the oxygen diffusion within the sphere and without solute.

5.3 Experimental

Preparation of EoITC silica spheres

The eosin-labeled silica spheres were prepared analogous to the synthesis of spheres tagged with fluorescein-isothiocyanate as described by van Blaaderen *et al.*[5] First, 6.52 mg ($9.25*10^{-6}$ mol) of eosin-5-isothiocyanate (EoITC, Molecular Probes) was added to 0.0212 g ($1*10^{-4}$ mol) of (3-aminopropyl) triethoxysilane (APS, 99%, Janssen) dissolved in 1.0 ml absolute ethanol. The coupling reaction between EoITC and APS proceeded for 17 hours in the dark under continuous magnetic stirring and under nitrogen atmosphere. The obtained solution was then added to a mixture of 500 ml (freshly distilled) ethanol, 40 ml ammonia (25% Merck) and 20.0 ml (freshly distilled) tetraethoxysilane (TES, Fluka, purum grade). The turbidity of the pink solution appeared gradually during a time span of several min utes due to the growth of silica particles. After 1 day, 4.0 ml TES were added to the stirred dispersion for additional silica growth. This additional silica stabilizes the surface of the silica particles, screening the dye molecules from the surface.[5] Excess free dye was removed by repeated centrifugation (3 times at 1500 rpm for 5 hrs) during which the particles were transferred into pure ethanol. The final concentration of EoITC-silica spheres (coded P113) amounted to 0.78 % (v/v).

One small batch of 62.5 ml of 0.78 % (v/v) silica spheres P113 was separated for further silica growth. To this batch 6.25 ml ammonia (25%, Merck) and 0.37 ml TES were added. The particles obtained from this growth procedure were coded P117. Both P113 and P117 formed stable dispersions with no (visible) signs of aggregation. Also centrifugation procedures did not induce any aggregation. Dynamic light scattering experiments confirmed the absence of aggregated spheres (see below). For the TPA measurements, the tracers were transferred into a mixture of *N,N`*-dimethylformamide (DMF, Sigma-Aldrich) and dimethylsulfoxide (DMSO, Sigma-Aldrich) (40:60) containing 10 mM LiCl one week before experimental use. Both solvents were spectroscopic grade (J.T. Baker Chemicals B.V.).

The oxygen concentrations for a sequence of dispersions were measured with an isolated dissolved oxygen meter (ISO_2) and an oxygen electrode from World Precision Instruments. The ISO_2 was calibrated with water, saturated with N_2 or air.

Dye concentration in tracer

The concentration of the dye within the eosin-labeled tracers was determined by optical absorption measurements after dissolution of the particles. To this end, a dispersion of tracer in ethanol (volume fraction of 0.78 %) was mixed with an equal volume of 0.4 M NaOH. This mixture was left overnight resulting in a clear solution the next day. Because the extinction coefficient of eosin depends on the solvent, the absorption of the solution at 522 nm was compared to that of a calibration series consisting of pure EoITC in a 50:50 v/v mixture of ethanol and 0.4 M NaOH in water. The molar extinction coefficient in the latter solution was found to be $103 \cdot 10^3\ M^{-1}\ cm^{-1}$ at 522 nm. Note that we assume that the small amount of dissolved APS does not influence the extinction coefficient of EoITC.

Particle size determination

The hydrodynamic radius of the tracers was measured with Dynamic Light Scattering (DLS) on a dilute dispersion of P113 in DMF and DMSO (40:60) with 10 mM LiCl. The krypton laser (647 nm, Spectra Physics) was used as excitation source in order to avoid fluorescence from the particles. The intensity correlation functions were taken at 16 angles ranging from 35° to 120°. The solvent viscosity η_0 was 1.38 cp, as determined with an Ubbelohde capillary viscometer. Intensity autocorrelation functions were fitted with a second order cumulant fit.

The particle size was also determined with transmission electron microscopy (TEM) using a Philips EM301 electron microscope. Particle size distributions were obtained by measuring radii of about 100 separate particles. The polydispersity is defined as the standard deviation of the distribution divided by the mean particle radius.

Spectral measurements

Time-integrated fluorescence and phosphorescence spectra were measured on a Perkin Elmer LS 50 B luminescence spectrometer following the application of an excitation light pulse (see chapter 2). The LS 50 was also used for phosphorescence lifetime measurements. Here, a gate width of 100 μs was used to integrate the signal while varying the delay time between the light pulse and the opening time of the gate between 0.1 and 5 milliseconds. The samples were excited at 527 nm with a slit width of 15 nm and the emission light was detected at 675 nm with a slit width of 20 nm.

Absorption measurements were performed on a DW2000 spectrophotometer (SLM-Aminco). This instrument is equipped with a special utility to measure the absorbance of scattering samples.

For all spectral measurements (including the time-resolved measurements) samples with an absorbance of 0.1 or lower were used.

Time-resolved fluorescence set-up

Time-resolved fluorescence measurements were carried out using excitation with mode-locked lasers and detection with time-correlated photon counting electronics.[13] A mode-locked continuous wave Nd:YLF laser (Coherent model Antares 76-YLF, Reed & Frangineas 1990) was equipped with a frequency doubler (Coherent model 7900 SHGTC) and frequency tripler (Coherent model 7950 THG) to obtain up to 1 W of continuous wave mode-locked output power at 351 nm wavelength. With this UV light a continuous wave dye laser (Coherent Radiation model CR 590) was synchronously pumped. The pulse duration of excitation pulses was 4 ps FWHM, the wavelength 500 nm and the maximum pulse energy about 100 pJ at a maximum repetition rate of 594 kHz.

The samples were kept at a temperature of 22 °C in a thermostated sample holder, using fused silica cuvettes with a volume of 0.5 cm^3 and 1 cm light path (Hellma model 114F-QS). At the front of the sample housing a Glen-Thomson laser polarizer was mounted, optimizing the vertical polarization of the input light beam. The fluorescence was collected at an angle of 90° with respect to the

direction of the exciting light beam. Between the sample and photomultiplier detector a set of single fast lenses with a rotatable sheet type polarizer were placed, followed by a monochromator and a second set of single fast lenses. The detection monochromator (CVI model Digikröm 112 double monochromator) was set at 551 ± 1 nm. The relative detection sensitivity for horizontally and perpendicularly polarized light (G-factor) was determined using the decay of a fast rotating fluorescent probe and applying a so-called tail matching procedure.

Detection electronics were standard time-correlated single photon counting modules. Single fluorescence photon responses from a microchannel plate photomultiplier (Hamamatsu model R3809U-50 at 3100 V) were amplified by a wide-band amplifier (Becker & Hickl model ACA-2), analyzed in another channel of the CFD and then used as the stop signal for the TAC. The output pulses of the TAC were analyzed by an ADC (Nuclear Data model 8715), used in Coincidence and Sampled Voltage Analysis mode, triggered by the Valid Conversion Output pulses of the TAC. The output of the ADC was gathered in 8192 channels of a multichannel analyzer (MCA board from Nuclear Data model AccuspecB).

Time-resolved phosphorescence set-up

The time-resolved phosphorescence depolarization set-up used here was discussed extensively in chapter 2 and the reader is invited to look there for details.

Analysis of the decay curves

In order to obtain a dynamic instrumental response of the fluorescence measurements for deconvolution purposes, the signal from a highly scattering sample was captured at the excitation wavelength. For the analysis of the phosphorescence decay curves no deconvolution was needed, because on the phosphorescence time-scale the laser pulse was effectively a delta pulse.

The numerical analysis of the time-resolved experimental data was carried out using the ZXSSQ routine from the IMSL program library to fit the data to the model of choice (in this case a mono-exponential anisotropy decay) with the nonlinear least-squares method of Levenberg and Marquardt. The experimental decay curves from the time-resolved experiment were analyzed using a reiterative nonlinear least-squares deconvolution technique.[14]

5.4 Results

Characterization of eosin-labeled silica spheres

The eosin-labeled silica spheres P113 and P117 proved to be very stable colloids, even after a number of centrifugation procedures. Furthermore, no leaching of dye from the particles was observed. The hydrodynamic radii obtained from DLS measurements and the TEM size of the tracer particles are given in Table 5.1. Both techniques indicate a polydispersity of 5-10%. The values of hydrodynamic radius were corrected for the polydispersity of the spheres.[15] The autocorrelation functions of the DLS measurements did not show any sign of aggregated particles.

The dye concentration within the tracer particles was 682 μM, which corresponds with an average dye-to-dye distance of 13.5 nm. The labeling efficiency, defined as the fraction of added dye molecules actually incorporated in the particles, was 23.8 %. The extinction coefficient of P113 in DMF:DMSO (40:60) was $78 \cdot 10^3$ $M^{-1}cm^{-1}$. The excitation, fluorescence and phosphorescence spectra of P113 in a mixture of DMF and DMSO (40:60) are shown in Figure 5.3. The mean fluorescence and phosphorescence lifetimes of P113 were t_f = 2.40 ns and t_f = 3.5 ms, respectively. For the intersystem crossing rate k_{isc} we found a value of $k_{isc} = 1.18 \cdot 10^8$ s^{-1}, solving the rate equations (2.2).

	R_{TEM} (nm)	R_{DLS} (nm)	R_{TPA} (nm)
P113	113 ± 11	137 ± 12	131 ± 3
P117	117 ± 12	133 ± 12	132 ± 5

Table 5.1 *Tracer sizes as determined by TEM, DLS, and TPA.*

Knowing t_f, t_p, and k_{isc}, we have all the information needed to calculate the ET decay factors $C_f^{ET}(t)$ and $C_p^{ET}(t_d)$ as described in the theory. $C_p^{ET}(t)$ decays to a value of $C_p^{ET}(t_d) = 0.68$ within tens of nanoseconds. The influence of $C_f^{ET}(t)$ is shown in Figure 5.2, where $r_f(0) \cdot C_f^{ET}(t)$ is plotted (dashed line). Note that the first few nanoseconds the rotational diffusion and ET are coupled. Therefore, $C_f^{ET}(t)$ is merely approximated by equation (5.6) in this time-window. The correctness of the decoupling of rotational diffusion and ET for $D_{dye}^r t \to \infty$ is demonstrated by the fact that $r_f(t)$ approaches a constant value with increasing *t*.

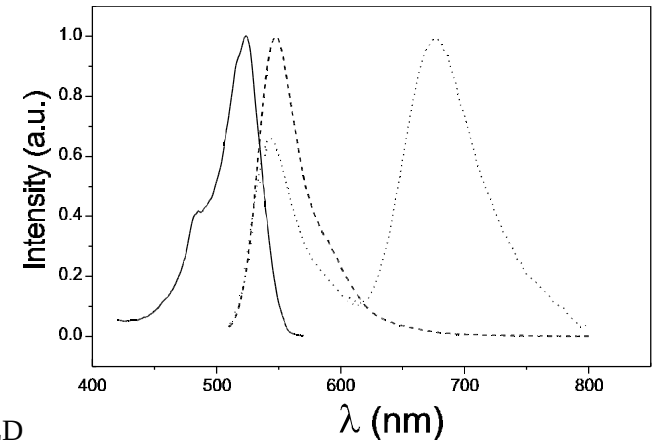

EMBED

Figure 5.3 *Excitation (solid line), fluorescence (dashed line), and delayed luminescence (phosphorescence and delayed fluorescence, dotted line) spectrum of P113 in a mixture of DMF and DMSO (40:60).*

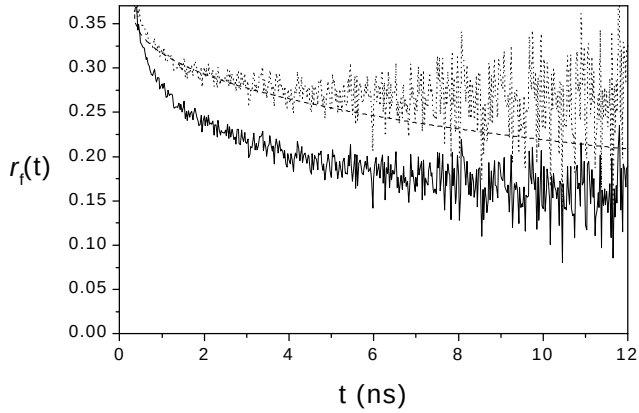

Figure 5.2 *Fluorescence anisotropy decay of P113 in DMF:DMSO for excitation at 500 nm and emission at 551 nm (solid line). The dashed line gives the decay caused by Energy Transfer, as calculated from equation (5.5). The dotted line gives the fluorescence anisotropy decay in the absence of ET, e.g. corrected with the calculated ET curve.*

Fluorescence anisotropy decay of eosin-labeled silica spheres

Time-dependent fluorescence anisotropy measurements were performed on P113 in a mixture of DMF and DMSO (40:60). The excitation wavelength was 500 nm and the fluorescence was detected at 551 ± 1 nm. In Figure 5.2 the measured fluorescence anisotropy decay is shown (solid line). The fluorescence anisotropy at t = 0 is 0.36. We also show the fluorescence anisotropy corrected for ET (dotted line). This corrected curve reached a plateau of $r_F^{rot}(D_{dye}^r t \to \infty) = 0.27$.

Time-resolved phosphorescence of eosin-labeled silica spheres

In Figure 5.4 we plotted the total phosphorescence intensity decay ($I_{VV}(t) + 2I_{VH}(t)$) and the phosphorescence anisotropy decay for P113 in a mixture of DMF and DMSO (40:60). We used a volume fraction of 0.15 % tracer particles. The sampling time was two minutes. Clearly, both the phosphorescence intensity and anisotropy decay take place on the same time-scale. The rotational diffusion time for P113 is $1/6D_o^r = 3.00 \pm 0.25$ ms.

The hydrodynamic radius for P113 and P117 was calculated from the phosphorescence anisotropy decays, R_{TPA}(P113) = 131 ± 3 nm and R_{TPA}(P117) = 132 ± 5 nm respectively. For the initial phosphorescence anisotropy we found $r_P(t_d) = 0.121 \pm 0.001$. Corrected for the ET effect this results in $r_P^{rot}(t_d) = 0.18$.

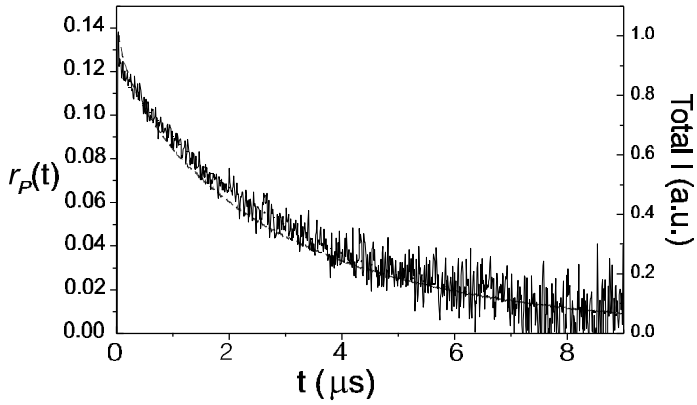

Figure 5.4 *Decay curves of the phosphorescence intensity (dashed line) and anisotropy (straight line) of P113 (0.15 % v/v) DMF:DMSO (40:60) with 10 mM LiCl. The phosphorescence anisotropy is best fitted with a single exponential decay (dotted line): $r_P(0) = 0.121 - 0.001$ and $1/6D_o^r = 3.00 - 0.25$ ms.*

Effect of solvent on the phosphorescence lifetime of eosin-labeled silica spheres

Both the phosphorescence lifetime and the phosphorescence quantum yield of eosin strongly depend on the environment of the dye. In order to find out if dyes embedded in silica particles are protected from the external bulk environment, the solvent in which the particles are dispersed was varied. All dispersions were prepared at least one week prior to the experiment. The values of the phosphorescence quantum yield and lifetime are given in Table 5.2, together with the maxima of the excitation and fluorescence peaks. The positions of the excitation and emission maxima of free eosin (<10 μM) in solution are given between brackets.

	EtOH	Propanol	Glycerol	DMF	DMF:DMSO	H_2O
Φ_p ($\cdot 10^{-3}$)	5.0	4.5	3.9	4.2	4.0	1.6
t_p (ms)	3.1	2.1	2.6	2.7	3.5	1.0
$\lambda_{exc,sil,}$ (nm)	527	528	527	529	528	518
$\lambda_{exc,free}$ (nm)	526	523	525	528	535	517
$\lambda_{flu,sil}$ (nm)	547	545	546	547	547	540
$\lambda_{flu,free}$ (nm)	544	545	544	548	552	537

Table 5.2 *Influence of solvent on the phosphorescence quantum yield Φ_p and the phosphorescence lifetime t_p of P113. The excitation and emission maxima of the fluorescence spectra are also given. The corresponding values for free eosin in solution are given between the brackets. The error in the wavelengths is 2 nm.*

The most significant influence of the solvent was found for H_2O. The phosphorescence lifetime decreased with a factor 3 and a spectral shift of 9 nm was found. To obtain more insight in the diffusion of water into (ethanol or DMF saturated) spheres, dispersions of P113 in ethanol and of P113 in DMF were mixed with water (1:10). In Figure 5.5 the observed phosphorescence lifetime as a function of time after mixing is given. For P113 in DMF and water we found that the initial phosphorescence lifetime is almost fully recovered after an initial fast decay. For P113 in ethanol and water we found a continuous decay eventually reaching a plateau. The same experiment was conducted for P117 particles, which are P113 particles with an extra layer of silica. For P117 we obtained similar results as for P113 (not shown).

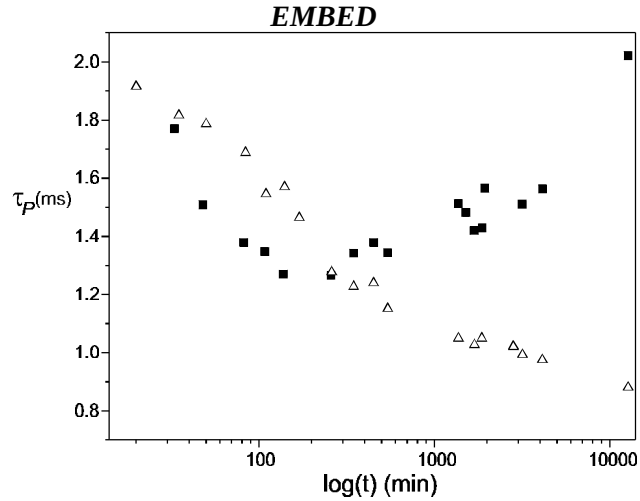

Figure 5.5 *Reduced phosphorescence lifetime vs. time after suspending dispersions P113 in water (1:10). P113:DMF in water (■) and P113:EtOH in water (Δ).*

Effect of oxygen on phosphorescence lifetime for eosin-labeled silica spheres

Oxygen is one of the most important quenchers of the excited triplet state. Its influence on the phosphorescence lifetime and quantum yield of eosin in a silica surrounding was studied by making a sequence of dispersions at different oxygen concentrations. We prepared two different series, namely P113 in ethanol and water (1:10) and P117 in ethanol and water (1:10). The results are shown in Figure 5.6, where the reduced phosphorescence lifetime t_P^0/t_P is plotted against the oxygen concentration. The quenching constant for P113 in a mixture of Ethanol and water (1:10) is $k_q = (4.0 \pm 0.3)\cdot 10^4\,M^{-1}s^{-1}$ and for P117 in the same mixture $k_q = (4.3 \pm 0.5)\cdot 10^4\,M^{-1}s^{-1}$. We checked that the phosphorescence lifetime at an oxygen concentration of 250 μM (saturated air) was the same as the value given in Table 5.2.

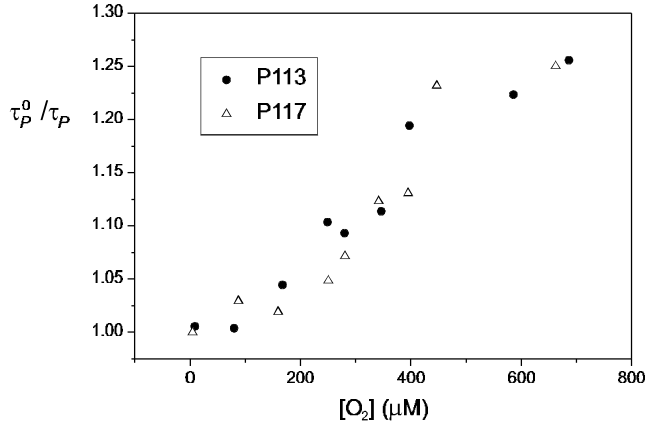

Figure 5.6 *Oxygen sensitivity of the phosphorescence lifetime of P113. The quenching constant for P113 in a mixture of Ethanol and water (1:10) is* $k_q = (4.0 - 0.3)\cdot 10^4\ M^{-1}s^{-1}$. *For P117 in the same mixture* $k_q = (4.3 - 0.5)\cdot 10^4\ M^{-1}s^{-1}$.

5.5 Discussion

Synthesis of eosin-labeled silica spheres

The eosin-labeled Stöber particles P113 and P117 proved to be colloidally stable particles. No aggregation was observed, which confirms that the colloidal stability of the particles remain unaffected by the incorporated dye. Since it is known that the stability declines when dye molecules are located on the surface of the particles,[5] we can conclude that the dye molecules are sufficiently screened from the surface by the extra silica layer. This is confirmed by the fact that no leaching of dye molecules from the silica sphere was observed. The spectra of P113 in different solvents were very similar to the spectra of the free dye, showing that the silica environment does not affect the spectral properties of the dye, which confirms similar results for fluorescein and rhodamin derivatives.[2,5] Finally, the relatively high concentration of dye molecules in the particles did not cause spectral shifts.[4]

The size of the particles was determined using three independent methods, namely DLS, TPA, and TEM. The hydrodynamic radius compared reasonably well with the hydrodynamic radius found with DLS. The hydrodynamic radius as determined by DLS and TPA is considerably larger than the TEM radius, which is considered to result from shrinkage under the electron beam, see Table

5.2.[16] In addition, in solution there is a layer of adhering solvent molecules around the particles, which may result in a larger effective radius.[15]

Sensitivity of the TPA experiment

TPA is clearly a very sensitive technique, with which enables us an easy and quick measurement at a very moderate tracer concentrations of 0.15 % v/v, using a dye concentration within the tracer particles comparable with concentrations used in earlier studies.[2,4] The typical capture time of the experimental trace was merely 2 minutes, which is very short as compared to the capture time of typical DLS and FRAP measurements (hours). From this we can conclude that the phosphorescent dye-labeled silica spheres are suitable for measuring the rotational dynamics of sphere-like particles. Moreover, the experiments were performed at such low tracer concentrations, so that we can safely assume that no interaction between tracers to take place, so that we observe free self-diffusion.

The influence of high dye concentrations on the fluorescence and phosphorescence anisotropy due to ET has to be considered when choosing the appropriate dye concentration for the synthesis. We have shown here that a dye concentration of 682 μM within the sphere causes a decrease of the initial phosphorescence anisotropy to 71 % of the theoretical value. The anisotropy was still sufficiently high to make the particles suitable for further use as rotational diffusion tracers in complex systems (see chapter 6). In view of the low tracer concentration used and the fast capture time of the experiment, even lower dye concentrations within the tracer particles might be applicable. When the dye concentration is halved, the initial anisotropy would be 84 % of the theoretical value. In order to preserve the same phosphorescence intensity a tracer concentration of 0.30 % v/v would be needed, which is still low enough to avoid tracer-tracer interactions.

Internal mobility of the dye in the silica sphere.

In the theoretical section 5.2 we showed how the fluorescence and phosphorescence anisotropy depend on the local order of the dye molecule and the orientations of the absorption and emission dipole moments within the frame of the dye molecule. We argued that the particle-in-a-box model is the simplest model to describe the orientational parameters. This model assumes that the dye molecules can move freely within a cone of angles $D\beta$ and $D\gamma$

The experimental values $r_F^{rot}(D_{dye}^r t \to \infty)$ and $r_P^{rot}(t_d)$ were fitted in the following way: equation (5.12) was used to calculate the two order parameters $\langle D_{02}^2 \rangle$ and $\langle D_{00}^2 \rangle$, taking $\beta_0 = \beta_{m,532}$ and $\gamma_0 = 0°$, while varying $\Delta\beta$ and $\Delta\gamma$. $r_F^{rot}(D_{dye}^r t \to \infty)$ and $r_P^{rot}(t_d)$ were calculated from the so-obtained values of $\langle D_{02}^2 \rangle$ and $\langle D_{00}^2 \rangle$ and the known orientations of the transition dipole moments (chapter 3 and 4), using equations (5.9) and (5.11). The results are given in Table 5.3.

	exp.	$\Delta\gamma$=40°, $\Delta\beta$=40°	$\Delta\gamma$=57°, $\Delta\beta$=1°	$\Delta\gamma$=1°, $\Delta\beta$=59°
$r_F^{rot}(D_{dye}^r t \to \infty)$	0.27	0.277	0.277	0.275
$r_P^{rot}(t_d)$	0.18	0.174	0.172	0.175

Table 5.3 *Comparison between experimental and calculated values of* $r_F^{rot}(D_{dye}^r t \to \infty)$ *and* $r_P^{rot}(t_d)$*, for three different combinations of* $\Delta\gamma$ *and* $\Delta\beta$.

From Table 5.3 it can be inferred that $\Delta\gamma$ and $\Delta\beta$ are correlated. This contradicts the assumption made in the particle-in-a-box model. We also found that the fit-values depend on the difference angles between absorption and emission dipole moments, but are independent of the orientation relative to the frame of the molecule. Both observations are caused by the fact that many features of the system are averaged out by the isotropic symmetry of the sample. One approach to extract extra information from the system is the use of two excitation wavelengths in the anisotropy experiments instead of one.

Regarding the requirement of a high initial phosphorescence anisotropy for TPA measurements, we can conclude that the free volume in which the dye molecule is confined is sufficiently small. Knowing the structure of EoITC from chapter 3, the average space between dye and silica can be estimated to be in the order of 3 Å. The high limiting value of the fluorescence is in contrast with the findings of Imhof *et al.*[4] for fluorescein-isothiocyanate labeled silica spheres. They found an instantaneous and complete depolarization at comparable dye concentrations. They suggested possible leaching from the dye out of the sphere indicating an insufficient binding. Clearly, using the synthesis procedure described in this chapter, these problems are avoided.

Influence of solvent and silica on spectral properties of eosin

The differences in the position of the fluorescence and absorption maxima between freely dissolved eosin and dispersions of the eosin-tagged particles are small for all solvents. In most solvents the spectral maxima of in P113 are slightly red-shifted (2 nm) as compared to those of eosin free in solution. The phosphorescence lifetime determined in the silica particles is only slightly shorter than the 4.7 ms found in a rigid matrix like dry PVA (see chapter 2). This implies that in the spheres collisional quenching of the excited triplet state is strongly hindered and that consequently the silica particles behave like a rigid matrix. Note that the relative diffusion of dye molecule and quencher is a determining factor for the quenching of phosphorescence.[12,17] The protective character of silica is a useful feature when eosin-labeled silica spheres are used as tracers for rotational dynamics studies. The silica-eosin complex has a phosphorescence quantum yield that is at least a factor 10 higher, as compared to proteins tagged with eosin.

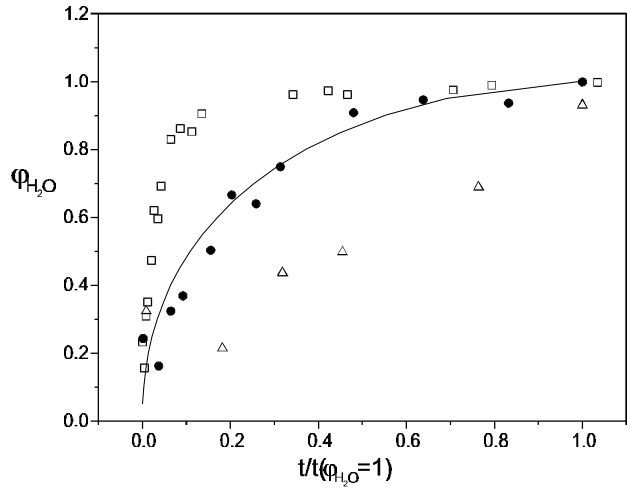

Figure 5.7 *The volume fraction of water in silica particle as a function of the reduced time for* $t(\phi_{H_2O})$ *= 110 minutes (□),* $t(\phi_{H_2O})$ *=540 minutes (●) and* $t(\phi_{H_2O})$ *)= 4000 minutes (Δ).*

Diffusion of water into the silica particle

We have shown that P113 dispersed in water has a much shorter phosphorescence lifetime than P113 dispersed in most other solvents, namely 1 ms vs. 3 ms. Furthermore, the positions of the excitation and fluorescence peaks are significantly blue-shifted relative to those in other solvents and are similar to those found for free eosin in water. Clearly, the triplet state is more quenched by water than by other solvents. But, more importantly, the results of P113 stabilized in ethanol and dispersed in water strongly suggest that in these spheres the ethanol is nearly fully replaced by water. This means that the microporosity of the Stöber particles is sufficiently large to allow for this exchange. The exchange was followed in time by measuring the phosphorescence lifetime (see Figure 5.5) as a function of the time after mixing.

The change in phosphorescence lifetime upon water diffusion into the sphere can be translated into the change of the volume fraction of the sphere occupied by water. The lifetime should then be analyzed as a sum of two lifetimes, varying the contribution a_1 of phosphorescent dyes in an ethanol surrounding with lifetime τ_P(ethanol) and the contribution a_2 of dye in a water surrounding with lifetime τ_P(water). Here, a_2 is proportional to the volume fraction of the sphere occupied by water. In the appendix we derive a simple model for the time dependence of the volume fraction occupied by water, assuming that diffusion flux of water into the sphere is stationary. This model depends only on one fit parameter, namely the time at which the sphere is completely saturated with water, $t(\phi_{H_2O}=1)$. However, the choice of τ_P(ethanol) and τ_P(water) plays an important role. We found that the phosphorescence lifetime measured 2 minutes after mixing was already much lower than the phosphorescence lifetime in ethanol. The origin of this immediate fast decrease is yet unclear. For our analysis we used the lifetime measured after 2 minutes as τ_P(ethanol). In Figure 5.7 we show the results for three different choices of $t(\phi_{H_2O}=1)$. The best fit was found for $t(\phi_{H_2O}=1)=540$ minutes. Using equation (A5.7), we can calculate the diffusion coefficient of water into the particle. Here we take for the porosity of 'Stöber' silica 12 %, as found by Bogush *et al.*[18] and Ketelson *et al.*[19] Together with the choice of $t(\phi_{H_2O}=1)=540$ minutes, this corresponds to a diffusion coefficient of water into the silica of $D = 4.8\cdot10^{-15}$ cm^2/s. It should be noted that we are interested in the order of magnitude for D, so any uncertainty in the porosity is not very important.

It is less straightforward to explain observations for P113 in DMF and water (see Figure 5.5). During the first hours, the decay of the phosphorescence

lifetime follows the same trend as for P113 in ethanol and water. Then, the phosphorescence lifetime starts to recover towards its initial value. The underlying mechanism is yet unclear, but may have to do with the strong polarity of DMF, which causes a high affinity for the silica.

Oxygen sensitivity of the phosphorescence lifetime of eosin in silica

The oxygen sensitivity of the phosphorescence lifetime can be characterized by the quenching constant k_q. For the suspension of P113 in water and ethanol (9:1) we found $k_q = (4.0 \pm 0.3)\cdot 10^4\ M^{-1}s^{-1}$ and for P117 in water and ethanol we found $k_q = (4.3 \pm 0.5)\cdot 10^4\ M^{-1}s^{-1}$. Comparing these values with the quenching rate of free Eosin Y in a sodium potassium buffer[11] ($k_q = 3.8\cdot 10^8\ M^{-1}s^{-1}$) the decrease in sensitivity is four orders of magnitude.

The low oxygen sensitivity observed for eosin-labeled silica particles may be caused by two mechanisms: the concentration of oxygen inside the silica sphere may be relatively low and the relative diffusion constant of oxygen may be small. The fact that the values of k_q within the experimental error are the same for P113 and P117, implies that the extra 4 nm silica layer does not hamper the diffusion of oxygen diffusion into the silica sphere. Based on this result, we assume that transport of oxygen throughout the particle has taken place before the experiment is performed. Under this assumption, the determining factor for the sensitivity is the relative diffusion of dye and quencher within the silica particle. Since the dye molecules are covalently bound, they cannot diffuse through the tracer, so that the diffusion of oxygen is the only diffusional process possible. Using equation (5.14), we conclude that the diffusion coefficient of oxygen in the silica particles is a factor $1.1\cdot 10^{-4}$ lower than that in water (approximately 10^{-5} cm^2/s). The observation that oxygen diffusion into the tracer is strongly hindered by the silica matrix with the findings oxidation of silica coated iron[20] and the reduced bleachability of fluorescein-tagged silica spheres with an extra layer of silica.[21]

Considering the requirement for TPA measurements of a high phosphorescence quantum yield, it can again be concluded that, although the silica surrounding still allows some diffusion of oxygen into the particle, it protects the dye molecule sufficiently against quenching by oxygen. The difference in phosphorescence lifetime between oxygen concentrations of 1 and 250 μM (saturated air) was around a factor 1.03, from which we conclude that deoxygenation of the TPA samples is not necessary.

Porosity of the Stöber silica

The influence of solvent on the phosphorescence lifetime and quantum yield of eosin (see Table 5.2) suggests that solvent molecules can get into close contact with the dye molecules incorporated in the silica. This is confirmed by the time-resolved fluorescence and phosphorescence anisotropy measurements, where it was shown that there is free volume available in the silica sphere for depolarizing motions. The order of the free volume corresponds with the 3 Å that has been found for the size of micropores with a molecular sieving technique.[22]

The porosity of Stöber silica has been already demonstrated in several studies. The penetration of water into silica has been measured with IR spectroscopy[23] and molecular sieving.[22] Ketelson *et al.*[19] estimated the particle porosity at 15 % by comparing particle sizes measured by DLS and by disk centrifuge particle size apparatus. Bogush *et al.*[18] found a microporosity between 10 and 15 %.

Diffusion of solvent through the silica sphere is exemplary for the solvent effect. The diffusion coefficient for this process is approximately $4.8 \cdot 10^{-15}$ cm^2/s, within the model of stationary diffusion. This value is about 10 orders of magnitude lower than unbounded diffusion of water. Note that the diffusion rate of oxygen in the silica spheres is only four orders of magnitude lower than that in water. The polarity and possible hydrogen bonding of water may explain the difference in the relative decrease of the diffusion rates. The diffusion of water thus is an activated process.

5.6 Conclusions

In this chapter we demonstrated that a novel, phosphorescent, colloidal silica sphere tagged with eosin-5-isothyocyanate represents a suitable tracer for studying rotational diffusion on the millisecond time-scale. The suitability of the tracer was based on the four criteria mentioned in the introduction.

First, the spheres are colloidal stable in the solvents of interest, i.e. the spheres do not show any sign of aggregation and no leaching of dye is observed. *Second*, the suitability of EoITC as dye molecule, based on the results shown in Figure 2.9, was demonstrated: the phosphorescence quantum yield is sufficiently high and the phosphorescence lifetime fits within the time-window of the rotational dynamics of the tracer particles. *Third*, the initial phosphorescence anisotropy is sufficiently high, although the internal motions of the dye and

energy transfer between dye molecules do cause a small decrease. *Finally*, the phosphorescence quantum yield of the tracer particles is for most investigated solvents close to the value of immobilized eosin in PVA (see chapter 2). Solvents do penetrate the sphere, but, because diffusion inside the sphere is very limited, the quenching of phosphorescence is very slow. This limited diffusion is especially convenient with regard to possible quenching by oxygen, since no measures need to be taken to deoxygenate the samples.

We also demonstrated that TPA is a very sensitive technique compared to other techniques like DDLS, which needs a higher tracer concentration and are usually slower. An additional advantage of eosin-silica tracers is that they can also be used for FRAP, since eosin is known for its bleachability and its strong fluorescence. Therefore sequential TPA and FRAP experiments on the same sample may provide the investigator with rotational as well as translation diffusion coefficients of the sample under investigation. The eosin-tagged tracers are less suited for microsensing, because of the strongly hindered diffusion of oxygen and water through the silica matrix.

Appendix: Diffusion of water into a sphere

The diffusion of solvent molecules into a dry spherical particle is modeled using a simple diffusion model. Consider a diffusion flux J of (solvent) molecules into a sphere with radius R:

$$J\,dr = 4\pi r^2 D\,dn\,. \qquad \text{(A5.1)}$$

Here n is the number concentration of molecules at a distance r from the sphere center and D is the diffusion coefficient of the molecules in the sphere (which may be much smaller than for free molecules in the surrounding solution). We assume that the concentration just outside the sphere remains constant at a bulk concentration n_∞, whereas the concentration is zero beyond a certain shell thickness yR, where $0<y<1$ (see Figure A5.1):

$$n = n_\infty \text{ for } r \geq R\,;\; n = 0 \text{ for } 0 \leq r < (1-y)\mathrm{R} \qquad \text{(A5.2)}$$

Figure A5. 1 *Model for diffusion of molecules into a dry sphere.*

For a stationary flux J is independent of r, so that integration of (A5.1) gives:

$$J = 4\pi DRn_{\infty} \Big/ \left[(1-y)^{-1} - 1\right] . \qquad \text{(A5.3)}$$

We now define φ as the fraction of the sphere volume that is occupied by the shell containing solvent molecules

$$\varphi = \frac{V_{wet}}{V_{sphere}} = 1-(1-y)^3 . \qquad \text{(A5.4)}$$

Let η be the shell volume per water molecule, then the change of the volume fraction in time is defined as

$$\frac{d\varphi}{dt} = J\eta \Big/ (\tfrac{4}{3}\pi R^3) . \qquad \text{(A5.5)}$$

The solution of (A5.5) can be written in the dimensionless form, using equations (A5.3) and (A5.4):

$$t/t(\varphi = 1) = 1 + 2(1-\varphi) - 3(1-\varphi)^{2/3} \qquad \text{(A5.6)}$$

Here,

$$t(\mathrm{j}=1) = R^2/6Dn_\infty v \qquad \text{(A5.7)}$$

is the time needed for the diffusing molecules to fill the whole sphere. Note that $n_\infty v$ is a measure for the volume fraction of molecules in the shell. Also note that v in the sphere may differ from the specific volume in the bulk. Equation (A5.6) shows that, within this simple "dry core-wet shell" diffusion model, the growth of the "wet" region is fixed by the choice (or estimate) of the time-scale in equation (A5.7), in which D is the essential (unknown) parameter. A characteristic feature of the growth is the rapid initial increase of j (see Figure 5.7).

Acknowledgements

Carlos van Kats is thanked for the synthesis of the eosin-silica spheres and the TEM measurements. Bonny Kuijper and Gijsje Koenderink are thanked for the viscosity and DLS measurements. Arie van Hoek of the Agricultural University of Wageningen is thanked for performing the time-resolved fluorescence depolarization experiments. Dave van den Heuvel is thanked for the determination of the dye concentration.

References

[1] A. van Blaaderen, I. Peetermans, G. Maret, and J.K.G. Dhont (1992), *J. Chem. Phys.* **96**, 4591-4603
[2] N.A.M. Verhaegh and A. van Blaaderen (1994), *Langmuir*, **10**, 1427-1438
[3] W.L. Vos, R. Sprik, A. van Blaaderen, A. Lagendijk, and G. H. Wegdam (1996), *Phys. Rev. B.* **53**, 16231-16235
[4] A. Imhof, M. Megens, J.J. Engelberts, D.T.N. de Lang, R. Sprikand, and W.L. Vos (1999), *J. Chem. Phys. B* **103**, 1408-1415
[5] A. van Blaaderen and A. Vrij, Langmuir (1992), **8**, 2921-2930
[6] C. Zannoni (1979) in *The molecular physics of liquid crystals*, G.R. Luckhurst and C.A. Veracini (Ed.). Academic Pres, New York
[7] M.D. Galanin (1955), *Sov. Physics-JETP.* **1**(2), 317-325
[8] J. Knoester and J.E. van Himbergen (1984), *J. Chem. Phys.* **81**, 4380-4388
[9] G.H. Fredrickson (1988), *J. Chem. Phys.* **88**, 5291-5299
[10] C. Zannoni, A. Arcioni, and Cavatore (1983), *Chem. and Phys. of lipids* **32,** 179-250

[11] J.M. Vanderkooi, G. Maniara, T.J. Green, and D.F. Wilson (1987), *J. of Biol. Chem.* **262** (12), 5476-5482
[12] M.R. Eftink (1991) in *Topics in Fluorescence Spectroscopy, Volume 2: Principles*, edited by J.R. Lakowicz, Plenum Press, New York
[13] A. van Hoek and A.J.W.G. Visser (1981), *Rev. Sci. Instruments* **52**, 1199-1205
[14] R.B. Cundall and R.E. Dale (1983), *Time-resolved Fluorescence Spectroscopy in Biochemistry and Biology*, Plenum Press, New York
[15] A. Imhof and J.K.G. Dhont (1995), **52** (6), 6344-6357
[16] A.K. van Helden, J.W. Jansen, and A. Vrij (1981), *J. Colloid Interface Sci.* **81,** 354-367
[17] R. Brennetot and J. Georges (1998), *Chem. Phys. Let.* **289** 19-24
[18] G.H. Bogush, M.A. Tracy, and C.F. Zukoski (1988), *J. Non-Cryst. Solids* **104**, 95-106
[19] H.A. Ketelson, R. Pelton, and M.A. Brook (1996), *Langmuir* **12**, 1134-1140
[20] A. Ohmori and E. Matijevic (1993), *J. Colloid Interface Sci.***160**, 288-292
[21] personal communication with A. van Blaaderen
[22] A. Walcarius, C. Despas, and J. Bessière (1998), *Micropores and Micromaterials* **23**, 309-313
[23] A. Burneau and B. Humbert (1993) *Colloids Surf. A* **75** 111-121

Chapter 6

Rotational diffusion of tracer spheres in random sphere packings and dispersions

Abstract

The rotational diffusion of spherical particles is difficult to access experimentally due to the intrinsic mechanical isotropy of spheres. In this study we apply the Time-resolved Phosphorescence Anisotropy (TPA) method for studying the rotational diffusion of phosphorescent silica spheres in dispersions and in random closed packings (rcp) of host spheres. The tracer diffusion coefficients in the sphere dispersions appeared to be in good correspondence with hard-spheres predictions, demonstrating that TPA is a reliable technique for studying rotational dynamics. An important advantage of the TPA technique is the possibility to perform measurements on scattering media. This feature was exploited assessing the rotational diffusion of the tracers in (occasionally turbid) packings. We find that the fraction of immobilized tracers directly reflects the pore size distribution as extracted from the Voronoi construction of a simulated rcp. Calculating the average distance between tracer and neighboring particle, we observe that the dependence of the rotational diffusion coefficient on the average distance between tracer and medium spheres is stronger for packings than for dispersions.

6.1 Introduction

The dynamics of colloidal particles in complex media plays an important role in a wide range of fields, from protein mobility in cells to oil recovery. The mobility of a particle in a confining geometry is predominantly determined by three factors, namely the geometrical constraints of the matrix, hydrodynamic interactions between tracer and matrix, and finally any potential interactions between the matrix and the particle, e.g. the van der Waals force and the Coulombic interactions. Because of the complexity of the diffusion process, many theoretical studies[1,2,3,4] have been performed to tackle the problem.

Most studies on particles in confining geometries consider long-time translational diffusion, where particles have moved over distances many times their own size and consequently had many encounters within the confining medium. Examples of phenomenological approaches to study this translational diffusion are peak broadening in chromatography[5] and diffusion across membranes driven by a concentration gradient.[6] *In situ* determination of translational long-time self-diffusion coefficients has been performed by dynamic light scattering (DLS) studies of silica spheres in (cross-linked) polymer systems.[7,8] Another popular method to study translational long-time self-diffusion is fluorescence recovery after photo bleaching (FRAP). This method has been used, for example, to study diffusion of macromolecules through dextran methacrylate gels[9] and the mobility of membrane proteins inside the cell.[10]

Interpretation of long-time self-diffusion coefficients is often troublesome because they are influenced by the geometrical constraints as well as by the hydrodynamic and potential interactions. One approach to study long-time self-diffusion in complex media is therefore to make use of model systems where specific interactions between tracer and host matrix can be controlled. This approach was followed by Kluijtmans.[11] He used DLS and FRAP to determine translational long-time self-diffusion of spherical silica particles through porous glasses[12] and random sphere packings,[13] varying pore size and ionic strength.[14]

The use of model systems offers a few advantages. First of all, the physical properties of the system, such as the size and surface of the tracer particles, are well defined. Moreover, the system is stable in the sense that sticking between tracer and matrix is avoided. Although the geometry and hydrodynamics of the systems are difficult to model, simulation results[15] and approximate models[1] have been used to account for the long-time self-diffusion behavior in the case of a random sphere packing.[12]

In this chapter we study the mobility of tracers with radius R_{tr} in random packings of host spheres with radius R_{pack} by time-resolved phosphorescence anisotropy (TPA). In this way we monitor the *rotational* diffusion D_r of the tracer rather than the translational diffusion D_L. One important difference between D_r and D_L is that the structure of the complex is probed on different spatial scales.[16,17] For example, D_L vanishes for b_{tr} (= R_{tr}/R_{pack}) larger than ≈ 0.15, since the tracer cannot escape from the interstitial holes.[13] D_r, in contrast, probably vanishes at much higher b_{tr}, because the confinement of a tracer to an interstitial space does not prohibit rotational diffusion of the tracer within this interstitial space. The study of rotational diffusion of tracers in random packings of host spheres therefore provides us with information on the local structure.

Furthermore, the interactions between tracers and host spheres can be studied when they come in close contact.

The structure of packed host spheres is static, provided the host spheres are large enough for their Brownian motion to be negligible. It would also be interesting to explore what happens if the confinement is thermally fluctuating, i.e. if the host spheres are Brownian particles in a colloidal dispersion. We therefore decided to study the rotational diffusion for a series of sphere dispersions at a fixed value of b_{tr} (=0.95). This also allows us a comparison with measurements and theory as described by Degiorgio *et al.*[18] They used depolarized dynamic light scattering (DDLS) to study the rotational diffusion of optically anisotropic spheres in colloidal dispersions.

This chapter is organized as follows. In section 6.2 we discuss how TPA can be applied to rotational diffusion measurements on colloidal systems. Section 6.3 describes the sample preparation and gives a brief description of the TPA technique and the method used for the analysis. In section 6.4 the TPA results on dispersions and sphere packings are summarized and discussed. We will pay special attention to the effect of the microstructure of the random closed packing (rcp) on the rotational and translational diffusion. For this purpose we used the Voronoi construction to analyse the structure of simulated random closed packings. Section 6.5 summarizes the main conclusions.

6.2 Theory

In a time-resolved phosphorescence anisotropy experiment the sample is illuminated with a short vertically (*V*) polarized light pulse. The horizontal (*H*) or vertical (*V*) component of the emitted light is detected in a standard 90° geometry (see chapter 2). The phosphorescence anisotropy $r_p(t)$ is then defined by

$$r_p(t) = \frac{I_{VV}(t) - I_{VH}(t)}{I_{VV}(t) + 2I_{VH}(t)} \ . \tag{6.1}$$

If the sample is macroscopically isotropic, the anisotropy can be expressed as a single correlation function:[19]

$$r(t) = 2\left\langle D_{00}^{2*}(\Omega_{Ln}^{t}) D_{00}^{2}(\Omega_{Lm}^{0}) \right\rangle \ , \tag{6.2}$$

where D^{L}_{mn} is the Wigner rotation matrix of angle Ω. Ω^{0}_{Lm} and Ω^{t}_{Ln} represent the orientations of the absorption dipole moment $\vec{m}$ at t = 0 and emission dipole moment $\vec{n}$ at time t relative to the director of the laboratory frame L. $\Omega_{Lm,n}$ can be separated into three sequential orientations: the orientation Ω_{Ld} of the local director of the tracer d in the laboratory frame L, the orientation Ω_{dl} of the long axis of the dye l relative to the local director d, and the orientation of the absorption and emission dipole moment $\vec{m}$ and $\vec{n}$ relative to the long axis of the dye l. Here we exploit the orthonormality of Wigner rotation matrices by using the closure relation, giving

$$r_P^{rot}(t) = \frac{2}{5}\sum \left\langle\left\langle D^2_{p'p}(\Omega^t_{Ld}) D^2_{q'q}(\Omega^0_{Ld}) D^2_{pm}(\Omega_{dl}) D^2_{qn}(\Omega_{dl})\right\rangle\right\rangle D^2_{mo}(\Omega_m) D^2_{no}(\Omega_n), \quad (6.3)$$

where Ω^t_{Ld} and Ω^0_{Ld} are the orientations of the tracer at the time of absorption and emission respectively. The double brackets $\langle\langle\ldots\rangle\rangle$ denote integration over Ω_{Ld} and Ω_{dl}. When the internal rotation of the dye relative to the local director of the tracer is orders of magnitude faster than the overall tumbling of the tracer, the first term in this equation can be separated:

$$r_P^{rot}(t) = \frac{2}{5}\sum \left\langle D^2_{p'p}(\Omega^t_{Ld}) D^2_{q'q}(\Omega^0_{Ld})\right\rangle\left\langle D^2_{pm}(\Omega_{dl}) D^2_{qn}(\Omega_{dl})\right\rangle D^2_{mo}(\Omega_m) D^2_{no}(\Omega_n) \quad (6.4)$$

Equation (6.4) can be simplified, considering the locally uniaxial distribution in the sphere and the uniaxial symmetry of the tracers themselves. Using these symmetries we have (see chapter 3)

$$\left\langle D^2_{qn}(\Omega_{dl})\right\rangle = \delta_{q0}\left\langle D^2_{on}(\Omega_{dl})\right\rangle \text{ and } \left\langle D^2_{q'q}(\Omega_{Ld})\right\rangle = \delta_{q'0}\left\langle D^2_{oq}(\Omega_{Ld})\right\rangle,$$

so that

$$r_P^{rot}(t) = \frac{2}{5}\left\langle D^2_{00}(\Omega^t_{Ld}) D^2_{00}(\Omega^0_{Ld})\right\rangle \times \left[\sum_{m=-2,0,2}\left\langle D^2_{0m}(\Omega_{dl})\right\rangle D^2_{mo}(\Omega_m) \times \sum_n \left\langle D^2_{0n}(\Omega_{dl})\right\rangle D^2_{no}(\Omega_n)\right] \quad (6.5)$$

The term within the square brackets gives the correlation function of the local reorientation of the dye molecules. The value of this term was evaluated in chapter 5.

The first term gives the rotational diffusion correlation function of the tracer particles, which is the function relevant in the present study. In the case of monodisperse and non-interacting spheres, this correlation function can be described by a single exponential

$$\left\langle D_{00}^{2}(\Omega_{Ld}^{t}) D_{00}^{2}(\Omega_{Ld}^{0}) \right\rangle = \exp(-6D_{o}^{r}t) \ , \tag{6.6}$$

where D_o^r is the rotational diffusion coefficient at infinite dilution. D_o^r is given by the Stokes-Einstein relation for rotating spheres, which depends on volume V of the rotating sphere, temperature T, and viscosity η of the solvent:

$$6D_0^r = \frac{k_B T}{\eta V} . \tag{6.7}$$

However, here we are dealing with the rotational diffusion of tracer particles with a polydispersity of about 10 % in a dense packing of host spheres. Because of the polydispersity of the tracers and the expected variation of the local micro-viscosity throughout the packing, for such a system a distribution of diffusion coefficients D_i^r should be considered in the analysis. Therefore, the data were analyzed using a multi-exponential as a model for the anisotropy decay $r_P(t)$.

$$r_P(t) = r_P(t_d) \sum_i a_i \cdot \exp(6D_i^r t) , \tag{6.8}$$

where a_i is the contribution of the diffusion coefficient D_i^r and $r_P(t_d)$ the effective initial anisotropy as determined in chapter 5.

The capacity to extract different exponents from the data analysis is limited.[20] As an example we consider two limiting cases. First, suppose there are two diffusion coefficients: $D_1^r = 0.8 \cdot D_2^r$ and $a_1 = a_2$. Simulations show for this case that the decay curve is equally well fit by a mono-exponential as by a bi-exponential. Thus, the polydispersity of the tracer particles of 10 % does not lead to a clearly detectable multi-exponential decay. If, on the other hand, D_2^r is much lower than D_1^r and $1/D_1^r$ is in the order of the phosphorescence lifetime, then the best fit is often a single decay component with a plateau (D_2^r=0). This limiting case is reached around $D_2^r = 0.1 \cdot D_1^r$. Note that spherical particles by definition do not have any orientational order. Therefore, a plateau in the anisotropy decay does not point to ordering, but to the presence of a very slow decay component.

6.3 Experimental

Preparation and characterization of the medium particles

Sphere packings were prepared from silica spheres of various sizes, some of which were used earlier by Kluijtmans *et al*.[13] Information on these silica spheres is summarized in Table 6.1. Particle sizes were determined with transmission electron microscopy (TEM) using a Philips CM10H electron microscope. Particle size distributions were obtained by determining the size of about one hundred separate particles. The polydispersity is defined as the standard deviation of the distribution divided by the mean particle radius.

The particles coded SC were made by a seeded growth procedure following the method of Giesche.[21,22] Silica seeds (R_{TEM} = 202 nm) were prepared by the Stöber method.[23] The particles were grown by continuously adding two feed solutions to 80 ml starting-dispersion of SiO_2 seeds (0.65 M) in ethanol with ammoniumhydroxide (0.5M, Merck) and H_2O (10M). The two feed solutions, ammoniumhydroxide (1.12M) and H_2O (16 M) in ethanol and 2M TES in ethanol, were added in equal amounts at a rate of 10 ml/hr. Samples were taken from the reaction vessel twice a day for five days and coded in chronological order. After two days the start of a second nucleation was observed. The particles were separated by repeated centrifugation and coded with a subscript. All SC-particles were transferred to a solution of *N*,*N*'-dimethylformamide (DMF, Sigma-Aldrich) by repeated centrifugation and redispersion.

Silica AS30 was obtained as powder from Alltech (Deerfield, IL, USA). The material, which is used as column packing, is readily redispersable. TEM showed no clustering or large aggregates. Its particle size polydispersity of 13 %, however, is substantial. The synthesis and characterization of the VIII particles is described by Kluijtmans.[11] SB284 en S163 were synthesized by Mr. C. van Kats (Utrecht Colloidal Synthesis Facility). The phosphorescent colloidal silica P113 and P117 were used as optical tracers. The synthesis and characterization of the tracer particles P113 and P117 are described in chapter 5.

For TPA measurements on tracer particles in a dense packing or dispersions of spheres it is necessary to optically match the porous medium. For this reason, the host spheres were transferred to a mixture of DMF and dimethylsulfoxide (DMSO) (40:60 v/v) with a refractive index of 1.46. The salt concentration was fixed at 0.01 M LiCl. The volume fractions of the so obtained stock dispersions (ϕ_{dry}) were determined by drying a known volume of the dispersion and dividing the weight of the solid residue by the silica mass density of 1.8 ± 0.1 g/ml. This density has been reported for various silica colloids.[24]

Packing Particle	R_{TEM} (nm)	Size polydispersity σ	b_{tr} (= 113/R_{TEM})
SC_{06}	123	0.06	0.862
S163	163	0.04	0.650
SC_{07}	204	0.02	0.520
SC_{08}	270	0.02	0.393
SB284	284	0.05	0.373
VIII	347	0.04	0.305
SC01	392	0.03	0.270
SC03	458	0.02	0.231
SC04	622	0.02	0.170
SC06	828	0.02	0.128
AS30	1675	0.13	0.063
Tracers			R_{TPA}
P113	113	0.10	131 ± 3
P117	117	0.10	132 ± 5

Table 6.1 *Characteristics of host and tracer spheres.*

Preparation of sphere packings and dispersions

A series of dispersions was prepared from a sediment of SC_{06} (R_{TEM} = 123 nm) with a volume fraction ϕ_{dry} = 0.46 in a mixture of DMF and DMSO (40:60) 10 mM LiCl. We used P117 as a tracer (R_{TEM} = 117 nm). The tracer concentration was for all dispersions 0.12 % v/v. For the effective volume fraction of the sediment we have to consider that the particles have an extra solvation layer of solvent molecules.[25,26] The radius of the dry particles R_{dry} can be found, assuming that the shrinkage of the particles due to radiation damage of the electron beam is 5 %.[25] R_{dry} = 123 nm for the tracer P117, which is 10 nm smaller than the hydrodynamic radius R_{DLS}. The solvation layer of 10 nm is comparable to the value found by Imhof and Dhont for pure DMF.[26] The effective volume fraction is now $\phi_{eff} = (132/123)^3 \cdot 0.46 = 0.57$.

The sphere packings were prepared as follows. In a small glass vial (100·4·0.4 mm, Vitro Dynamics) 50 µl of a concentrated dispersion of host spheres (ca. 20 % v/v) and phosphorescent tracers P113 (between 0.7 and 3 % v/v, increasing with R_{pack}) was centrifuged. The centrifugation time was chosen between 5 min at 2000 rpm for AS30 and 40 min at 3000 rpm for SC_{06}. Following this procedure

we took care that the final tracer concentration in the packing was approximately of the same order for all packings. The samples were used the same day for the TPA experiment. The volume fraction of the packings was determined by preparing a packing with a dispersion of known volume fraction and measuring the height of sediment relative to the total height of the fluid in the vial. A few dried packings were inspected with scanning electron microscopy (SEM, Philips, XL30FEG at 10 kV).

TPA measurements and analysis

The time-resolved phosphorescence set-up is described in detail in chapter 2. Here we summarize the most significant features of the set-up. A vertically polarized excitation source (Nd:YAG-laser 10 Hz (Continuum)) was used to excite the sample at 532 nm. The vial with the sample was placed at an angle of 45° with the incident beam in a cuvette containing toluene for optical matching. The emission light was detected under 90° with the excitation beam (similar to Figure 2.2). A sheet polarizer was used to select the polarization direction of the emission light. In this way two signals were captured: $I_{VV}(t)$ for the vertically polarized emission light and $I_{VH}(t)$ for the horizontally polarized emission light. The anisotropy is calculated from these two signals (see equation (6.1)).

The numerical analysis of the time-resolved experimental data was carried out using the ZXSSQ routine from the IMSL program library to fit the data to the model of choice (see equation (6.6)) with the nonlinear least-squares method of Levenberg and Marquardt. The experimental decay curves from the time-resolved experiment were analyzed using a reiterative nonlinear least-squares deconvolution technique.[27]

6.4 Results and discussion

Rotational diffusion in sphere dispersion

We have measured the rotational diffusion of P117 (R_{TEM} = 117 nm) in a SC_{06} dispersion (R_{TEM} = 123 nm) as a function of the volume fraction of host spheres in a mixture of DMF and DMSO (40:60) 10 mM LiCl. The TPA data were fitted using a mono-exponential decay. In Figure 6.1 the reduced diffusion coefficient (D/D_0) is plotted as a function of the effective volume fraction. Our results are in good correspondence with the experimental and theoretical results of Degiorgio *et al.*[18] The latter authors used DDLS to measure the rotational diffusion in dispersions of 110 nm optically anisotropic spheres and compared their results with theoretical calculations on the short-time rotational diffusion of hard spheres with hydrodynamic interactions. Our results confirm that TPA is a reliable technique and that the tracers as characterized in chapter 5 behave as hard spheres. Therefore TPA can be used to follow the rotational diffusion of phosphorescent spherical tracers in confining media.

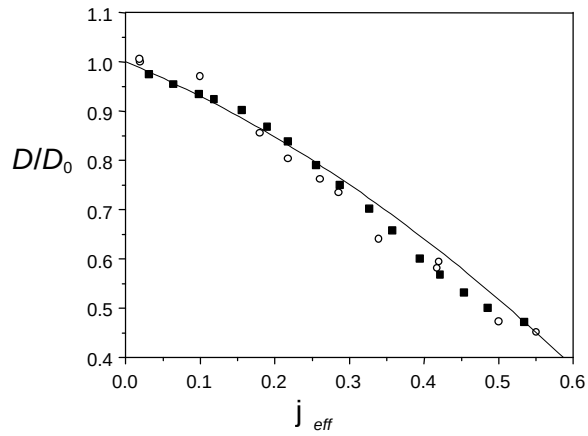

Figure 6.1 *Reduced rotational diffusion coefficient of P117 in a dispersion of SC_{06} host spheres (ϕ$_{tr}$ = 0.95) as a function of the volume fraction j $_{eff}$ of host particles (○), compared with the data of Degiorio et al.*[18] *(|). The full line is the theoretical prediction for hard spheres with hydrodynamic interactions.*[18]

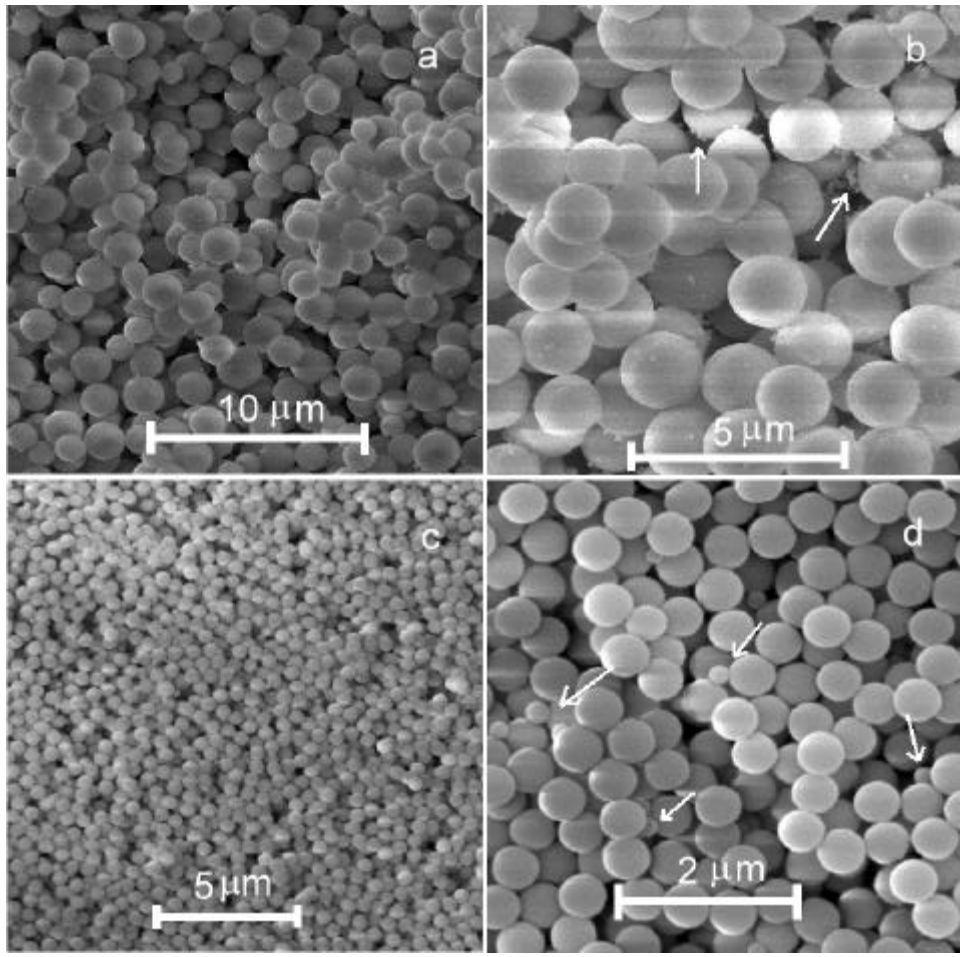

Figure 6.2 *Scanning electron micrographs of a cross-section of a dried packing with AS30 (upper graphs) and SC_{08} (bottom graphs) spheres, containing the tracer P113. The graphs on the left give an overview of the cross-section area. The graphs at the right show the tracer particles present in the sample, some of which are indicated by the arrows. Due to the capillary forces when the sample is dried the tracers accumulate in the narrow inclusions between touching AS30 spheres (b). For SC_{08} there is no accumulation due to the small pore sizes (c).*

Characterization of the tracers and the sphere packings

The tracer concentration in the sphere packings was estimated comparing the phosphorescence intensity detected from the packings with the phosphorescence intensity detected from a solution with a known tracer concentration. For most values of β_{tr} (= R_{tr}/R_{pack}), tracer concentrations in the packing were typically 0.1 % v/v, starting with concentrations of circa 0.3 % v/v in the dispersion before centrifugation. A sediment of tracer particles was formed on top of the packing for these samples. At higher values of β_{tr} (> 0.5) the tracer concentration in the packing increased, while smaller sediments of tracer particles were observed on top of the packings.

The sphere packings were transparent for host spheres SC_{06} to VIII (Table 6.1). For larger host spheres, packings had a slightly opaque homogeneous appearance and looked 'glassy'. In none of the packings Bragg reflections were observed and therefore we assume that the host spheres were randomly packed. This is confirmed by the SEM micrographs shown in Figure 6.2 and similar micrographs made by Kluijtmans.[13] The random sphere packings have a volume fraction in the range of 65 ± 5 %, which is comparable to the random close packing value of 64 %. Our packing density range is comparable to other values found for silica sphere packings.[24]

For the optically clear packings of SC_{06} to VIII and AS30, we found an effective initial anisotropy of 0.12. However, for the particles SC01 to SC04 the effective initial anisotropy decreased to 0.09. This decrease is probably due to depolarization effects caused by scattering of the packing. This effect does not hinder the analysis of the anisotropy decays.

Rotational diffusion in sphere packings

Typical TPA curves are shown in Figure 6.3, where the TPA is given for four values of the size ratio $\beta_{tr} = R_{tr}/R_{pack}$ of tracer and host spheres. For small values of β_{tr} (up to $\beta_{tr} = 0.178$) the phosphorescence anisotropy decays were best fitted with a double exponential decay. The typical slow decay time component for these fits was 5 to 9 times the phosphorescence lifetime, i.e. between 15 and 27 ms. For higher values of β_{tr} the curves were best fitted using a mono-exponential decay with a plateau. The level of this plateau indicates the fraction of tracer molecules that are immobilized on the phosphorescence time-scale, i.e. which have a decay time of around 30 ms or higher.

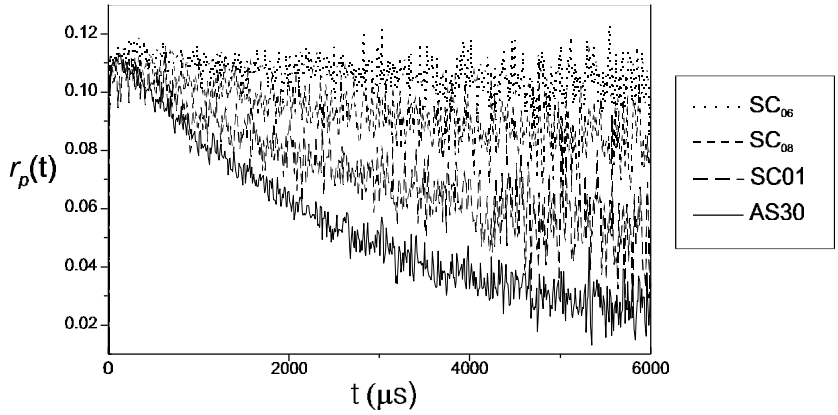

Figure 6.3 *TPA decay curves showing the rotational diffusion of eosin-labeled tracers with a TEM radius of 113 nm in four different packings of host spheres. The radius of the host spheres is varied between 1675 nm and 213 nm (see Table 6.1).*

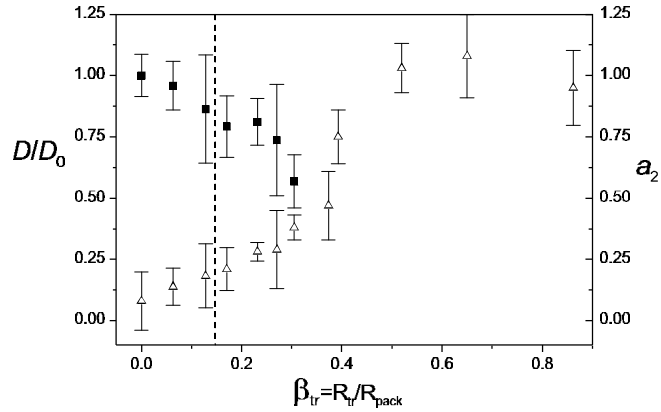

Figure 6.4 *Reduced rotational diffusion coefficient D/D_0 (|) and contribution of immobilized tracers a_2 (Ä) as a function of* b_{tr}*. The values are obtained from a mono-exponential fit with a plateau a_2 of the TPA decay curves. The dashed line marks the point after which translational diffusion is prohibited (*b_{tr} » *0.15).*[13]

The reduced diffusion coefficient and the fraction of immobilized tracers are plotted in Figure 6.4 as a function of b_{tr}. Because the differences in quality between the double exponential fit and the mono-exponential fit with plateau were marginal for $b_{tr} < 0.178$, we used the results of the mono-exponential fit

plus plateau for all values of b_{tr}. Each point is an average of 4 to 8 measurements and the error margins are given by the standard deviation. The values for $b_{tr} = 0$ represent the rotational diffusion of P113 in solution. In the ideal case the value for a_2 is zero. Here we find however a value of 0.08 ± 0.13. This deviation may indicate that there were some aggregates in the sample. For $b_{tr} > 0.4$ it is virtually impossible to accurately determine the reduced diffusion coefficient because of the very small population of freely rotating particles.

Pore size distribution in random closed packing (rcp): Voronoi construction

For the interpretation of the rotational diffusion in sphere packings a theoretical model is needed describing the effect of hydrodynamic interactions on the rotational diffusion of a spherical tracer in a confined space. In addition, information on the microstructure of the random closed packing of spheres has to be implemented in the analysis.

For long-time translational self-diffusion measurements one can use as a reference model the translational diffusion of a sphere in a capillary or slit[13] for which the hydrodynamic effects can be calculated.[28] A similar reference for rotation is to our knowledge not available yet. There are several references where the influence of the volume fraction of hard sphere-dispersions on the rotational diffusion is calculated[18,29] or simulated.[30] Jones and Alavi[31] calculated the influence of a hard wall potential on the rotational diffusion. Calculations for a rotational diffusion model in Brinkman fluids have been reported.[32] It has been shown, however, that the Brinkman approach does not correctly describe the hydrodynamic permeability at high densities near or close to rcp.[24] Our system of hard sphere packings is best approximated by Philips *et al.*,[33] who performed Monte Carlo simulations on suspensions of immobilized hard spheres using Stokesian dynamics to calculate the rotational diffusion of a free tracer sphere. Their work does not apply to our measurements in a straightforward way, but it may be used for a qualitative comparison.

Though theory on the influence of hydrodynamic interactions on rotational diffusion in confined media is not available yet, we do have reliable information on the relative coordinates of spheres in a rcp.[34] Kluijtmans *et al.*[13] used the coordinates of the rcp to calculate the conductivity of their packings. However, the conductivity of the packing does not have any effect on the rotational diffusion of the tracers, since it is defined as the change in the *translational* diffusion due to geometrical constraints of the matrix. The parameter that does probably determine the rotational diffusion is the distribution of distances between tracer and host

spheres. Considering the hard sphere character of the host and tracer particles we can make the assumption that during the sedimentation of tracer-host mixtures the tracer particles are pushed towards the nearest available free volume. This free volume can be estimated from the distance between the center point of the tracer sphere and the surface of the nearest host sphere. If the real-space structure of the sphere packing is known, then the center points can be found in a unique way through the Voronoi construction, see Figure 6.5.

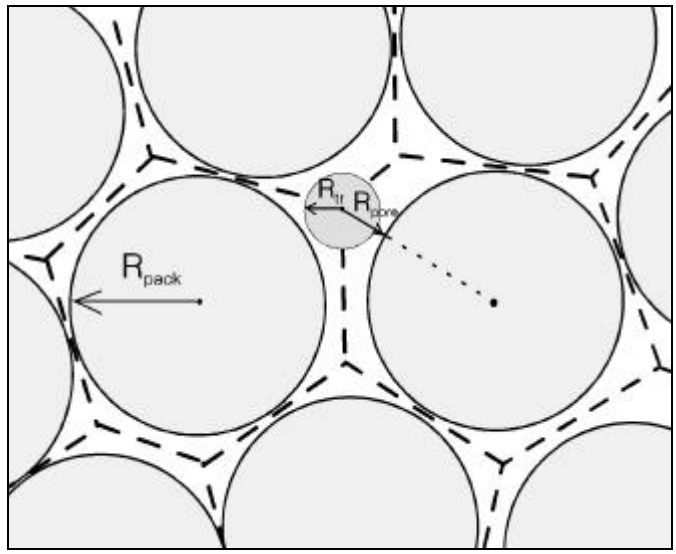

Figure 6.5 *Illustration of the Voronoi construction of a random closed packing in 2 dimensions. The edges of the Voronoi polyhedron, for which every point has an equal distance to two spheres centers, are given by the dashed lines. The gray sphere is the tracer particle.*

A Voronoi polyhedron contains all the points in space that are closer to the center of the particle than to all other particles. All particles share a face of their Voronoi polyhedron with another particle. The vertices of the polyhedron are the points where three faces intersect. A good estimate of the free space is therefore given by the distance between a vertex and its center, minus the radius of the host sphere (R_{pack}). This typical distance will be called the pore size R_{pore}, with the corresponding relative distance $\delta_{pore} = R_{pore} / R_{pack}$.

Here we perform an analysis on a computer-simulated rcp, using an adapted version of the program voron3d.[35] The resemblance between the real-space structure of the simulated rcp and an actual rcp of dye-labeled silica spheres was demonstrated elsewhere, using confocal fluorescence microscopy.[34] The pore size

distribution $P(\beta_{pore})$ is given in Figure 6.6. For this figure we analyzed 30 cubes each containing up to 95 spheres taken at random from the simulated rcp and calculated the Voronoi construction. Doing so, we collected up to 110000 vertices.

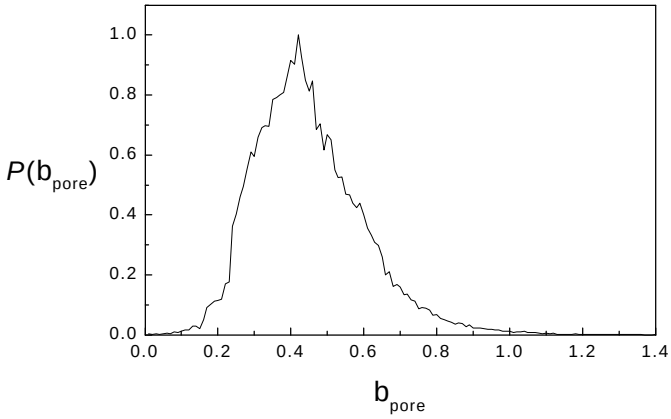

Figure 6.6 *Pore size distribution $P(\beta_{pore})$ as obtained from a Voronoi construction of a simulated random closed packing of spheres.*

A simple method to estimate the amount of immobilized tracer particles in a random close packing is to assume that the particles are immobilized when the distance between tracer and host particle is smaller than a certain distance ΔR. In order to find an estimate for the fraction of immobilized particles a_2 at a ratio β_{tr}, the integral over $P(\beta_{pore})$ from $\beta_{pore} = 0$ to $\beta_{tr'} = (R_{tr}+\Delta R)/R_{pack} = \beta_{tr}(1+\Delta R/R_{tr})$ has to be divided by the total integral taken from $\beta_{pore} = 0$ to β_{pore}^{max}, the highest value for β_{pore} found from the Voronoi construction:

$$a_2(\beta_{tr}) = \frac{1}{N}\int_o^{\beta_{tr}'(\beta_{tr})} P(\beta_{pore})\,d\beta_{pore} \tag{6.9}$$

with

$$N = \int_o^{\beta_{pore}^{max}} P(\beta_{pore})\,d\beta_{pore} \tag{6.10}$$

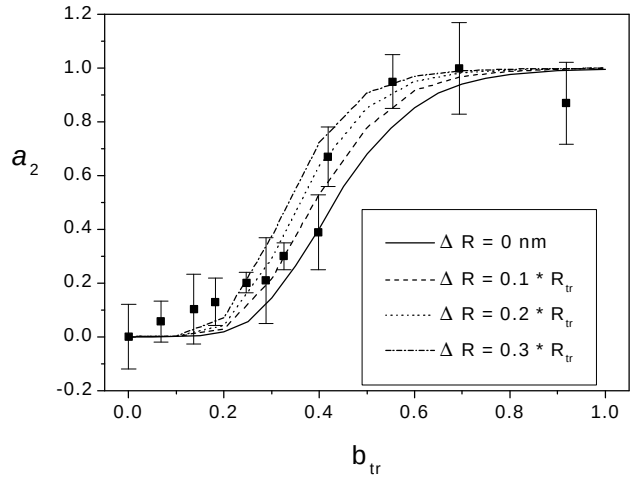

Figure 6.7 *Fraction of immobilized tracer particles. Experimental values as compared to the values calculated using equation 6.9, for four threshold radii* ΔR.

The result of this model and a comparison with our experimental data are shown in Figure 6.7. We used a ratio of $\Delta R/R_{tr}$ between 0 and 0.3. The better fit from the four curves is given by $\Delta R = 0.2*R_{tr}$. Taking for the tracer radius the hydrodynamic radius of 132 nm, this suggests that the rotational diffusion is at least ten times reduced compared to D_0 when the distance between the surfaces of the tracer and the host spheres is less than 26 nm. The deviations for small values of b_{tr} may indicate that the tracer particles occasionally stick to the sphere packings. This is however contradicted by the results of the dispersion series, where we found a good correspondence between our rotational diffusion data and the theoretical predictions for hard spheres (Figure 6.1). More probably, a small fraction of tracer is jammed between the packing spheres during the sedimentation procedure used to prepare the packing. From the analysis of the fraction of immobilized tracers we can conclude that the pore size distribution $P(b_{pore})$ found from the Voronoi construction of the computer simulated rcp models the microstructure of the rcp satisfactorily.

Comparison between rotational dynamics of tracers in random sphere packings and dispersions

In order to compare the reduced rotational diffusion coefficients in a static (packing) and a fluctuating (dispersions) environment, our data should be rescaled, so that we can compare our experimental results with simulations performed by Phillips *et al.*[30,33] Instead of the effective volume fraction of the dispersion ϕ_{eff} and the ratio β_{tr} of the sphere packings, we now use the average reduced free distance $\langle\lambda\rangle$. In the case of sphere packings $\langle\lambda\rangle$ is the ratio of the tracer radius to the average pore size: $\langle\lambda\rangle_{pack} = R_{tr}/\langle R_v\rangle = \langle\beta_{tr}/\beta_{pore}\rangle$. $\langle\lambda_{pore}\rangle$ is calculated by

$$\left\langle \lambda_{pore}(\beta_{tr}) \right\rangle = \int_{a}^{\beta_{pore}^{max}} P(\beta_{pore}) \frac{\beta_{tr}}{\beta_{pore}} d\beta_{pore} \Bigg/ \int_{a}^{\beta_{pore}^{max}} P(\beta_{pore}) d\beta_{pore}, \tag{6.11}$$

where a equals $a = (R_{tr} + \Delta R)/R_{pack}$, the cut-off ratio under which the tracer particles are immobilized.

For dispersions, $\langle\lambda\rangle$ is the ratio of the tracer radius to the average distance between the center of the tracer and the surface of a medium sphere.

$$\left\langle \lambda_{disp} \right\rangle = \frac{R_{tr}}{R_{tr}} \cdot \left[\left(\tfrac{4}{3}\pi \frac{1}{\phi_{eff}} \right)^{1/3} - 1 \right]^{-1} \tag{6.12}$$

The results are in qualitative agreement with the results of Philips *et al.*, who simulated the volume fraction dependence of the rotational diffusion of a tracer sphere in a suspension of mobile[30] and immobilized[33] medium spheres. Like Philips *et al.*, we find that the rotational diffusion in a surrounding of immobilized spheres depends slightly stronger on the relative distance than in a surrounding of mobile spheres.

Opportunities for TPA measurements in complex media

We have shown in this chapter that results of TPA measurements on phosphorescent spherical colloids convincingly reflect the pore size distribution of a rcp, as found by computer simulations and CLSM measurements. This indicates that TPA is a useful tool to recover the pore size distribution of more complex structures that are difficult to simulate by a computer or to image by CLSM. Here the capability to make tracers of a desired size between approximately 30

nm and 1 μm may be decisive. More importantly, we can manipulate the direct interactions between the tracers and the host medium by chemical modification of the silica surface.[25] Furthermore, the tracers are specifically labeled, and therefore also specifically detected. Scattering of the host complex does not significantly hamper the experiment or its interpretation, in contrast to dynamic light scattering-experiments.

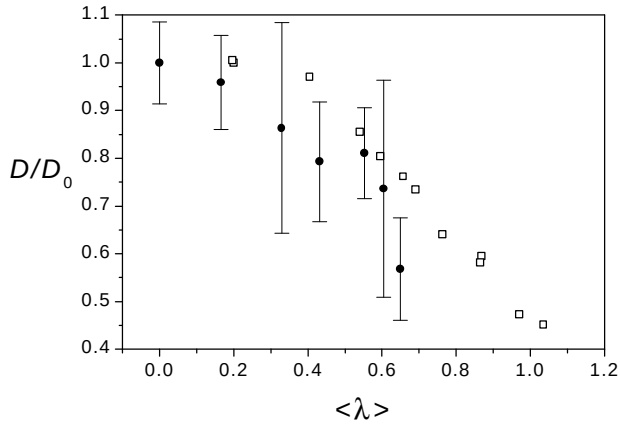

Figure 6.8 *Reduced rotational diffusion coefficient as a function of the average reduced free volume* ⟨l ⟩*. The solid circles give the results for tracer diffusion in packings. The open cubes give the results for tracer diffusion in dispersions.*

6.5 Conclusions

TPA measurements were used to study the rotational diffusion of phosphorescent silica spheres in dispersions of different volume fractions and in static random packings of host spheres. The measurements on dispersions were in good correspondence with theoretical predictions for hard sphere interactions, demonstrating the suitability of the tracers as well as the TPA technique. The measurements on sphere packings showed that the fraction of immobilized tracers corresponds with the pore size distribution as found by a Voronoi analysis on a simulated rcp. The reduced rotational diffusion coefficients for the dispersions and packings showed the same qualitative dependency on the average reduced free distance as had been found by computer simulations.

Our results for the rotational diffusion measurements of spherical tracers in a rcp show that rotational diffusion measurements yield different information on the behavior of tracers in complex media than translational long-time self-diffusion measurements.[13] The translational diffusion depends on the conductivity of the complex, whereas rotational diffusion depends on the local pore size of the complex. In practice this means that tracer rotation can still occur at pore sizes where long-time translational self-diffusion is impossible. Thus by combining translational and rotational diffusion measurements a distinction can be made between sterical entrapment by the complex and immobilization caused by physical interactions between tracer and complex.

An important advantage of the TPA technique is the possibility to perform measurements on scattering media, as a result of the selectivity of the technique. Although the dynamic range is affected by scattering, the time-dependence of the anisotropy curve remains the same. The low tracer concentration needed for the experiments is exemplary for the sensitivity of the technique. An additional advantage of the organo-silica tracer particles is that the surface and dimensions of the particles can be modified. In this way we created the unique possibility to study complex (local) interactions in a controlled manner.

Acknowledgements

Carlos van Kats from the Utrecht Colloidal Synthesis Facility is thanked for the preparations of silica particles and the SEM measurements. Gijsje Koenderink is thanked for the fruitful discussions.

References

[1] I.C. Kim and S. Torquato (1992), *J. Chem. Phys.* **96**, 1499-1503
[2] A.G. Ogston (1958), *Trans. Faraday Soc.* **54,** 1754-1757
[3] J. Tong and J.L. Anderson (1996), *Biophys. J.* **70**, 1505-1513
[4] A.G. Ogston, B.N. Preston, and J.D. Wells (1973), *Proc. R. Soc. Lond.* **333**, 297-316
[5] V. Hejtmanek and P. Schneider (1994), *Chem. Eng. Sci.* **49**, 2575
[6] D.M. Malone and J.L. Anderson (1978), *Chem. Eng. Sci.* **33**, 1429
[7] G.D.J. Phillies and D. Clominel (1993), *Macromolecules* **26**, 167-170
[8] J.G.H. Joosten, E.T.F. Geladé, and P. N. Pusey (1990), *Phys. Rev. A* **42** 2161-2175
[9] S.C. De Smedt, T.K.L. Meyvis, J. Demeester, P. van Oosteveldt, J.C.G. Blonk, and W. E. Hennink (1997), *Macromolecules* **30**, 4863-4870
[10] B. Storrie and T. E. Kreis (1996), *Trends in Cell Biology* **6**, 321-324

[11] S.G.J.M. Kluijtmans (1998), *Dynamics of colloids in porous media*, Thesis Utrecht University, The Netherlands
[12] S.G.J.M. Kluijtmans, J.K.G. Dhont, and A.P. Philipse (1997), *Langmuir* **13**, 4976-4981
[13] S.G.J.M. Kluijtmans and A. P. Philipse (1999), *Langmuir* **15,** 1896-1898
[14] S.G.J.M. Kluijtmans, E. H. A. de Hoog , and A. P. Philipse (1998), *J. Chem. Phys.* **108**, 7469-7477
[15] I. Pagonabarraga, M. H. J. Hagen, C. P. Lowe, and D. Frenkel (1999), *Phys. Ref. E* **59**. 4458-4469
[16] T. Jamil and P. S. Russo (1998), *Langmuir*, **14**, 264-270
[17] D. Lavalette, C. Tétreau, M. Tourbez, and Y. Blouquit (1999), *Biophys. J.* **76,** 2744-2751
[18] V. Degiorgio, R. Piazza, and R. B. Jones (1995), *Phys. Rev. E* **52**, 2707-2712
[19] C. Zannoni (1979), Distribution functions and order parameters. *The molecular Physics of Liquids, eds.* G. R. Luckurst and G. W. Gray, Academic Press, London
[20] D.A. van der Sijs, E.E. van Faassen, and Y.K. Levine (1993), *Chem. Phys. Let.* **216**, 559-565
[21] H. Giesche (1994), *J. of the Eur. Cer. Soc.* **14**, 189-204
[22] H. Giesche (1994), *J. of the Eur. Cer. Soc.* **14**, 205-214
[23] W. Stöber, A. Fink, and E. Bohn (1968), *J. Colloid Interface Sci.* **26,** 62-69
[24] A. P. Philipse and C. Pathamanoharan (1993), *J. Colloid Interface Sci.* **159**, 96-107
[25] A.K. van Helden, J.W. Jansen, and A. Vrij (1981), *J. Colloid Interface Sci.* **81**, 354-358
[26] A. Imhof and J.K. Dhont (1995), *Phys. Rev. E* **52**, 6344-6357
[27] R. B. Cundall and R.E. Dale (1983), *Time-resolved Fluorescence Spectroscopy in Biochemistry and Biology*, Plenum Press, New York
[28] J.L. Anderson and J.A. Quinn (1974), *Biophys. J.* **14**, 130-141
[29] M. Watzlawek and G. Nägele (1997), *Physica A* **235,** 56-74
[30] R.J. Philips, J. F. Brady, and G. Bossis (1988), *Phys. Fluids* **31,** 3462-3472
[31] R.B. Jones and F.N. Alavi (1992), *Physica A* **187,** 436-455
[32] Y.E. Solomentsev and J.L. Anderson (1996), *Phys. Fluids* **8**, 1119-1121
[33] R.J. Philips, J.F. Brady, and G. Bossis (1988), *Phys. Fluids* **31,** 3473-3479
[34] A. van Blaaderen and P. Wiltzius (1995), *Science* **270**, 1177-1179
[35] M.P. Allen and D.J. Tildesley (1987), *Computer Simulations of Liquids*, Clarendon Press, Oxford, Great-Britain

Summary

The technique of Time-resolved phosphorescence anisotropy (TPA) has been frequently used to study rotational motions of particles on the micro- to millisecond time-scale. The interpretation of the observed TPA signals is, however, not straightforward. The theoretical description of the physical processes often requires more parameters than can be determined experimentally. This is often due not only to the complex interaction within and between the particles, but also to the incomplete knowledge of the photophysics of the dye molecules.

This thesis had therefore two scopes. In the first place, dye molecules were scanned for their suitability for TPA experiments and their polarization properties were identified. The second goal of this thesis was the synthesis and use of colloidal silica spheres tagged with a phosphorescent dye, where the interactions underlying the dynamic processes can be modulated systematically.

In chapter 2 we demonstrated how the number and type of substituted heavy atoms in the dye molecule influence the phosphorescence quantum yield, lifetime and zero-time anisotropy. To this end, spectral parameters were determined for the commonly used probes erythrosine (4-iodo-fluoresein), eosin (4-bromo-fluorescein), as well as for 2-iodo- and 2-bromo-fluorescein. We found that the Z number of the substituted heavy atoms primarily influences the luminescent properties of the dyes. The number of substituted heavy atoms appears to play a subsidiary role. More importantly, we have formulated a quantitative measure to select dye molecules for particular phosphorescence experiments. In addition, we have delineated the optimal concentration range of dye molecules for phosphorescence depolarization experiments.

The absolute orientation of the absorption and fluorescence dipole moments in the frame of the molecule, in this case erythrosine and eosin, was our focus in chapter 3. This information is required for the interpretation of fluorescence depolarization experiments on orientationally anisotropic systems. The orientations of the transition dipole moments were recovered from angle-resolved fluorescence depolarization measurements on dye molecules, macroscopically aligned in stretched polymer films. The relative orientation of the fluorescence dipole moment is between the visible and UV absorption dipole moments for both eosin and erythrosine.

In chapter 4 the orientations of the phosphorescence dipole moments relative to the absorption and fluorescence dipole moments were investigated for the four fluorescein derivatives. The combination of the absolute orientations of the fluorescence and absorption dipole moments (determined in chapter 3) with measurements of the fluorescence and phosphorescence anisotropies at two excitation wavelengths yielded the orientation of the phosphorescence dipole moment. It was demonstrated that the tilt of the phosphorescence dipole moment relative to the S_0-S_1 absorption dipole moment is primarily sideways towards the fluorescence dipole moment and not so much out of the molecular plane. The effect of the spin-orbital coupling is to pull the phosphorescence dipole moment towards the fluorescence dipole moment.

A novel, phosphorescent, colloidal silica sphere tagged with eosin-5-isothyocyanate was introduced in chapter 5 as a tracer for the study of rotational diffusion with TPA. The suitability of the tracer was tested by a combination of spectral and time-resolved fluorescence and phosphorescence measurements. The silica environment of the eosin proved to be useful: quenching processes are reduced markedly and the internal motion of the dye is restricted to a small cone. The hydrodynamic radius of the tracer found from the TPA measurements coincides with the value obtained from dynamic light scattering. This shows that eosin has a suitable phosphorescence lifetime and confirms the colloidal stability of the tracers.

In chapter 6 we presented a study of the rotational diffusion rates of the phosphorescent tracer spheres in packings and dispersions of host spheres. The measurements on tracers in dispersions agree fairly well with calculations for hard spheres. This confirms the suitability of the tracers as well as the TPA technique for studying rotational dynamics. An important advantage of the TPA technique is that it can be used for experiments on slightly scattering media. This feature was exploited for assessing the rotational diffusion of the tracers in occasionally turbid packings. We found that the fraction of immobilized tracers can be estimated accurately by the pore size distribution extracted from the Voronoi construction of a simulated random close packing. We found that the dependence of the rotational diffusion coefficient on the average distance between tracer and medium spheres is stronger for packings than for dispersions.

Samenvatting (voor niet-vakgenoten)

Rotatie en Translatie

Stel, een deeltje neemt een warm bad. Wanneer het deeltje niet te groot is, zal het niet naar de bodem zinken, maar kris-kras door het bad crossen, terwijl het om zijn as tuimelt. Kortom, het zal willekeurige *translatie-* en *rotatie-bewegingen* uitvoeren. Deeltjes van deze grootte worden *colloïden* genoemd.

Als we het deeltje nu uit bad halen en in een lange dunne buis stoppen, zal de translatiebeweging van het deeltje zich beperken tot één dimensie, terwijl de rotatie niet echt gehinderd wordt. Sterker nog, wanneer het deeltje in een (te ingewikkeld) labyrint wordt gestopt, dan zal het niet over grote afstanden kunnen bewegen en in zijn kleine beschikbare ruimte blijven rondtollen. Stel nu dat de beweging van het deeltje met een microscoop bekeken wordt (want dat heb je minstens nodig om colloïdale deeltjes te bekijken). Door de beperkte mogelijkheden van een microscoop kan het zijn dat translatiebewegingen te klein zijn om waar te nemen, terwijl het deeltje wel degelijk beweegt. Hierdoor zouden verkeerde conculsies getrokken kunnen worden over de interactie tussen het deeltje en zijn omgeving, bijvoorbeeld dat het deeltje vastplakt.

Een praktijkvoorbeeld uit de macroscopische wereld: stel dat men geïnteresserd is in de bewegingen van het kindje dat zich in de beperkte ruimte van de buik van een zwangere vrouw bevindt. Als we van een afstandje naar die buik kijken, zouden we kunnen concluderen dat de baby vastgeplakt zit aan de wand van de buik, omdat geen translatiebeweging waargenomen kan worden. Het enige bewijs van leven zou dan de translatiebeweging zijn die het kindje ondergaat bij de geboorte. Zou men andere technieken toepassen om het kindje te zien, door een hand op de buik te leggen of door een echoscopie te maken, dan zou men merken dat het kindje wel degelijk rotaties over een van zijn draaiassen kan uitvoeren. Het kind leeft en zit niet vastgeplakt.

Wanneer men geïnteresseerd is in de lokale mobiliteit van een deeltje, zou het handiger zijn om de rotatie van het deeltje te volgen en niet de translatie. Het probleem is echter dat rotatiebewegingen in het algemeen lastiger te bepalen zijn. Stel bijvoorbeeld dat de deeltjes perfect rond, dus perfect *isotroop*, zijn. In dat geval kan er visueel geen onderscheid gemaakt worden tussen draaiende en stilstaande deeltjes. Van een bal in een flipperkast is het bijvoorbeeld duidelijk dat hij transleert, maar het is niet te zien of hij ook om zijn as draait.

Om de rotatie van een bal te kunnen volgen, moet de bal gemerkt worden met bijvoorbeeld een streep. Op dezelfde manier moeten de colloïdale bolletjes gemerkt worden met iets dat zich als 'streep' gedraagt wanneer er met een bepaalde techniek naar gekeken wordt. Deze 'strepen' zijn vaak moleculen die een *anisotrope* eigenschap hebben, oftewel *verklikkermoleculen*. Dit wil zeggen dat er iets aan het gedetecteerde signaal verandert, zodra het betreffende molecuul van oriëntatie verandert. – Stel bijvoorbeeld dat de meettechniek bestaat uit een bundel tennisballen waarvan de baan gemeten kan worden. Wanneer een egaal witte voetbal in de bundel geplaatst wordt, dan zal de baan van de afgeketste tennisballen niet veranderen als de stand van de voetbal verandert. Wanneer een tennisracket in de bundel geplaatst wordt, verandert de baan van de afgeketste ballen wel degelijk met de stand van het racket. De stand van het racket kan ook in de tijd worden gevolgd: draai je het langaam om zijn as, dan verandert de baan van de afgeketste ballen langszaam; draai je het racket snel, dan verandert de baan snel. Het racket is mechanisch anisotroop, dus kan de rotatiesnelheid van het racket bepaald worden.

Het probleem is de verklikkermoleculen in een bol te stoppen zonder dat de isotrope eigenschappen van de bol veranderen en de anisotrope eigenschappen van de verklikkermoleculen behouden blijven. Bovendien moet de wisselwerking tussen de verklikkers en de meettechniek zo specifiek zijn dat de omgeving van het veklikkermolecuul de meting niet beïnvloedt.

Verklikkermoleculen

Vaak zijn de anisotrope verklikkers moleculen die een lichtdeeltje (*foton*) kunnen absorberen en weer uitzenden. De kans dat het molecuul een foton absorbeert (*geëxciteerd* wordt), hangt af van de kleur (energie) van het licht én van de *polarisatie* (trillingsrichting) van het licht. Door een verzameling van willekeurig verdeelde moleculen met een puls van gepolariseerd licht aan te stralen, worden de moleculen geselecteerd die de juiste oriëntatie hebben om het licht te absorberen. Zo'n molecuul zendt gemiddeld na een karakteristieke tijd t_{leef} (de *levensduur*) weer een foton uit, dat een andere polarisatie heeft (zie Figuur 1.1). Wanneer het deeltje waaraan het molecuul vastzit tussen t=0 en t=t_{leef} bewogen heeft, dan zal de polarisatie van het uitgezonden licht veranderd zijn. Deze verandering wordt gemeten als functie van de tijd en is een maat voor de rotatiesnelheid van het deeltje; dit heet *anisotropie*. De polarisatie van de eerste uitgezonden fotonen zal al een beetje veranderd zijn. Dat kan zelfs zoveel zijn dat het molecuul hierdoor niet meer geschikt is voor rotatiemetingen. Het verschil in polarisatierichting noemt men de *intrinsieke anisotropie* $r(0)$.

Of een verklikkermolecuul geschikt is om de rotatiesnelheid van een deeltje te volgen waaraan het is vastgeknoopt, hangt vooral af van de levensduur van het deeltje. Als het deeltje al een paar keer om zijn as heeft gedraaid voordat het zijn

verklikkende foton heeft uitgezonden, valt er niks meer te zeggen over de draaisnelheid, behalve dat het een stuk sneller is dan 1/ t_{leef}. Het is ook mogelijk dat het deeltje zo langzaam beweegt dat het verklikkermolecuul al zijn licht al heeft uitgezonden voordat er sprake is van iets wat op een draai lijkt. Vrije colloïdale deeltjes hebben een rotatiesnelheid tussen de honderd tot een miljoen omwentelingen per seconde. Geschikte verklikkermoleculen moeten dus een levensduur in dit tijdsvenster hebben.

Een ander aspect dat van belang is, is het aantal uitgezonden fotonen dat de detector uiteindelijk bereikt. Dit is afhankelijk van de kans dat een molecuul daadwerkelijk een foton uitzendt nadat het geëxciteerd is. Die kans wordt de *quantum yield* genoemd. De quantum yield hangt niet alleen af van het soort deeltje, maar ook van de temperatuur, de moleculen in de omgeving van de verklikker en vele andere zaken. In het algemeen kun je zeggen dat de quantum yield kleiner wordt naarmate het aantal botsingen van de verklikker met zijn omgeving groter wordt.

Fosforescentie

Geschikte verklikkers die aan dit eisenpakket voldoen, zijn moleculen die zowel snel (in een miljardste van een seconde: *fluorescentie*) als langzaam (in een honderdduizendste tot honderdste van een seconde: *fosforescentie*) licht uitzenden. Voor het volgen van colloïdale deeltjes moet het fosforescentielicht gedetecteerd worden. Het probleem met fosforescentie is echter dat de quantum yield laag is en dat de polarisatie-eigenschappen van de fosforescentie niet goed gekarakteriseerd zijn. Al deze eigenschappen van de fosforescentie worden beïnvloed door het aantal en soort zware atomen dat aan het verklikkermolecuul vastzit. Het zijn deze atomen die ervoor zorgen dat het molecuul niet alleen maar fluoresceert, maar ook fosforesceert.

In de hoofdstukken 2, 3 en 4 van dit proefschrift zijn vier moleculen behandeld die identiek zijn, afgezien van het aantal en soort zware atomen (Jood en Broom) dat aan het molecuul (Fluorescine) vastzitten. De *spectrale* eigenschappen van de vier moleculen (de interactie tussen licht en de moleculen) worden bepaald met behulp van metingen aan plastics waarin de moleculen zijn ingebed. Daarmee hebben we niet alleen een overzicht gekregen van welk molceuul het beste gebruikt kan worden voor welk experiment, maar ook de invloed van de zware atomen op de spectrale eigenschappen gekarakteriseerd. Deze spectroscopische karakterisatie is gedaan bij de vakgroep Moleculaire Biofysica.

Toepassing: Rotatie van ronde silica-bolletjes

Het markeren van deeltjes wordt veel toegepast bij het onderzoeken van de rotatie van eiwitten. De omgeving van eiwitten is echter vaak complex, en de interactie tussen het eiwit en zijn omgeving al helemaal. Fosforescentie-anisotropiemetingen aan eiwitten zijn daarom vaak lastig te interpreteren.

Om op een gecontroleerde manier naar interactie tussen deeltjes en hun omgeving te kijken, worden bij de vakgroep Fysische- en Colloïdchemie modelsystemen gemaakt. Hiervoor worden colloïdale bollen (rond de 100 nm) van silica gemaakt waarin fluorescente moleculen zijn ingebouwd. Dit is niets anders dan heel fijn gekleurd zand. De beweging van deze deeltjes in complexe media, zoals poreus glas, kan selectief gevolgd worden zonder dat de meting verstoord wordt door allerlei verstrooiïngen van het omringende complex.

In hoofdstuk 5 wordt dezelfde synthesetechniek gebruikt om bolletjes te maken die fosforescente moleculen bevatten. Daarvoor is een van de vier moleculen geselecteerd die in hoofdstuk 2 t/m 4 behandeld zijn, namelijk eosine (bekend als kleurstof voor lippenstift). We laten zien dat eosine goed afgeschermd wordt van de omgeving van het deeltje, en dat de rotatiebeweging van eosine in het deeltje heel klein is. Voor dit laatste werd het fluorescentielicht gebruikt. – Er is aan het hele eisenpakket voor een goed fosforescentie-experiment voldaan. Het is daarom geen verassing meer dat de draaisnelheid van de colloïdale bollen in een vloeistof inderdaad bepaald kon worden met fosforescentie-anisotropie-metingen. Wel is het de eerste keer dat de rotatiesnelheid van dit soort fijne zanddeeltjes gemeten is.

In hoofdstuk 6 hebben we de rotatiesnelheid van deze gemerkte bollen in vrij troebele pakkingen van andere, ongelabelde, bollen gemeten. We hebben laten zien dat we met deze metingen een schatting kunnen maken van de grootte van de ruimtes tussen de bollen in de pakking. Bovendien hebben we aangetoond hoe de rotatiesnelheid beperkt wordt door de grootte van de ruimte om de testbolletjes. Dit was met de gebruikelijke technieken niet gelukt, omdat deze teveel last hebben van de niet specifieke verstrooing van de andere bollen.

Hiermee komt een wijd gebied aan toepassingen vrij, waarin fosforescentie-anisotropie-metingen aan gemerkte testbolletjes gebruikt kunnen worden om informatie over de structuur van en wisselwerkingen in complexe media te bestuderen.

Nawoord

Promoveren in tijden van bezuinigingen, herstructureringen, herver-bouwingen (en daardoor spontaan in de brand vliegende opstellingen), het ontstaan van onderzoeksinstituten en wat dies meer zij, is een enerverende aangelegenheid. Tijdens de afgelopen vier jaar en-een-beetje heb ik daardoor niet alleen wetenschappelijke toppen en dieptes voorgeschoteld gekregen, maar ook een scala aan menselijke gedragsvormen.

Het is erg plezierig terugkijken op deze periode, met een dieprood gekleurd proefschrift in de hand (de kleur heeft te maken met de kleur van het fosforescentielicht). Het moet wel gezegd worden dat het boekje er niet was geweest als een paar mensen er niet ook waren geweest. Daarom lijkt het me een goed idee die mensen te bedanken. Allereerst is dat mijn (co-pro)motor Marc (A. M. J. van Zandvoort), die mij vanaf mijn eerste stappen als student bij Moleculaire Biofysica begeleid heeft. Ik ben benieuwd of ik hem in de toekomst nog binnen werktijd zal tegenkomen, maar in ieder geval zal dit buiten werktijd het geval zijn.

Het rode boekje is een beetje schizofreen omdat het twee promotores heeft. Yehudi (K. Levine) heeft de hoofdstukken 2 t/m 4 door de mangel gehaald. Door hem heb ik enigszins een vermoeden gekregen wat het echte Engels is, zoals het door de wetenschappers op dat eiland gebezigd wordt. Bovendien heeft hij mij laten zien hoe een brij van metingen toch tot iets transparants omgevormd kan worden.

Albert (P. Philipse) heeft me ingewijd in de wereld van de tollende bolletjes en de verstrikte staafjes, oftewel de wereld van de colloïden. Vanaf het begin van ons contact waren onze sessies hersenbestormend. Dat resulteerde in de twee vlot ontstane laatste hoofdstukken.

De breedgeschouderde Gijs van Ginkel heeft als een bulldozer voor mij wegen gebaand en obstakels van kant gemaakt. Hierdoor leek het junglepaadje naar het eind van mijn promotie soms haast een lekker lopende weg.

Op een gegeven moment wist ik me omringd door zoveel mensen die voor mij aan het sloven waren dat ik als een pasja in een constante delegeertoestand kwam. Daarvoor wil ik mijn excuses aanbieden aan Willie en Marie-Lousie, mijn geliefde en al lang voormalige analistes, die inmiddels een even geliefde opvolger hebben gevonden in Dave, mijn hoofdvakstudenten Edwin, Thijs, en Martin, en het handjevol ‘driemaanders’ (dat werd meestal wat meer) Carlijn, Marleen, Leon en Bart. De laatste jaar heb ik bij Colloïdchemie nieuwe slachtoffers gevonden in Carlos, die al mijn bollen gebakken heeft, en Gijsje, die elke verkeerde zin en gedachte zachthandig neerzabelde. Evert de Beer bedank

ik voor het gebruik van zijn laser en de gastvrijheid bij de vakgroep Fysiologie en Sportgeneeskunde.

Voor alle mensen die niet bij Moleculaire Biofysica rondlopen: deze groep is klein en fijn!

Mijn ouders ben ik diep dankbaar voor de manier waarop zij meegeleefd en meegedacht hebben.

Juliane is mijn meisje. Daarvoor dank, en ook voor het zetten van komma's en thee.

Alle mensen die zich te kort gedaan voelen hebben een probleem, maar kunnen zich (of hadden zich kunnen) beklagen bij mij na afloop van de promotie.

List of publications

1. M.P. Lettinga, C. M. van Kats and A.P. Philipse, Rotational diffusion of tracer spheres in random sphere packings and dispersions. *To be Published*

2. M.P. Lettinga, M.A.M.J. van Zandvoort, C.M. van Kats and A.P. Philipse, Phosphorescent colloidal silica spheres as tracers for rotational diffusion studies. *To be Published*

3. M.P. Lettinga, M.A.M.J. van Zandvoort and Y. K. Levine, Luminescent characterisation of fluorescein derivatives in various immobilising matrices. *To be Published*

4. M.P. Lettinga, E.M. Klarenbeek, H. Zuilhof and M. A. M. J. van Zandvoort (1999), The orientation of the phosphorescence dipole moment of Erytherosine within its molecular frame. *Journal of Fluorescence* **9** (3), 265-279

5. Barbon, P. Lettinga, P.L. Nordio (1995),Analysis of temperature dependent fluorescence polarization for dimethylaminobenzonitrile. *Chemical Physics* **200,** 41-47

6. M.A.M.J. van Zandvoort, D. Wróbel, P. Lettinga, G. van Ginkel and Y.K. Levine (1995), Chlorophylls in polymers. I. State of chlorophyll *a* in unstretched polymer systems. *Photochem. and Photobiol.* **62**, 279-289

7. D. Wróbel, M.A.M.J. van Zandvoort, P. Lettinga, G. van Ginkel and Y.K. Levine (1995), Chlorophylls in polymers. II. Pheophytin *a* in polymer and the influence of stretching on the state of chlorophylls in anhydrous polymer films. Ph*otochem. and Photobiol.* **62**, 290-298

8. M.A.M.J. van Zandvoort, D. Wróbel, P. Lettinga, G. van Ginkel and Y.K. Levine (1995),The orientation of the transition dipole moment of chlorophyll *a* and Pheophytin *a* in their molecular frame. *Photochem. and Photobiol.* **62**, 299-308

Curriculum Vitae

Pavlik Lettinga werd op 15 juni 1970 geboren te Delft. Hij behaalde in 1988 het VWO-diploma aan de Rijksscholengemeenschap 'Het Wagenings Lyceum' te Wageningen. Datzelfde jaar begon hij met zijn studie Natuur- en Sterrenkunde aan de Universiteit Utrecht met als hoofdvak Moleculaire Biofysica. Het keuzevak Fysische Chemie volgde hij gedurende een vier maanden durende stage aan de Universiteit van Bologna (Italië). Na het behalen van zijn doctoraalbul in 1994 was hij voor tweeëneenhalve maand werkzaam als toegevoegd onderzoeker aan de Universiteit van Padova (Italië). In december van hetzelfde jaar trad hij als AiO in dienst van de Universiteit Utrecht bij de vakgroep Moleculaire Biofysica van het Debye Instituut. Het resultaat van het aldaar verrichte onderzoek is weergegeven in dit proefschrift.